Peninsula Technikon

Faculty of Engineering

Centre for Research in Applied Technology (CRATECH)

SINGULAR BEHAVIOUR OF NON-NEWTONIAN FLUIDS

Abed Mennad

BSc. (Eng.) (University of Blida, Algeria)

A Thesis Submitted Towards the Degree of
Master of Technology (M Tech)

Supervisor: N. Mahomed, BSc. (Eng), MSc. (Eng), PhD (Warsaw)

CAPE TOWN, 1999

ACKNOWLEDGEMENTS

I would like to thank my supervisor and the father of research at Peninsula Tecknikon, Dr Nawaz Mahomed, for patiently providing me with invaluable advice and insight during the course of this work, without his constant assistance and encouragement, it is improbable that this work would have been completed.

I would like also to express my gratitude to Dr Bohua Sun for his comments and suggestions. I express my sincere appreciation to Mr Anthony Staak, the Dean of the Faculty of Engineering, Mr Keith Jacobs, the Head of Mechanical Engineering, and Mr Walter Kohloffer, all for their friendly advice and encouragement.

I would also like to acknowledge useful discussions with the expert of the singular finite element in fluids, Dr G. Georgio from the Department of Mathematics and Statistics, University of Cyprus, Dr Ahmed ould Khaoua from the Departamento de mathematics Universdad de los Andes in Columbia, and Prof E Shnack from Universiatat Karlsuhe (TH).

I would like also to acknowledge the financial support received from the National Research Foundation NRF, and that received from Peninsula Technikon.

In addition, I would like to thank my many colleagues, starting with Mogammad Tawhir, who encouraged me to be equally motivated at the end as at the beginning, and assisted with the linguistic correctness of the text of this dissertation. Marino Kekana was of noteworthy assistance with the programming. Also to be mentioned are Brian Hendricks, my brother in South Africa, Da Huang, Mark Ludick, Xun Li, Cheng Wei, post-doctorate from Beijing University, Larissa Stepanova, post-doctorate from Semara University in Russia, Philemon Simelane, Oscar Philander, Momay Riddles, Leon Navarro, Bart Riedstra, Bernadette Gonzalves, Elvina Moosa, and all the members of the Centre for Research in Applied Technology, and all those responsible for the new research at Peninsula Technikon.

DEDICATION

I dedicate this modest work to my father for his untiring and patient support for my aspirations, and to the memory of my mother; to all my brothers and sisters, and to my future wife.

ABSTRACT

Since 1996, a team at the Centre for Research in Applied Technology (CRATECH) at Peninsula Technikon, under NRF sponsorship and with industrial co-operation, has been involved in the simulation of Non-Newtonian flow behaviour in industrial processes, in particular, injection moulding of polymers.

This study is an attempt to deal with some current issues of Non-Newtonian flow, in small areas, from the viewpoint of computational mechanics. It is concerned with the numerical simulation of Non-Newtonian fluid flows in mould cavities with re-entrant corners. The major complication that exists in this numerical simulation is the singularity of the stresses at the entry of the corner, which is responsible for non-integrable stresses and the propagation of solution errors.

First, the study focuses on the derivation of the equations of motion of the flow which leads to Navier- Stokes equations. Thereafter, the occurrence of singularities in the numerical solution of these equations is investigated.

Singularities require special attention no matter what numerical method is used. In finite element analysis, local refinement around the singular point is often employed in order to improve the accuracy. However, the accuracy and the rate of convergence are not, in general, satisfactory. Incorporating the nature of singularity, obtained by an asymptotic analysis in the numerical solution, has proven to be a very effective way to improve the accuracy in the neighborhood of the singularity and, to speed up the rate of convergence. This idea has been successfully adopted in solving mainly fracture mechanics problems by a variety of methods: finite difference, finite elements, boundary and global elements, and spectral methods.

In this thesis, the singular finite elements method (SFEM), similar in principle to the crack tip element used in fracture mechanics, is proposed to improve the solution accuracy in the vicinity of the singular point and to speed up the rate of convergence. This method requires minor modifications to standard finite element schemes.

Unfortunately, this method could not be implemented in this study due to the difficulty in generating the mesh for the singular element. Only the standard finite element method with mesh refinement has been used. The results obtained are in accordance with what was expected.

LIST OF FIGURES

LIST OF TABLES

NOMENCLATURE

a	Acceleration
$BMESH$	Background mesh
$CMESH$	Cavity mesh
CV	Control volume
dS	Surface element
e	State variable
E_a	Activation energy
F	Local deformation gradient
g	Gravitational force vector
h	Half gape width of the mould
i	Unit vector in x direction
I	Spatial unit tensor
$IMESH$	Input mesh data of boundary segments and nodes
$IMOLD$	Input mesh data for time integration
J	Jacobian determinant
j	Unit vector in y direction
k	Thermal conductivity
k	Unit vector in z direction
M	Preliminary interpolation function the velocity
M_i	Interpolation function in ξ direction
M_1	Mesh 1 used for the computation
M_2	Mesh 2 used for the computation
N	Interpolation function for isoparametric element
$\widetilde{N}$	Interpolation function for no-isoparametric element
$\widetilde{N}_i$	Interpolation function for the geometry of singular element
n	Unit normal pointing out the surface
$OMOLD$	Output file for CRATMOLD
P_i	Interpolation function in η direction
$P=P(X,t)$	Pressure depends on the space and time
q	Heat flux
R	Constant of gas
r	Radial coordinate
R	Radius
R_e	Reynolds number
S	Surface of fluid element
$S(x,t,p)$	Fluidity
s_i	Rate of the strain
T	Temperature
T	Transpose
u	Velocity weighting function
v	Velocity vector
v_e	Entrance velocity
v_r	Radial velocity

v_θ	Angular velocity
X	Spatial position vector

Greek Letters

δ_{ij}	Kronecker delta
φ_0	Stream function Corresponding to Stokes solution
θ	Angular coordinate
η_a	Apparent viscosity
ρ	Density
Γ_e	Entrance boundary
λ	Exponent of the singularity
β	Global angle of the singular element
$L^2(\Omega)$	Hilbert space
σ_{ij}^p	Hydrostatic pressure tensor
ϕ_i	Interpolation function for the velocity for singular element
(ξ,η)	Local coordinate for master element
$\bar{\dot{\epsilon}}$	Magnitude of the strain rate
$(\sigma \cdot n)$	Normal stress on the free surface
Λ	Penalty parameter
$Re(\lambda)$	Real part of the eingenvalue
$\dot{\epsilon}_{ij}$	Shear rate tensor (strain tensor)
φ	Stream function
$(\sigma \cdot t)$	Tangential stress on the free surface
λ	The coefficient of bulk viscosity
σ_i	The total stress tensor
τ^*	Transition stress
ξ	Vector position used (initial position)
η	Viscosity
η_0	Viscosity at zero shear stress
σ_{ij}^v	Viscous stress tensor
υ	Volume element fluid
Γ_w	Wall boundary
W_i	Weighting function for Gauss quadrature
$H^1(\Omega)$	Soblev space
Γ_f	Free surface boundary
∇	Spatial gradient
$\aleph(\xi,t)$	Fluid properties

Abbreviation

CAD/CAM	Computer aided design/ computer aided manufacturing
CRATMOLD	A code for simulation of Non-Newtonian Fluid
FAN	Flow analysis network
FEM	Finite element method
FIB	Flow Induced Birefringence
LDV	Laser Doppler Velocimetry
SFEM	Singular finite element method
PDE	Partial differential equation
POLYFLOW	A commercial code for simulation of free surface flow
UCM	Upper Convected Maxwell Model

CHAPTER 1

INTRODUCTION

1.1 Background

For the past several years, numerical simulation of Non-Newtonian flow has been a powerful tool for understanding the fluid behaviour in a variety of industrial processes and scientific interests. Non-Newtonian fluids, owing to their inelastic or viscoelastic character, are of particular interest in the numerical simulation community. Their wide applications in materials processing, and their different behaviour from that of Newtonian fluids, are often complex and striking.

The origin of this work is an attempt to deal with an industrial problem concerning the injection of thermoplastics. It is concerned with the numerical simulation of Non-Newtonian fluid flow in injection moulding filling processes. One of the difficulties in treating such flow is the presence of the re- entrant corner of the mould cavity, where the stress becomes extremely higher resulting in numerical instability and loss of convergence of the solution.

Great strides have been made in understanding the complexity of Non-Newtonian fluid behaviour. This understanding has led to further challenges in mathematics and numerical methods. In injection moulding, this complexity is particularly displayed in the details in the vicinity of a sudden change of geometry of a cavity, the details of a re-entrant corner, as well as those when the free surface leaves the die of the mould. It is well known that, under these circumstances, the flow develops a singular behaviour, which leads to a singular problem.

In this Chapter, the occurrence of singularity in mechanics in general is introduced. Thereafter singularity in fluid mechanics has been attended to. The different types of fluids are also addressed. Our application is injection moulding, thus a brief introduction to this process as well as the difficulties associated with singularity in this process, are also given. The objectives of this study, the numerical method that deal with singularity, and our proposed method of approach has been discussed. Further, some of the related literature to singularity that occurs in non-Newtonian fluid is given consideration. The Chapter ends with the dissertation outline.

1.2 Singularity problems

Singularities are present in many of natural and engineering systems around us. Examples of singular phenomena in fluid mechanics include three-phase moving

contact lines, cusps generated in interface with surface tension, flow around sharp corners, break-up of liquid drops and threads, and the shape of drops when they freeze. In solid mechanics, examples include crack initiation and propagation, stress field around sharp corners and cracks, penetration of indentures into a plastic medium, strain localization and shear bands.

Since the problem is a fluid mechanics problems, Figure 1.1 shows the set up for the three singular problems in fluids, namely the die-swell, the stick slip and the corner problems. These are often used as model problems for the various numerical methods proposed for Newtonian or Non-Newtonian flows. These problems are important in injection moulding processes and in other industrial applications, and have been the subject of a considerable amount of experimental and numerical work.
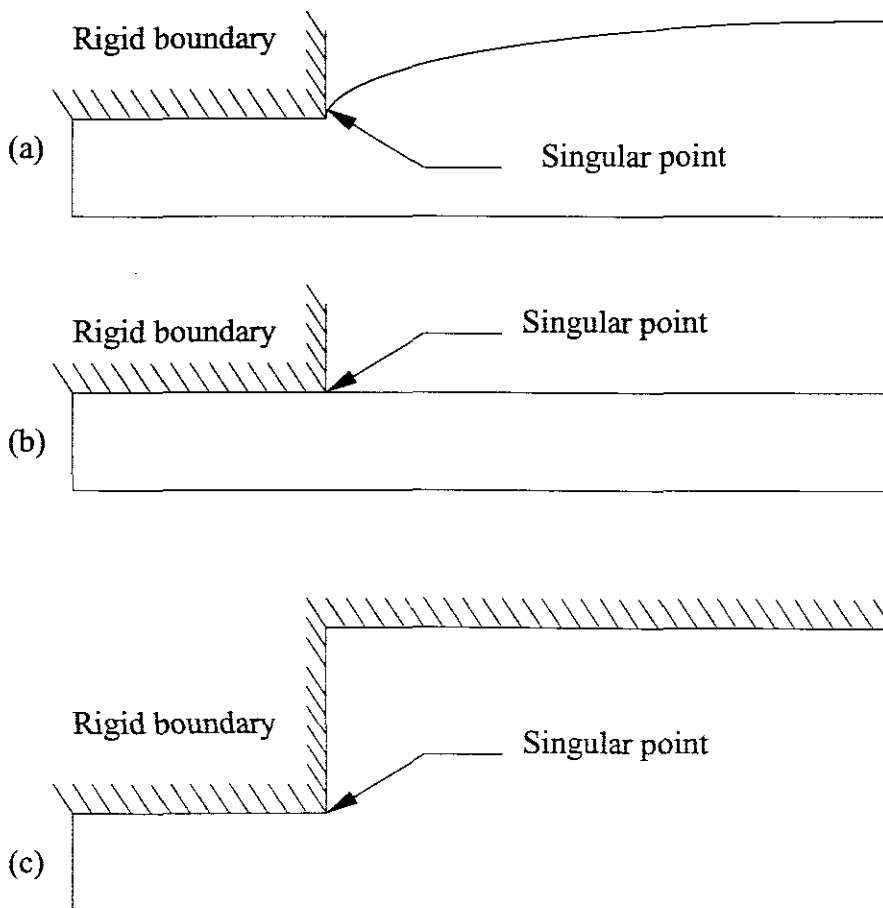
Figure 1.1 Singular problems in fluid

(a) The die swell problem
(b) The stick slip problem
(c) The corner flow

In these three problems the solution of the equation of behaviour of the flow is smooth (regular) in the whole domain, except in the neighborhood of the singular point as shown in Figure 1.1.

Since the geometry of the mould has a right angle corner, it is chosen to solve the flow of a Non-Newtonian fluid around a corner, as in Figure 1.1(c), which is more challenging than that of a Newtonian fluid.

1.3 Types of fluids

A fluid is called Newtonian if the dependence of the stress tensor on the spatial variation of the velocity is linear. This model was introduced by Stokes in 1844 and is very well applicable for describing flows of many fluids including water and air in the standard regime. On the other hand, there are many problems in different areas of science and industry where it is necessary to study flows of fluids, which are not described by Stokes's model. Such fluids are called Non-Newtonian.

Due to the negative definition of Non-Newtonian fluids, it is useful to define some important points of non-Newtonian behaviour. The most significant characteristics are:
- The ability of the fluid to shear thin or thicken in a simple shear flow
- The presence of non-zero normal stress differences in a simple shear flow
- The ability of the fluid to yield stress
- The ability of the fluid to exhibit stress relaxation
- The ability of the fluid to creep.

A particular Non-Newtonian fluid can exhibit just one or all of the above mentioned characteristics. Using these characteristics Crochet and Walters (1983) classified the fluid into four groups, namely, purely viscous or time independent fluids, time dependent fluids, viscoelastic fluids and complex rheological fluids. Since we will use the model of a purely viscous fluid, the main departure from Newtonian behaviour will be shear thinning and shear thickening. All other characteristics are somehow connected to visco-elastic qualities and we will not discuss them here.

Now, let us take a look at just the first phenomenon. It can be typically found with polymer melts, polymer solutions, or solid-in-liquid suspensions. Let us consider a two-dimensional simple shear flow. Then the velocity field has the following form:

$$v(x,y) = (v_x(y),0)$$

And the symmetry part of the velocity gradient and the viscous stress tensor can be written in the form:

$$\dot{\epsilon}_{ij} = \begin{bmatrix} 0 & \frac{1}{2}\frac{dv_x}{dy} \\ \frac{1}{2}\frac{dv_x}{dy} & 0 \end{bmatrix}$$

$$\sigma_{ij}^v = \begin{bmatrix} 0 & \tau \\ \tau & 0 \end{bmatrix}$$

If laminar-shearing flow can be generated in a viscometer, then it is possible to measure the dependence of the shear stress $\tau = \sigma_{ij}^{v}$ on the shear rate $k = \dot{\epsilon}_{ij}$. The apparent viscosity η_a is defined by

$$\eta_a(k) = \frac{\tau}{|k|}$$

and the difference between the shear thinning and shear thickening can be described as follows:

1.3.1 Newtonian fluids

The Newtonian fluid shows the simplest behavior of the purely viscous fluids. The apparent viscosity is constant, equal to the dynamic viscosity of the fluid, i.e.

$$\frac{d\eta_a}{dk} = 0$$
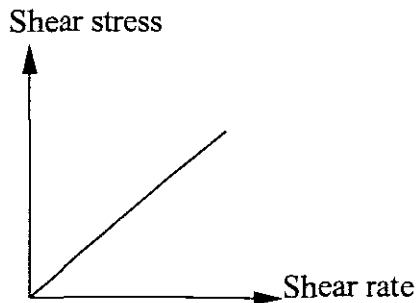
Newtonian behavior has been found for all glasses and in general for liquids or solutions of materials of lower molecular weight. However, there is speculation and some supporting evidence that fluids which are normally considered to be Newtonian may exhibit some non-Newtonian behavior under conditions of very high shear, so the classification of a fluid may change with imposed conditions.

1.3.2 Pseudo-plastic fluids (Shear thinning)

The apparent viscosity is a decreasing function of k, one which concave downward:

$$\frac{d\eta_a}{dk} \leq 0$$
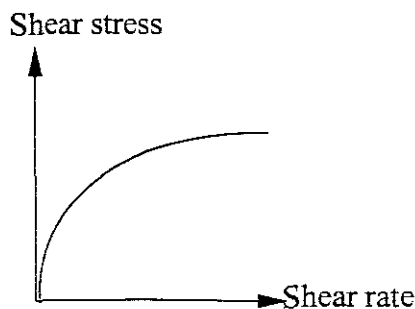
Examples of fluids, which show pseudo-plastic behavior include polymeric solutions or

melts such as rubbers, cellulose, acetate, and napalm, suspensions such as paints and detergent slurries, and dilute suspensions of inert solids.

1.3.3 Dilatant fluids (Shear thickening)

This model shows rheological behavior essentially opposite to that of pseudo-plastic. The apparent viscosity is an increasing function of k, that is:

$$\frac{d\eta_a}{dk} \geq 0$$

Shear stress

Shear rate
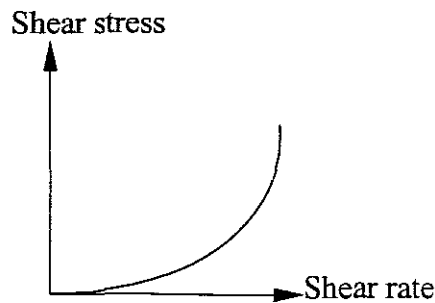
Examples of fluids that are reported as exhibiting dilatancy are pigment-vehicle suspensions, such as paints and printing inks. Dilatant fluids are much less common than pseudo-plastic fluids and have received much less study.

1.4 Introduction to injection moulding

Today injection moulding (IM) is one of the most important polymer processing techniques. The commercial importance of injection moulding comes from the high level of automation and high production rate that is possible. Furthermore, injection moulding allows complex parts to be produced in a single operation. The resulting surface is often good enough and moulded articles require little or usually no extra effort for finishing. The advantages and weaknesses of the technique can be summarized as follows...

    Advantages...
- The procedure is fast and can be performed at a high level of automation.
- Very complex articles can be manufactured.
- The resulting surface often requires no extra effort for finishing.
- There is little waste of material in the process.
    Weaknesses...
- The moulds are very expensive, and difficult to make.
- The moulding machinery is very complex and therefore expensive.

The result of the injection moulding process depends significantly on the conditions under which the part is moulded. The complexity of the moulding process makes it difficult to predict the quality of the resulting product. This complexity makes it interesting to develop theoretical models that describe the moulding process. This issue will be discussed in Chapter 2.

1.4.1 A survey of the production method

In the injection moulding of thermoplastics, molten material is forced into a mould where it is cooled and hardens. The working procedure of the injection moulding machine is as follows… (See Figure 1.2)

Polymer granules fill the barrel. The polymer material is melted by heating elements. The screw acts as a ram and pushes the molten polymer into the mould until the mould is just filled. This is called the *filling phase*. The clamping unit holds the mould in position during this period of time.

At the end of the filling phase pressure is maintained for an extra period of time, called the *packing phase*. During this period a small amount of extra material can enter the mould. This compensates for the decrease in density of the polymer at higher temperatures.

The final phase is called the *cooling phase*. The mould has cooling channels that increase the cooling rate. At the end of this phase the mould opens and the product is pushed out from the mould. During this period, new polymeric material is fed into the barrel and the process can start again.
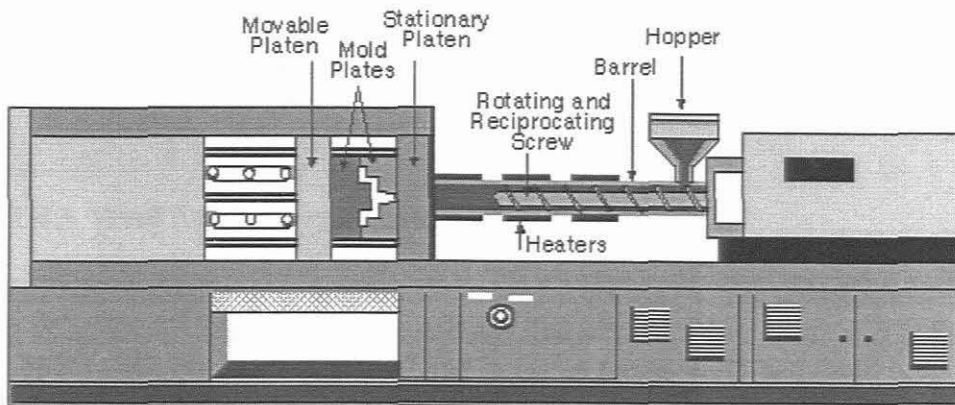
Figure 1.2 Injection moulding machine

1.4.2 Air traps

In addition to the singularity that arises from the abrupt change in the geometry of the mould, when the melt front arrives at the corner, another singularity called interface singularity arises in the injection moulding. This singularity comes from the interface between the polymer melt and the air that is caught inside the mould cavity. The air becomes trapped by converging polymer melt fronts, or because it failed to escape from the mould vents. Air-traps locations are usually in areas that fill last. Lack of vents or undersized vents in these last-to-fill areas are a common cause of air traps and the resulting defects. Air trap is crucial because the two fluids represent radically different

behaviour which gives a strong discontinuity of certain physical coefficients at the interface. The numerical solution is then delicate. Figure 1.3 shows the air trap location.
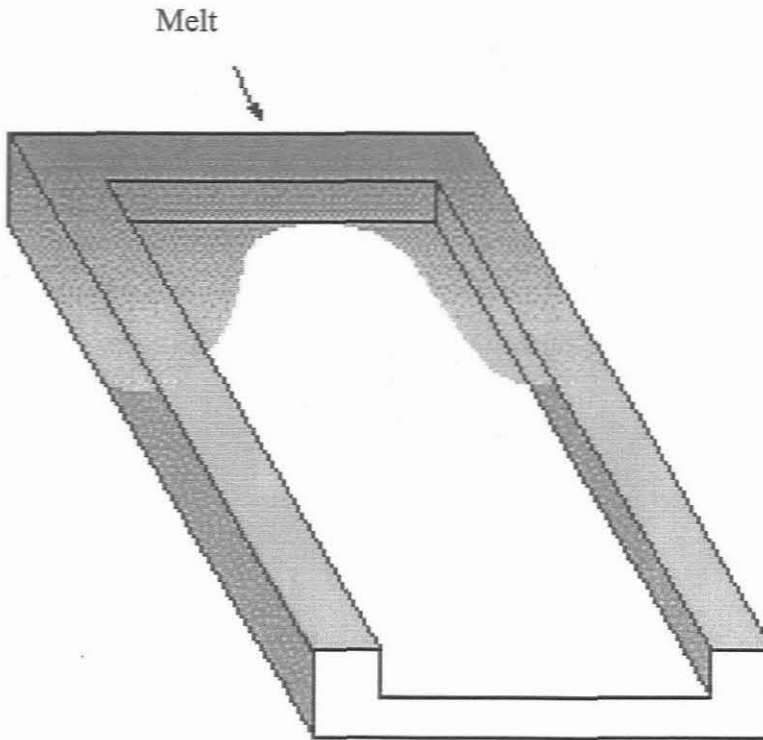
Melt

Figure 1.3 Air trap location

1.4.3 Weld lines and meld lines location

A weld line (also called a weld mark or knit line) is formed when separate melts fronts travelling in opposite directions, meet. A meld line occurs if two emerging melt fronts flow parallel to each other and create a bond between them. Weld and meld lines can be caused by holes, or inserts in the part, multiple gates, or variable wall thicknesses where Hesitation or race tracking occurs. If weld or meld lines cannot be avoided, they should be position them at low-stress and low visibility areas by adjusting the gate position and dimension. The strength of weld and meld lines can be improved by increasing the local temperature and pressure at their locations.

Traditionally, the "meeting angle" is used to differentiate weld lines and meld lines. As illustrated in Figure 1.4 below, a meeting angle θ smaller than 135^0 produces a weld line; greater than 135^0, a meld line. Note that the weld line surface mark disappears when the meeting angle reaches 120^0 to 150^0. Normally, weld lines are considered to be of lower quality than meld lines, since relatively less molecular diffusion occurs across a weld line after it is formed.

There are some other difficulties and problems associated with the injection moulding method. These difficulties are summarized as follows:

- The polymer can solidify before the mould is completely filled.
- Differences in the mould thickness and in the cooling system capacity between different parts of the mould can cause cooling rate, and therefore the shrinking rate to differ at different parts of the product. This can cause the final product to become warped.
- Polymer can leak out of the mould if the clamping units are not pressed together using enough force.
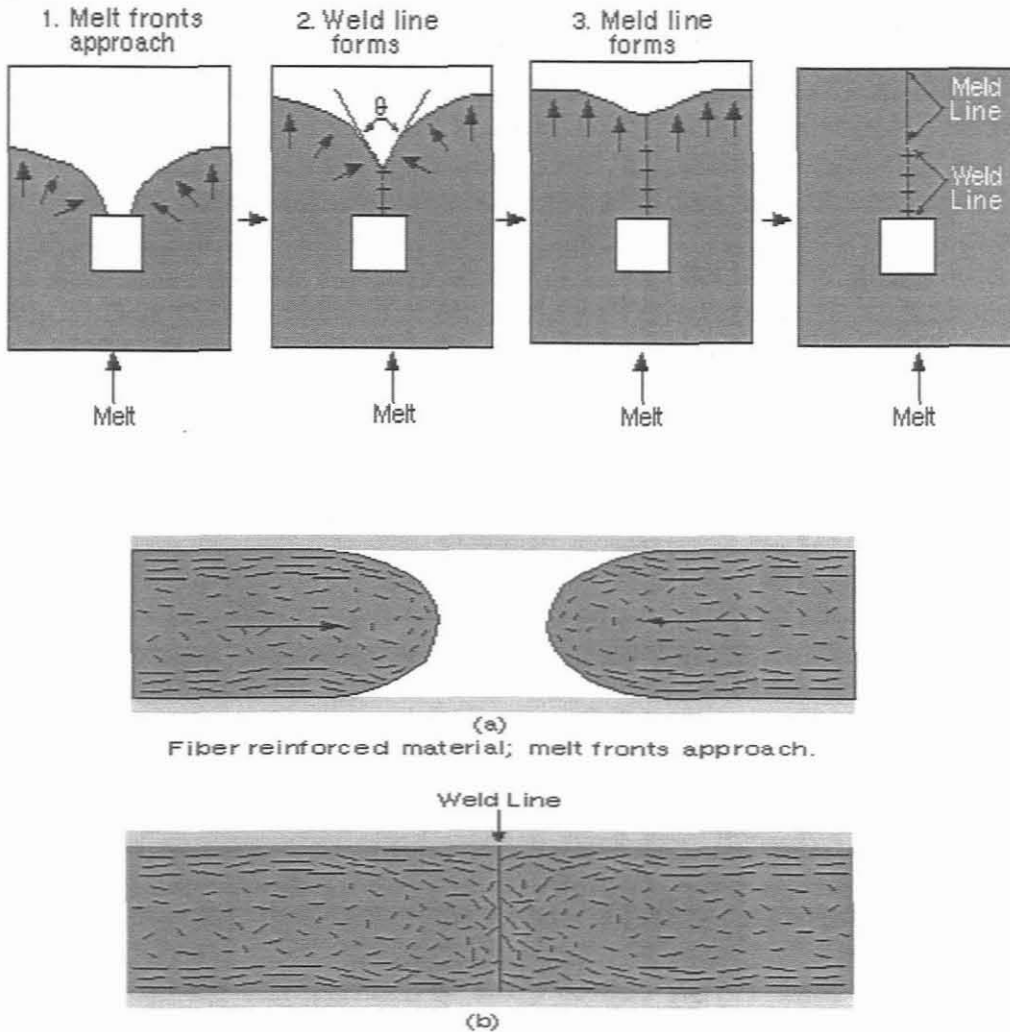
Figure 1.4 Interface singularity due to the meld and the weld line

1.5 Previous related studies

The problems of singularities have always attracted the attention of mathematicians, scientists and engineers IACM (1997). The flow of Non-Newtonian liquids involving

abrupt changes in geometry has been the subject of experimental and numerical study for over a decade (see Crochet et al., 1984). Walters and Webster (1982) were the first who noted the strong interaction between fluid and the corner conditions. In some of their experiments they reported that corner conditions had a far greater influence on the flow field as a whole in non-Newtonian flows, than was the case for corresponding Newtonian flows. Madrers et al., (1990) used an iterative linking of the singular analytical solution with a steady numerical finite element solution to study the flow in a converging channel with re-entrant corner. Pogu and Tournemine (1990) have studied a viscous flow in domains with corner. Kim et al., (1983) addressed the roles of shear thinning and inertia on axisymmetric sudden contraction flows. Rosenberg et al., (1988) reported new finite elements of creeping flows through a sudden planar contraction, the re-entrant corner which is defined by a circular arc of small radius. Song et al., (1988) simulated the flow of upper convected Maxwell fluids through a planar 4:1 contraction using type dependent difference approximation of the vorticity equation. A very good review of both experimental and numerical studies of axisymmetric and planar entry flows has been given by White et al., (1987). Mendelson et al., (1982) presented results for two viscoelastic models, the convected Maxwell model and the second order fluid model in a planar sudden contraction and in the wall driven cavity flow. Keunings and Crochet in (1984) analyzed the flow through an abrupt 4:1 contraction by means of finite elements. The effects of the memory in flows involving abrupt change in geometry has been given first by Perera and Walters (1977) in their work concerned with L- shaped and T-shaped geometry. They give further consideration to the solution of problems involving abrupt changes in geometry using implicit rheological equations of state in (1977), this idea has been extended by Davies et al., (1979) to the moving boundary problem. An analytical asymptotical solution has been proposed by Moffatt (1964) and Micheal (1958) for Newtonian flow to point out the presence of the stress singularity near geometrical singularity. Hassager (1988) solved a shear thinning power law fluid Lipscomb (1987) has studied the implications of boundary singularities in complex geometries for second order fluid. Davies (1988) has also given the theory of re-entrant singularities. He used biorthogonal series expansions to study creeping flow in re-entrant and non-reentrant corner sectors. Killer (1991) examined the flow around a 3/2 π corner of suspension of non-Brownian rigid rods. Renardy (1993) proposed a scheme to integrate the stresses of the UCM fluid, which avoids the downstream instability near the re-entrant corner. The scheme is based on representing the stress in a natural basis that is aligned with the streamlines. An exact series solution for planar creeping flows in the neighborhood of sharp corners are presented and discussed by Davies and Delvin(1993).

1.6 Numerical methods for singularity problem

The numerical simulation of Non-Newtonian flow involves the solution of the continuity and momentum equations with a specified constitutive equation and specified boundary conditions. The descriptions of the free surface offer a particular challenge especially when the melt front reaches the singular point. It is not understood how the solution behaves at this point. The free surface can be treated numerically from either the Eulerian or Lagrangian view. The Eulerian mesh remains fixed in space with

the flow moving through it, while the Lagrangian mesh is convected with the flow. Many of the computational codes use either a Eulerian mesh together with a control volume (CV) approach (also referred to flow analysis network (FAN)), to track the motion of the flow front (see Broyer et al., 1977; Tanguy and R Lacroix 1991), or remesh either locally at the flow front or remesh completely over the domain covered by the fluid (for more detail see Subbiah et al., 1989; Garcia 1991). However, in this study we are not interested in treating the melt front tracking and the free surface problem by determining the shape and the location of the free surface. Mahomed (1998) has solved this problem. We are interested only in the behaviour of the solution at the singular point. It is very important to improve the accuracy and to speed up the rate of convergence in the neighborhood of the singularity. A variety of methods have been successfully proposed to deal with this problem. These methods are:
The Spectral method (see for instance Lee et al., 1987; Cai et al., 1993; Lucas et al., 1993), the finite difference method Holsten and Paddon (1981), the boundary and global elements method Kermode et al., (1985), the J integral based schemes (see Tanner and Huang 1993; Hassanger and Laurdissen 1988) and the most popular finite element method (FEM). The work by Baker (1983) and Zienkiewwicz (1988) provide a general reference for the FEM.

In the finite element method, the approximate solution must be smooth (non-singular). In order to get the smoothness, it is convenient to modify the boundary by local mesh refinement or replace the corner by an arc with a small radius, or use a special finite element. These three approaches to smoothening are now discussed in the following section.

Local mesh refinement. Babuska and Rheinboldt (1978) have pioneered the adaptive placement of irregularity embedded finite elements in crude meshes for increased accuracy in regions of the domain where the solution varies greatly. The mesh refinement is based on the three versions of the finite elements, which are the h-version, the p-version and the h-p version (see Babuska and Miller 1994). Recently, adaptive h-p finite element methods have been used for analysis of significant classes of incompressible flows (see Oden et al., 1993) including generalized Newtonian fluids Lagat and Oden 1996), and extended to viscoelastic fluids by Warichet and Legat (1996). These techniques automatically adjust the parameters h and p (the mesh size and the degree of the polynomial). The accuracy can be achieved by refining the mesh, (small h) while the p remain fixed, usually at lower level $p=1$, 2, or 3. Also, it is possible to increase the degree p of the element uniformly or selectively while the mesh size is fixed, or to vary both of them. For some conception of remeshing (mesh size and computation of the mesh size) and treatment of the singularity, (see Zienkiewicz et al., 1988 for more details).

Replacing the corner by an arc. In this case, the boundary is smoothed by replacing the corner with a circular arc of a small radius as shown in Figure1.5. To increase the accuracy, mesh refinement is also necessary.
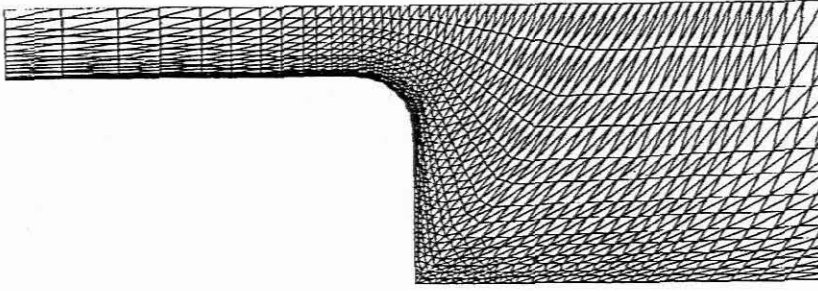
Figure 1.5 Replacing the corner with small arc (Bloch et al., 1994)

Singular finite element method (SFEM). This method has been developed in solid mechanics to deal with the crack propagation and the stress intensity factor. The singular finite element method has been extended to fluid mechanics by Georgiou et al., in (1988) and (1990). This idea used a special element with a special shape function around the singular point and ordinary finite elements elsewhere. This issue is one of the main objectives of this study and will be discussed in detail in Chapter 5.

1.7   Objectives of this study

The goal of this dissertation is to study the flow around the singularities in injection moulding. Such singularities occurs when the free surface of polymer melts flow in a mould with a sharp corner.

This research effort focuses on investigating the occurrence of the singularities in the numerical solution of the equations defining the flow behaviour, particularly the Navier-Stokes equations. The existing techniques for overcoming the problem of the singularities are further investigated. In this investigation, a suitable method for solving this problem has been proposed. The proposed method is called the singular finite element method (SFEM). This idea has been used in solid mechanics, but received limited attention in fluid mechanics, especially for Non-Newtonian fluids.

Considerable progress has recently been made in developing the finite element codes for free surface problems. These have been incorporated in CRATMOLD, a Fortran code for the computational simulation of Non-Newtonian fluids in injection moulding processes.

The scope of this project includes the assessment of the capability of CRATMOLD to deal with singularity and the investigation of the possibility of implementing the new method through the modifications of CRATMOLD. This requires the development of an additional routine for generating the singular element mesh, shape function, *Jacobian* transformation and the integration routines to the CRATMOLD code.

1.8 Dissertation outline

The Chapters of this dissertation are organised in the following manner. In Chapter 2 the mathematical model for injection moulding filling that is used throughout this work is derived from a fundamental viewpoint which serves as a rigorous basis for the dissertation. The solution of this model involves the solution of the equations of continuity and momentum with specified boundary conditions. The equation of energy has been derived, but it is not solved due to the isothermal condition of the filling phase. The free surface offers a particular challenge, but here again this problem is not investigated.

In Chapter 3, the occurrence of the singularity in the Stokes model is investigated. This investigation needs to solve a fourth order biharmonic equation in polar coordinates to find the analytical solution. This solution gives the stress and the velocity field distribution near the singular point. The order of the singularity is determined here, and is used to construct the singular element in Chapter 5.

In Chapter 4, the full finite element formulation of the problem is given. The formulation is based on the Galerkin weighted residual method, which transforms the classical form of the problem to the weak variational form. The penalty method to eliminate the pressure from the momentum equation is presented. The shape function, the coordinate transformation, the numerical integration, and some of the conditions for the mixed formulation for four noded isoparametric element that is used in the CRATMOLD code, are described in detail in this Chapter.

To achieve maximal accuracy of the flow field near the corner of the cavity, special finite element analysis have to be used. In Chapter 5 the singular finite element method (SFEM), which is one of the methods used to solve singular problems in solid mechanics, is introduced. The types of SFEM are discussed, which are the singular basis function approach and the singular element approach. Furthermore, only the singular element approach is concentrated upon. Two special shape functions have been developed, starting from knowing the analytic solution that has been given in Chapter 3, one for the velocity and the other for the geometry. The *Jacobian* transformation for the geometry is given. It is noticed that at a certain point the *Jacobian* becomes singular. It was attempted to implement this element into the CRATMOLD code, but for some difficulties that will be exposed in the recommendations, it was not used.

In Chapter 6, a general overview of the CRATMOLD code and its implementation is given. Four input files BMESH, CMESH, IMESH, and IMOLD are needed and one output file called OMOLD is generated (see Appendix D). A special routine has been added to the code for computing the two components of the normal stress and shear stress. The Chapter ends with the results and discussions.

Chapter 7 ends the dissertation with a conclusion for the entire work that was done, along with recommendations for further study.

CHAPTER 2

MATHEMATICAL DESCRIPTION OF CONSERVATION EQUATIONS FOR MODELLING OF INJECTION MOULDING

2.1 Introduction

Modelling of injection moulding has been an area of considerable research over the last two decades. In these processes, the modelling of the fluid flow represents several major challenges, since the flow is inherently transient, non-isothermal, non-Newtonian, and includes a free surface moving through cavities of highly irregular geometry.

Three conservation laws, namely, the conservation of mass momentum and energy, mathematically describe the fluid flow. These completely determine the physical behaviour of the fluid and are totally independent of the nature of the fluid, which is defined by additional properties such as viscosity, heat conductivity and compressibility. These fundamental laws can be expressed in terms of mathematical equations, which their most generals form, are usually partial differential equations.

In this Chapter, it is proposed to establish a mathematical model for polymer melt flow in a cavity mould with complex geometry. The mathematical model is derived from the fundamental principle of the fluid mechanics and thermodynamics. Some of the boundary conditions for the process are needed. This issue will be discussed at the end of this Chapter.

2.2 Fluid Dynamics

2.2.1 Continuum model

"Fluid mechanics" is the way of looking at a large collection of particles, so as to avoid dealing with each particle separately. Consider a volume of fluid. At microscopic level, we see lot of molecules and lot of empty spaces between them. The density (mass per unit volume) at each point in the volume is either zero if there is no molecule, or high value if there is one. In other words, density is a discontinuous function of the space variables. To simplify matters mathematically, we approximate this discontinuous function with a continuous one by associating each point in space with the average density over a sufficiently large neighborhood of that point. This is the basis of the continuum model.

2.2.2 Variables and notation

Three physical quantities, velocity, pressure and density, will be of particular interest in what follows. Velocity is a vector-valued function of space and time variables.   It will be denoted by $v = v(X,t)$ which means that v is a vector quantity, i.e.,

$$v = \begin{pmatrix} v_x(X,t) \\ v_y(X,t) \\ v_z(X,t) \end{pmatrix} \tag{2.1}$$

Pressure, which is scalar valued, also depends on space and time. It will be denoted by $p = p(X,t)$. The density of the fluid, denoted by ρ, is assumed to be constant. This implies that the fluid is incompressible, which is a realistic assumption for the mould filling stage.

Mathematically speaking, v, p, ρ, are considered to be the dependent variables of the flow that are functions of the independent variables X and t. This general description is termed a field description, and the dependent variables are called field variables. Thus, the terms such as velocity field used to imply the dependence of the velocity and the pressure on the independent variables X and t.

In this thesis, the Cartesian coordinates have been used to describe the position vector X,

$$X \equiv xi + yj + zk$$

The following tensor notation will be used throughout this Chapter:

$$a_i b_i = a_x b_x + a_y b_y + a_z b_z$$

$$\frac{\partial a_i}{\partial X} = \frac{\partial a_x}{\partial x} + \frac{\partial a_y}{\partial y} + \frac{\partial a_z}{\partial z}$$

The motion of a fluid is assumed to be completely known if we have expressions for the functions $v(X,t)$ and $p(X,t)$. The objective of the remaining sections is therefore to find (differential) equations from which these functions may be determined. Since v has three components, then a total of four scalar valued variables v_x, v_y, v_z and p have to be evaluated. it require four independent equations to determine these variables. One equation can be obtained from the principle of the continuity (mass conservation) and the remaining three from the principle of conservation of momentum.

2.2.3 Kinematics of the fluid

Suppose there is a fluid particle moving in space (see Figure 2.1). At time $t=0$ the position of the particle is specified by ξ and at a later time the particle is at position X. The spatial position can be represented parametrically by Aris (1989):

$$X = X(\xi,t) \tag{2.2}$$

In general, near P if $\xi + \delta\xi \rightarrow X + \delta X$, and $X(\xi,t)$ is differentiable
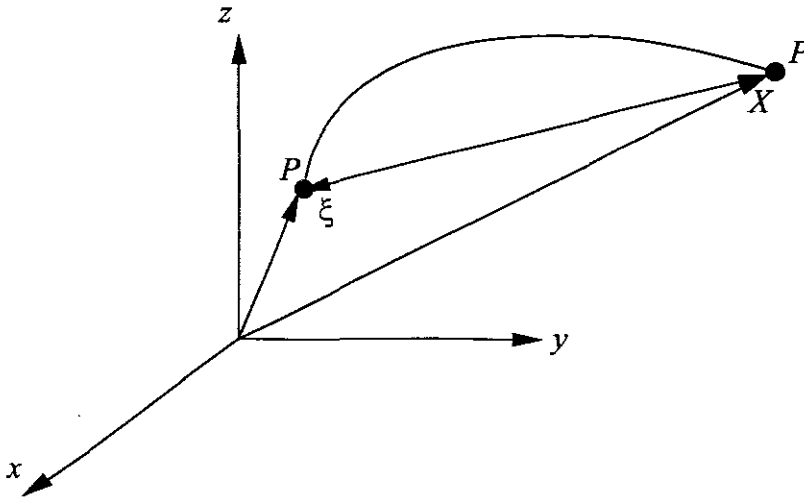
Figure 2.1 Particle trajectory description

$$dX_i = \left(\frac{\partial X_i}{\partial \xi_j}\right)d\xi$$

or, symbolically,

$$dX = F(\xi,t)d\xi$$

The matrix $F \equiv \left(\dfrac{\partial X_i}{\partial \xi_j}\right)$, is called the local deformation gradient, and for (1,1) mapping the *Jacobian* $J = det\, F \neq 0$.

Note: Under change of the background coordinates, F transforms like a second rank tensor.

The point trajectory may be inverted (assuming a non-singular *Jacobian*, i.e., the fluid particle does not break up during the motion or two particles do not occupy the same space at the same time) to give the initial position or material coordinates of the particle which is at any position X and time t.

$$\xi = \xi(X,t) \tag{2.3}$$

and $d\xi = F^{-1}(\xi,t)dX$

with $F_{kl}^{-1} = \partial\xi_k/\partial X_l$

Any properties of the fluid, say $\aleph(\xi,t)$, may be observed along the particles path. The description of the change of the properties $\aleph(\xi,t)$ may be changed into a spatial description by Equation (2.3):

$$\aleph(X,t) = \aleph[\xi(X,t),t] \tag{2.4}$$

This says that the value of the property at position x and time t is the same as the value appropriate to the particle at (X,t). The material description may be derived from the spatial description (2,2):

$$\aleph(\xi,t) = \aleph[X(\xi,t),t] \tag{2.5}$$

meaning that the value as seen by the particle at time t is the value of the position it occupies at that time. Let the change in the property observed at a fixed point X be:

$$\frac{\partial\aleph}{\partial t} \equiv \left(\frac{\partial\aleph}{\partial t}\right)_X \tag{2.6}$$

Let the change in the property observed when moving with the particle be:

$$\frac{D\aleph}{Dt} \equiv \left(\frac{\partial\aleph}{\partial t}\right)_\xi \tag{2.7}$$

The velocity of the particle is the material derivative of its position $\left(\aleph = X^i\right)$ and is defined by:

$$v(X,t) \equiv \left(\frac{\partial X}{\partial t}\right)_\xi \tag{2.8}$$

The two derivatives (2.7), (2.8) may be related by differentiating the material description (2.5) and using the chain rule:

$$\frac{D\aleph}{Dt} \equiv \left(\frac{\partial\aleph}{\partial t}\right)_\xi = \frac{\partial}{\partial t}\aleph[X(\xi,t),t] = \left(\frac{\partial\aleph}{\partial t}\right)_X + \left(\frac{\partial X}{\partial t}\right)_\xi \cdot \left(\frac{\partial\aleph}{\partial X}\right)_t \tag{2.9}$$

or

$$\frac{D\aleph}{Dt} = \frac{\partial\aleph}{\partial t} + (v.\nabla)\aleph \tag{2.10}$$

The acceleration field is then:

$$a \equiv \left. \frac{\partial}{\partial t} \right)_X v(X,t) + \left(v \cdot \frac{\partial}{\partial X} \right) v \tag{2.11}$$

2.2.4 Conservation of mass

The conservation of mass requires that the accumulation of mass inside a control volume υ is accounted for by the net flow of mass across the surface S (see Figure (2.2)).
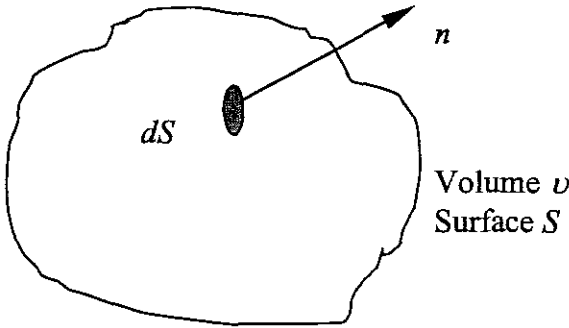
Figure 2.2 Arbitrary "CV" fixed in space.

Mathematically, this can be stated as (see Bird et al., 1987):

$$d \left(\iiint_\upsilon \rho d\upsilon \right) = - \left(\iint_S \rho v \cdot n dS \right) dt \tag{2.12}$$

Dividing by the time increment dt, we obtain an expression for the time rate of increase of mass inside the control volume

$$\frac{d}{dt} \iiint_\upsilon \rho d\upsilon + \iint_S \rho v \cdot n dS = 0 \tag{2.13}$$

by bringing the time differentiation inside the volume integral and applying the divergence theorem to the surface integral, gives

$$\iiint_\upsilon \left(\frac{\partial \rho}{\partial t} \right) d\upsilon + \iiint_\upsilon \nabla \cdot (\rho v) d\upsilon \tag{2.14}$$

$$\iiint_\upsilon \left(\frac{\partial \rho}{\partial t} + \nabla \cdot (\rho v) \right) d\upsilon = 0 \tag{2.15}$$

Because this holds for all control volumes, the integrand must be zero:

$$\frac{\partial \rho}{\partial t} + \nabla \cdot (\rho v) = 0 \tag{2.16}$$

Using the incompressibility condition, the continuity equation takes the simpler form

$$(\nabla \cdot v) = 0 \tag{2.17}$$

which must be satisfied for all x, y, z.

This equation expresses the conservation of mass applied to a fixed control volume. It is a scalar equation and is not sufficient by itself to determine the velocity field v. Sometimes the fluid mass conservation is called the *continuity equation* in recognition of the constraint it imposes on the velocity field.

2.2.5 Conservation of momentum

A basic principle of Newtonian mechanics is the following: whenever there is no net external force acting on a system, its momentum is conserved. The only way the momentum inside a volume can change is therefore through:
- The total force exerted on particles inside υ,
- The rate of momentum influx through S,
- The total forces acting on S.

The discussion of each of this component is as follows:

Body forces: These are forces such as gravity that act on the particles inside a volume, thus changing their momentum. The total effects of these forces simply given by integrating them over the volume. For the *ith* component of momentum, the rate of change due to the body forces is given by:

$$\iiint\limits_{\upsilon} \rho g_i d\upsilon \tag{2.18}$$

Momentum influx: The *ith* component of momentum per volume is $\rho v_i = v_i$ and the *ith* component of the momentum influx into υ is consequently

$$-\iint\limits_{S} v_i v \cdot dS \tag{2.19}$$

Surface forces: The description of these forces is a rather complicated matter (see Figure 2.3). The force acting on S has three spatial components; its effects on the surface depends on the surface's orientation, which has three components as well; and finally, the

resulting force on v again has three components. Some thought reveals that the ith component of the resulting force can be written in the form:

$$\iint_S \sigma_{ij} dS_j \tag{2.20}$$

Here, σ_i is a Cartesian tensor, which for proposes of this study is a spatial type of 3×3 matrix. The notation in the above integral is a tensor form that is equivalent to a dot product, i.e., it really means

$$\iint_S (\sigma_{i1} dS_1 + \sigma_{i2} dS_2 + \sigma_{i3} dS_3) \tag{2.21}$$
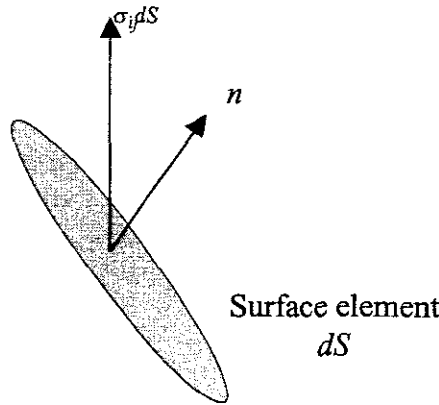
Figure 2.3 Element of surface dS across which the force $\sigma_{ij} dS$ is transmitted

Note that: in the above notation 1, 2 and 3 represent x, y and z respectively.

then σ_i can written in this form (see White 1991 for more detail):

$$\sigma_{ij} = \begin{bmatrix} \sigma_{xx} & \sigma_{xy} & \sigma_{xz} \\ \sigma_{yx} & \sigma_{yy} & \sigma_{yz} \\ \sigma_{zx} & \sigma_{zy} & \sigma_{zz} \end{bmatrix} \tag{2.22}$$

The linear momentum balance is given by the definition:
The rate of the total linear momentum is equal to the sum of the external forces, this gives:

$$\frac{d}{dt} \iiint_v \rho v_i dv = \iiint_v \rho g_i dv - \iint_S \rho v_i v \cdot dS + \iint_S \sigma_{ij} dS_i \tag{2.23}$$

Equation (2.23) is called the linear momentum balance.

2.2.6 Constitutive relations

The balance law for linear momentum (2.23) do not make any reference to the properties of the fluid. The full specification of the mechanical and thermal properties of the fluid requires further information as to the relation between the stress and the rate of the strain. This is provided by the constitutive equation which give a mathematical representation of functional dependence between stress and rate of the strain.

The fluids can be characterised a constitutive equation in which stress depends on the rate of strain In terms of the velocity gradient $\partial v_i / \partial v_j$, density ρ, and temperature T as follows:

$$\sigma_{ij} = s_{ij}(\partial v_i / \partial x_j, \rho, T) \tag{2.24}$$

Generally, the motion of a fluid involves translation, deformation and rotation. The local translation is described by the velocity vector v. The deformation and rotation are obtained from the velocity gradient tensor ∇v. In the study of the filling phase of injection moulding, the interesting part is the rate of deformation of the fluid. This is described by the rate of strain tensor defined as:

$$\dot{\epsilon}_{ij} = \frac{1}{2}\left(\frac{\partial v_i}{\partial x_j} + \frac{\partial v_j}{\partial x_i} \right) \tag{2.25}$$

The rate of strain tensor is symmetric and can be written as a matrix of its components as follows:

$$\dot{\epsilon}_{ij} = \frac{1}{2} \begin{bmatrix} 2\dfrac{\partial v_x}{\partial x} & \dfrac{\partial v_x}{\partial y} + \dfrac{\partial v_y}{\partial x} & \dfrac{\partial v_x}{\partial z} + \dfrac{\partial v_z}{\partial x} \\[2mm] \dfrac{\partial v_x}{\partial y} + \dfrac{\partial v_y}{\partial x} & 2\dfrac{\partial v_y}{\partial y} & \dfrac{\partial v_y}{\partial z} + \dfrac{\partial v_z}{\partial y} \\[2mm] \dfrac{\partial v_x}{\partial z} + \dfrac{\partial v_z}{\partial x} & \dfrac{\partial v_y}{\partial z} + \dfrac{\partial v_z}{\partial y} & 2\dfrac{\partial v_z}{\partial z} \end{bmatrix} \tag{2.26}$$

The isotropy property of deformation rate tensor requires that $\sigma_{ij} = s_{ij}(\dot{\epsilon}_{ij}, \rho, T)$ and $\dot{\epsilon}_i$ are coaxial (see Emanal (1994)). The most general form for σ_i is therefore:

$$\sigma_{ij} = aI + b\,\dot{\epsilon}_{ij} + c\,\dot{\epsilon}_{ij}^2 \tag{2.27}$$

where a, b, c are functions of ρ and T and the invariant of $\dot{\epsilon}_i$.

In the absence of the motion $\dot{\epsilon}_i = 0$ which gives:

$$\sigma_{ij} = s_{ij}(0, \rho, T) = -p(\rho, T)I \tag{2.28}$$

where $p(\rho,T)$ is the hydrostatic pressure. It is easy to write down the corresponding tensor:

$$\sigma_{ij}^p = \begin{bmatrix} -p & 0 & 0 \\ 0 & -p & 0 \\ 0 & 0 & -p \end{bmatrix} \tag{2.29}$$

The classical Newtonian viscous fluid is a special case of Equation (2.27) in which the stress is linear in the velocity gradient

$$\sigma_{ij} = \underbrace{-p(\rho,T)\delta_{ij}}_{\sigma_{ij}^p} + \underbrace{b_{ijkl}\,\dot{\in}_{kl}}_{\sigma_{ij}^v} \tag{2.30}$$

σ_{ij}^v is called the viscous stress tensor. The b_{ijkl} are the component of a fourth order isotropic tensor with $i-jk-l$ symmetry so that

$$b_{ijkl} = \lambda\delta_{ij}\delta_{kl} + \eta(\delta_{ik}\delta_{jl} + \delta_{il}\delta_{jk}) \tag{2.31}$$

Equation (2.30) therefore becomes:

$$\sigma_{ij} = \left[-p(\rho,T) + \lambda(\rho,T)\right]\delta_{ij} + 2\eta(\rho,T)\dot{\in}_{ij} \tag{2.32}$$

In the theory of elasticity λ is called Lame's constant. It is customary to call it the coefficient of *bulk viscosity* (see Chung (1988)). In this study, the term $\lambda(\rho,T)\delta_i$ can be ignored and the explicit form of the stress tensor can be written as:

$$\sigma_{ij} = -p(\rho,T)\delta_{ij} + \eta\left(\frac{\partial v_i}{\partial x_j} + \frac{\partial v_j}{\partial x_i}\right) \tag{2.33}$$

This gives an excellent description of many fluids. The additional dependence on $\dot{\in}_{ij}^2$ in Equation (2.27) is insufficient to provide an adequate description of many materials for example, blood, polymeric liquids, which deviate from linear dependence on rate of strain. These materials have a memory of deformation, which can be described using viscoelastic constitutive laws.

2.2.7 Navier Stokes Equation

The formulation of the equation of motion is obtained by equating the rate of change of momentum with the sum of the expressions for the body forces, the momentum influx, and the surface forces.

The density ρ is supposed constant; this will simplify the mathematical exposition.

$$\frac{d}{dt}\iiint_{\upsilon}v_i d\upsilon = \iiint_{\upsilon}g_i d\upsilon - \iint_{S}v_i v \cdot dS + \iint_{S}\sigma_{ij}dS_j \qquad (2.34)$$

using tensor notation to write $v_i v dS = v_i v_j dS$ and applying the divergence theorem, we rewrite this equation as:

$$\iiint_{\upsilon}\left\{\frac{\partial}{\partial t}v_i + \frac{\partial}{\partial X_j}\left(v_i v_j\right) - g_i - \frac{\partial}{\partial X_j}\sigma_{ij}\right\}d\upsilon = 0 \qquad (2.35)$$

Note the special meaning of the symbols in the above equation:

$$\frac{\partial}{\partial X_j}\left(v_i v_j\right) = \frac{\partial}{\partial x}\left(v_i v_x\right) + \frac{\partial}{\partial y}\left(v_i v_y\right) + \frac{\partial}{\partial z}\left(v_i v_z\right) \qquad (2.36)$$

and

$$\frac{\partial}{X_j}\sigma_{ij} = \frac{\partial\sigma_{ix}}{\partial x} + \frac{\partial\sigma_{iy}}{\partial y} + \frac{\partial\sigma_{iz}}{\partial z} \qquad (2.37)$$

Since υ can be any arbitrary volume, Equation (2.35) can rewritten

$$\frac{\partial v_i}{\partial t} + \frac{\partial v_i v_j}{\partial X_j} = g_i + \frac{\partial\sigma_{ij}}{\partial X_j} \qquad (2.38)$$

Switching to vector notation, the above equation can be written in the form

$$\frac{\partial v_i}{\partial t} + \nabla\cdot\left(v_i v\right) = g_i + \nabla\cdot\sigma_i \qquad (2.39)$$

The first component of this equation gives

$$\frac{\partial v_x}{\partial t} + \nabla\cdot\left(v_x^2 + v_x v_y + v_x v_z\right) = g_i + \nabla\cdot\sigma_{xx} \qquad (2.40)$$

Evaluating the divergence term in Equation (2.40) gives

$$\frac{\partial v_x}{\partial t} + 2v_x\frac{\partial v_x}{\partial x} + v_y\frac{\partial v_x}{\partial y} + v_x\frac{\partial v_y}{\partial y} + v_z\frac{\partial v_x}{\partial z} + v_x\frac{\partial v_z}{\partial z} = g_x + div\sigma_{xx} \qquad (2.41)$$

or

$$\frac{\partial v_x}{\partial t} + v_x \frac{\partial v_x}{\partial x} + v_y \frac{\partial v_x}{\partial y} + v_z \frac{\partial v_x}{\partial z} + v_x \left(\frac{\partial v_x}{\partial x} + \frac{\partial v_y}{\partial y} + \frac{\partial v_z}{\partial z} \right) = g_x + div\sigma_{xx} \qquad (2.42)$$

The same form of equation is obtained for the second and third components of force. In vector notation we have

$$\frac{\partial v}{\partial t} + (v \cdot \nabla)v = div\sigma + g \qquad (2.43)$$

where

$$div\sigma = \left(div\sigma_{xx} \quad div\sigma_{yy} \quad div\sigma_{zz} \right) \qquad (2.44)$$

and

$$(v \cdot \nabla)v = \left(v_x \frac{\partial}{\partial x} + v_y \frac{\partial}{\partial y} + v_z \frac{\partial}{\partial z} \right) v = \begin{pmatrix} v_x \dfrac{\partial v_x}{\partial x} + v_y \dfrac{\partial v_x}{\partial y} + v_z \dfrac{\partial v_x}{\partial z} \\[2mm] v_x \dfrac{\partial v_y}{\partial x} + v_y \dfrac{\partial v_y}{\partial y} + v_z \dfrac{\partial v_y}{\partial z} \\[2mm] v_x \dfrac{\partial v_z}{\partial x} + v_y \dfrac{\partial v_z}{\partial y} + v_z \dfrac{\partial v_z}{\partial z} \end{pmatrix} \qquad (2.45)$$

Finally, it necessary to evaluate $div\sigma$. To see the general pattern, consider the first component of $div\sigma$. The first component of the stress tensor is:

$$\sigma_{xx} = \left(-p \quad 0 \quad 0 \right) + \eta \left(\frac{\partial v_x}{\partial x} + \frac{\partial v_x}{\partial x} \quad \frac{\partial v_x}{\partial y} + \frac{\partial v_y}{\partial x} \quad \frac{\partial v_x}{\partial z} + \frac{\partial v_z}{\partial x} \right) \qquad (2.46)$$

hence,

$$div\sigma_{xx} = -\frac{\partial p}{\partial x} + \eta \left(\frac{\partial}{\partial x} \left(\frac{\partial v_x}{\partial x} + \frac{\partial v_y}{\partial y} + \frac{\partial v_z}{\partial z} \right) + \left(\frac{\partial^2 v_x}{\partial x^2} + \frac{\partial^2 v_x}{\partial y^2} + \frac{\partial^2 v_x}{\partial z^2} \right) \right) \qquad (2.47)$$

$$= -\frac{\partial p}{\partial x} + \eta \frac{\partial}{\partial x}(\nabla \cdot v) + \eta \nabla^2 v_x \qquad (2.48)$$

From the incompressibility condition, $\nabla \cdot v = 0$, Equation (2.48) becomes

$$div\sigma_{xx} = -\frac{\partial p}{\partial x} + \eta \nabla^2 v_x \qquad (2.49)$$

for the other two components of $div\sigma$, the expressions are analogy. In vector notation, this can be written as:

$$div\sigma = -\nabla p + \eta \nabla^2 v \qquad (2.50)$$

inserting these results into the equation of motion, we obtain Navier-Stokes equation

$$\frac{\partial v}{\partial t} + (v \cdot \nabla)v = g - \nabla p + \eta \nabla^2 v \qquad (2.51)$$

which has explicit non-linearity through the convected derivative term. Note that Equation (2.51) will be used intensively in Chapter 3

2.2.8 Material properties

When constructing a model of the injection moulding process it is important to understand the mechanical behavior of the polymeric material used. The viscosity is usually the most important property in polymer processing. There is difficulty in using the above equations for a polymer melt since the viscosity of macromolecular fluids depends on the rate of deformation and is therefore not constant. In order to obtain a simple formulation applicable to polymeric systems, rheologists have employed the *generalized Newtonian* fluid equation. In these types of fluids, the viscous stress tensor in Equation (2.30) is expressed linearly as a function of $\dot{\epsilon}_{ij}$, but the viscosity depends on the temperature, the pressure and the magnitude of the deformation as follows:

$$\sigma_{ij}^v = 2\eta(\bar{\dot{\epsilon}}, T, p)\dot{\epsilon}_i \qquad (2.52)$$

where $\eta(\bar{\dot{\epsilon}}, T, p)$ is the apparent viscosity as shown in Figure 2.4.
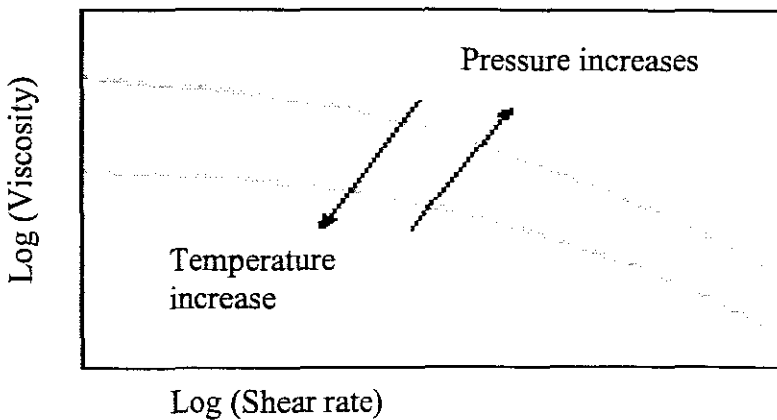
Figure 2.4 The viscosity of polymer melt depends on the shear rate, pressure, and temperature.

In general, the viscosity is a function of temperature, pressure and the magnitude of the rate of deformation $\bar{\dot{\epsilon}}$:

$$\bar{\dot{\epsilon}} = \sqrt{2(\dot{\epsilon}_{ij}\dot{\epsilon}_{ij})} \qquad (2.53)$$

The laws that give the fluid viscosity as a function of pressure and temperature represent an important part of *Rheology*, i.e.,

$$\eta(\bar{\dot{\epsilon}},T,p) = A\,exp\left(\frac{T_a}{T}\right)\bar{\dot{\epsilon}}^{n-1}\,exp(\beta p), \qquad 0 \le n \le 1 \qquad (2.54)$$

In this Equation, the coefficient β varies between $2,3.10^{-8}$ and 6.10^{-8} Pa^{-1} depends on the type of thermoplastic, the temperature T_a can be written in the form $\frac{E_a}{R}$ where R is the constant of gas and E_a the activation energy, which varies between, 3.10^4 and 13.10^4 *J/mole* depending on the type of the polymer used. Finally the coefficient A has an order of 10^2 *PL* (Poiseuille=*Pa.s*); for polyamides, for example equal to $6.4.10^3$ *Pa.s*. For lower shear stress, the viscosity given above becomes infinite. The 5-constant $(\eta,\tau^*,B,T_b,\beta)$ Cross-Exponential Model for incompressible flow and sufficient temperature is given by Mahomed and Kleiber (1998):

$$\eta(\bar{\dot{\epsilon}},T,p) = \frac{\eta_0(T,p)}{1 + \left(\eta_0(T,p)\,\bar{\dot{\epsilon}}\,/\,\tau^*\right)^{1-n}} \qquad (2.55)$$

with

$$\eta_0(T,p) = B\,exp\left(\frac{T_b}{T}\right)exp(\beta p) \qquad (2.56)$$

For the filling stage, the fluid pressure is relatively low and the above equation may be reduced to:

$$\eta_0(T,p) = B\,exp\left(\frac{T_b}{T}\right) \qquad (2.57)$$

the constants B and T_b related to A and T_a by

$$A = B^n\left(\tau^*\right)^{n-1} \text{ and } T_a = nT_b$$

It is clear for this model that for large $\bar{\dot{\epsilon}}$, the viscosity η can become very small, giving rise to a singularity condition. This typically occurs near flow boundaries or where the fluid encounters a sharp bend. Techniques to counter such singular behaviour is the subject of this study, and the particular case of the singular behaviour of Cross-type fluids in Stokes flow will be investigated in the following Chapters.

2.3 Thermodynamic

The mechanical aspects of the deformation cannot separate from the thermal and other changes and have therefore to introduce the concepts of continuum thermodynamics. In the filling phase of injection, thermal effects are small and are often neglected due to the isothermal condition. In this section, a brief description to the energy equation has been given to help future workers in the CAD/CAM project.

2.3.1 State equation and variables

The thermodynamics is an essay to give an important number of properties in a small number of variables, named state variables. Examples of these variables are pressure p, temperature T, density ρ, specific entropy s, internal energy e, specific enthalpy h. A state equation is a relation between many of these variables.

The thermodynamic state of a system is totally determined by two variables independent from the state variables. Example, for the pressure p and the temperature T, the density is given by the state equation:

$$\rho = \rho(p,T) \tag{2.58}$$

If this law is derivable, the differential of ρ is expressed in terms of the differential of p and T,

$$\aleph T = \frac{1}{\rho}\left(\frac{\partial \rho}{\partial p}\right)_T \geq 0 \text{ the compressibility coefficient is isotherm}$$

$$\aleph p = -\frac{1}{\rho}\left(\frac{\partial \rho}{\partial T}\right)_p \geq 0 \text{ the compressibility coefficient is isobar}$$

2.3.2 Energy equation and first principle

For a fluid in local thermodynamic equilibrium, there exists a state variable e where,

$$\frac{D}{Dt}\iiint_\upsilon \left(\frac{1}{2}|v|^2 + e\right)\rho d\upsilon = \iiint_\upsilon \rho f \, d\upsilon + \iint_S [\sigma \times n]v dS - \iint_S q \cdot n dS \tag{2.59}$$

the heat flux q is related to the temperature by *Fourier's* law:

$$q = -k\nabla T \tag{2.60}$$

where k is the thermal conductivity and may be a function of temperature. The local form for the energy equation can be obtained using the notation of the stress tensor σ, and the

equations of dynamic. This equation is valid in the entire fluid domain where the quantities are considered continuous. Here the form

$$\rho \frac{De}{Dt} = -p(\nabla . v) + \eta \, \overline{\dot{\epsilon}}^2 + \nabla \cdot (k\nabla T) \qquad (2.61)$$

Remark: The term $\eta \, \overline{\dot{\epsilon}}^2$ represents the dissipation energy.

2.3.3 Energy equation function of temperature

A simple calculus shows that the energy equation can be expressed in terms of temperature and pressure (see Bird et al (1987)) as follows:

$$\rho C_p \frac{DT}{Dt} = \aleph pT \frac{Dp}{Dt} + \eta \, \overline{\dot{\epsilon}}^2 + \nabla \cdot (k\nabla T) \qquad (2.62)$$

In this equation, the term $\dfrac{Dp}{Dt}$ represents heating by compression, the term $\eta \, \overline{\dot{\epsilon}}^2$ represents the viscous heating and the last terms represent heat diffusion.

2.4   The mould cavities geometry

In the previous sections, the governing equations of the polymer flow are presented. These equations express the conservation of momentum, conservation of mass and the fluid response to the deformation. Now in modelling of injection moulding, the cavities are considered to have shall geometry. This means that the thickness is negligible compared with the other dimension. Examples of plastic components in our daily life to verify the good foundation of this restriction are:
Bumper, computer keyboard, floppy disks... etc.

Consider a process where molten polymer is injected into a planar mould cavity with thickness $2h$ (see Figure (2.5)). Introduce a Cartesian coordinates system such that the flow is confined between $-h < z < h$. The flow will be parallel to the x-y plane in this coordinate system. Introducing some of the assumptions known as *Hele-Shaw assumptions* to simplify the flow. These assumptions are summarised as follows:

- $v_z = 0$, i.e., all flow is parallel to the x-y plane. The viscosity force in the z direction is also neglected.
- The flow in such that viscous forces and pressure differences are dominating in the momentum equations, i.e., inertia and body forces are ignored.
- Derivatives of v_x and v_y with respect to z are usually bigger than the derivatives with respect to x and y. This is due to the geometrical proportions and non-slip conditions

for $z = \pm h$. This is allows us to ignore the contributions of $\dfrac{\partial v_x}{\partial x}, \dfrac{\partial v_x}{\partial y}, \dfrac{\partial v_y}{\partial x}, \dfrac{\partial v_y}{\partial y}$ to

$\dot{\in}_{ij}$.

Using these assumptions in the expressions for the rate of the strain tensor, the following expression for the rate of strain tensor and the shear rate is obtained

$$\dot{\in}_{ij} = \frac{1}{2}\begin{bmatrix} 0 & 0 & \dfrac{\partial v_x}{\partial z} \\ 0 & 0 & \dfrac{\partial v_y}{\partial z} \\ \dfrac{\partial v_x}{\partial z} & \dfrac{\partial v_y}{\partial z} & 0 \end{bmatrix} \Rightarrow \bar{\dot{\in}} = \sqrt{2\,\dot{\in}_{ij}:\dot{\in}_{ij}} = \sqrt{\left(\dfrac{\partial v_x}{\partial z}\right)^2 + \left(\dfrac{\partial v_y}{\partial z}\right)^2} \qquad (2.63)$$
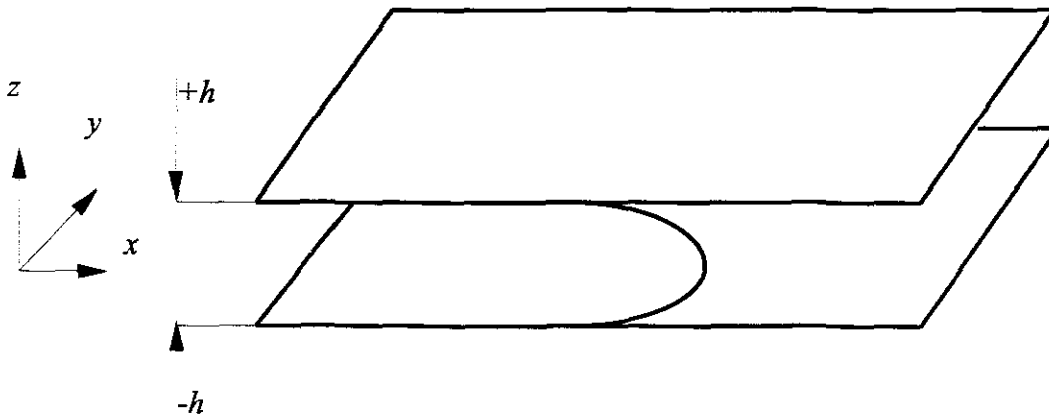
Figure 2.5 Representation of the Hele-Shaw flow

The pressure is constant along the thickness of the cavity, and fluid velocity is proportional to the pressure gradient: there exists a coefficient $S(x,t,p)$ where:

$$v(x,t) = -S(x,t,p)\nabla p \qquad (2.64)$$

on all points x in the cavity and for all time t, for more details (see Appendix A).

The equations for conservation of mass and momentum are also simplified by these assumptions. They can be written in the following form:

$$\frac{\partial v_x}{\partial x} + \frac{\partial v_y}{\partial y} = 0 \qquad (2.65)$$

$$\nabla p = div\left(\sigma_{ij}^v\right) \qquad (2.66)$$

The analysis of the Hele-Shaw flow for generalized Newtonian fluid was made by Hieber and Shen (1980) and extended by Hassager and Laurdissien in (1988) to the power law fluids.

2.5 Restrictions for our study

The main disadvantage of the Hele-Shaw flow model in injection moulding, its gives rise to errors in the entrance region and cannot capture the details of the flow field whenever out of plane flows are present such as in the vicinity of the flow front Kamal et al. (1988); Friedrichs and Guceri (1993). In an attempt to develop a model to represent the entry regions and the front regions, some assumptions, less restrictive than those for Hele-Shaw flow, have to be used in regard to the geometry of the cavity and the fluid.

In his study, Mahomed (1998) has used the Stokes model to simulate generalized Newtonian flow. The assumptions that were made are listed below:
- The fluid motion is laminar
- The unsteady state terms in the momentum and continuity equations are neglected in view of the comparatively long duration of the flow.
- The body forces are negligible.
- There are no velocity components in the z direction.

From the Navier-Stokes equation (2.49) and using the above assumptions then:

$$-\nabla p + \eta \nabla^2 v = 0 \qquad\qquad (2.67)$$

This model is called the Stokes flow model, and is composed only from the continuity equation and the momentum equation to be solved for the two components of the velocities and pressure. The energy equation is not considered here, so there is no unknown temperature. It should also be noted that the motion and position of the free surface is not considered in this study.   The occurrence of the singularity of this model will be investigated in the next Chapter.

2.6 Initial and Boundary conditions

In order to completely specify the mathematical model it is necessary to define the initial conditions as well as the conditions at the boundary of the flow domain. Mathematically there are two types of boundary conditions, namely Dirichlet (fixed value) conditions or Von Neuman (fixed gradient) conditions. However, in a complicated mixture of elliptic, parabolic and hyperbolic behaviours this oversimplified mathematical classification is of little use. It is more appropriate to define the conditions.
The equations of continuity and momentum previously derived are quite general. For the application to injection moulding, specific boundary conditions are needed. These boundary conditions in terms of velocity and its variations. Boundary conditions related to energy and temperature will not be needed here.

2.6.1 Boundary condition at the inlet

An inlet boundary is a boundary where the polymer has specified velocity distribution. The pressure at the inlet is unknown and a boundary value is extrapolated from the interior of the flow domain. However, if the gradient of the pressure at the inlet is small, it is sufficient to apply a zero gradient boundary conditions.

$$v = v_e$$ (2.68)

2.6.2 Boundary condition on the free surface

At the free surface both normal and tangential stresses vanish. This leads to

$$(\sigma \cdot n) = 0$$
$$(\sigma \cdot t) = 0$$ (2.69)

2.6.3 Boundary condition on the rigid boundaries (walls)

At the wall, the fluid takes the velocity of the wall, which means no slip of the fluid at the wall. This condition is called the zero slip condition.

$$v = 0$$ (2.70)
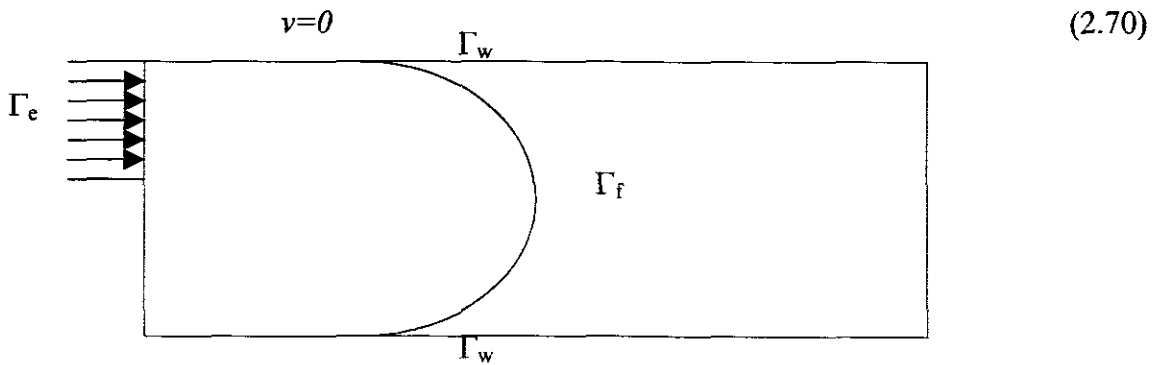
Figure 2.6 Boundary conditions

2.7 Closure

In these sections, the equations that reflect the mechanical aspect of injection molding, and define clearly the variable to be used, are derived. In most cases the model to be used can not solved analytically and therefore a numerical methods have to be applied. The next Chapter concerns the investigation of the occurrence of the singularity in this mathematical model.

CHAPTER 3

STOKES FLOW AND SINGULARITY ANALYSIS

3.1 Introduction

In this Chapter, the occurrence of the singularities in the Stokes model is investigated. The analysis is based on stream function concepts. The stream function gives rise to a partial differential equation called the *biharmonic equation*. This equation is a Laplace equation and shows the boundary value problem. Many papers have been published to deal with singularities in the Laplace equation (see for instance (Wigley, 1988; Olson et al., 1991; Gergiou et al., 1991, 1996). The solution of the Laplace equation in polar coordinates with proper boundary conditions gives the real flow field behaviour around the corner of the cavities for the velocity, pressure and stress.

In this Chapter, however, the analysis of Micheal (1958) and Moffatt (1964) was followed to give the complete picture of the asymptotic behaviour of the flow field near the singular point. Note that this analysis will be used in Chapter 5 to derive the shape functions for the velocity field.

3.2 Stream function

In Chapter 2, the Stokes flow model has been presented to simulate the behaviour of *generalized Non-Newtonian* flow in injection moulding. The exact solution of this model is obtained using the stream function concepts. In this model, Only two independent spatial variables are involved. The flow is considered to be creeping e,.i $Re \ll 1$ where Re is the Reynolds number, and the inertia forces are negligible (Isayev, 1987). Equation (2.16) and Equation (2.66) rewritten here,

$$\nabla \cdot v = 0 \tag{3.1}$$

$$-\nabla p + \eta \nabla^2 v = 0 \tag{3.2}$$

The solution of these equations will be in special domain in the cavity, where the geometry of the cavity is suddenly changed. Geometrically, this domain represents a re-entrant corner and is defined by:

$$0 < r < R, \quad 0 < \theta < \frac{3\pi}{2}$$

It is not understood how the solution of Equation (3.1) and Equation (3.2) behave at this domain.

The velocity v can be eliminated form the Equation (3.2) by taking the divergence of the entire equation, the result is:

$$\nabla^2 p = 0 \qquad (3.3)$$

Which is Laplace's equation and is elliptic. Thus the pressure shows pure boundary value behaviour.

The continuity Equation (3.1) can be satisfied by taking the velocity components in terms of the stream function φ such as:

$$v_x = \frac{\partial \varphi}{\partial y} \quad v_y = -\frac{\partial \varphi}{\partial x} \qquad (3.4)$$

The curves $\varphi = constant$ represent streamlines since $v \cdot \nabla \varphi = 0$ and $\nabla \varphi$ will be normal to the surface $\varphi = constant$. The x and y components of Equation (3.2) take the form:

$$\frac{\partial p}{\partial x} = -\frac{\partial}{\partial y} \eta \left(\nabla^2 \varphi \right) \qquad (3.5)$$

$$\frac{\partial p}{\partial y} = \frac{\partial}{\partial x} \eta \left(\nabla^2 \varphi \right) \qquad (3.6)$$

The variable p can be eliminated to give:

$$\nabla^2 \left(\nabla^2 \varphi \right) = \nabla^4 \varphi = 0 \qquad (3.7)$$

which is a fourth-order differential linear equation with the stream function only the variable. This equation is known as the *biharmonic equation in two dimensions*. It happens that this equation is governing relation in the theory of two dimensional elasticity, so that a large number of practical solutions already exist from solid mechanics (Tomoshenko and Goodier, 1970). These can be applied to our types of flow. The Equation (3.7) can be written as:

$$\frac{\partial^4 \varphi}{\partial y^4} + 2 \frac{\partial^4 \varphi}{\partial x^2 \partial y^2} + \frac{\partial^4 \varphi}{\partial x^4} = 0 \qquad (3.8)$$

It is usual to use the operator ∇^2, defined as:

$$\nabla^2 = \frac{\partial^2}{\partial x^2} + \frac{\partial^2}{\partial y^2} \qquad (3.9)$$

so that

$$\nabla^2 \varphi = \frac{\partial^2 \varphi}{\partial x^2} + \frac{\partial^2 \varphi}{\partial y^2} \qquad (3.10)$$

And operating a second time gives:

$$\nabla^4 \varphi = \left(\frac{\partial^2}{\partial x^2} + \frac{\partial^2}{\partial y^2} \right) \nabla^2 \varphi \qquad (3.11)$$

The solution of Equation (3.11) would correctly simulate all singular flow problems that include flow around corner, the die-swell, the stick slip and the driven cavity problems, which are often used as model problems for various numerical methods proposed for Newtonian or non-Newtonian flow. The particular form of φ is determined by the boundary conditions of the problem considered. The solution here, however, will not conducted in Cartesian coordinates, but in terms of polar coordinates, since this system is more convenient to use.

3.3   Polar Coordinates

It is convenient to formulate the flow around the corner using the polar coordinates. In this section, the detail of the transformation between the Cartesian and the polar coordinate is presented. The coordinates are related by:

$$x^2 + y^2 = r^2 \quad \text{and} \quad \tan \theta = \frac{y}{x}$$

The derivative relationships in the two coordinate systems are:

$$\frac{\partial r}{\partial x} = \frac{x}{r} = \cos \theta \qquad\qquad \frac{\partial r}{\partial y} = \frac{y}{r} = \sin \theta$$

$$\frac{\partial \theta}{\partial x} = -\frac{y}{r^2} = -\frac{\sin \theta}{r} \qquad\qquad \frac{\partial \theta}{\partial y} = \frac{x}{r^2} = \frac{\cos \theta}{r}$$

Now the derivatives of φ with respect to y may be written as:

$$\frac{\partial \varphi}{\partial y} = \frac{\partial \varphi}{\partial \theta} \frac{\partial \theta}{\partial y} + \frac{\partial \varphi}{\partial r} \frac{\partial r}{\partial y} \qquad (3.12)$$

$$\frac{\partial \varphi}{\partial y} = \frac{r \cos \theta}{r} \frac{\partial \varphi}{\partial \theta} + \sin \theta \frac{\partial \varphi}{\partial r} \qquad (3.13)$$

Differentiating a second time and substituting for the derivatives with respect to x and y gives:

$$\frac{\partial^2 \varphi}{\partial y^2} = \sin^2 \theta \frac{\partial^2 \varphi}{\partial r^2} + \cos^2 \theta \left(\frac{1}{r} \frac{\partial \varphi}{\partial r} + \frac{1}{r^2} \frac{\partial^2 \varphi}{\partial \theta^2} \right) + 2 \sin \theta \cos \theta \frac{\partial}{\partial r} \left(\frac{1}{r} \frac{\partial \varphi}{\partial \theta} \right) \qquad (3.14)$$

Similarly

$$\frac{\partial^2 \varphi}{\partial x^2} = \cos^2 \theta \frac{\partial^2 \varphi}{\partial r^2} + \sin^2 \theta \left(\frac{1}{r} \frac{\partial \varphi}{\partial r} + \frac{1}{r^2} \frac{\partial^2 \varphi}{\partial \theta^2} \right) - 2 \sin \theta \cos \theta \frac{\partial}{\partial r} \left(\frac{1}{r} \frac{\partial \varphi}{\partial \theta} \right) \qquad (3.15)$$

Adding Equation (3.14) and Equation (3.15) gives:

$$\nabla^2 \varphi = \frac{\partial^2 \varphi}{\partial x^2} + \frac{\partial^2 \varphi}{\partial y^2}$$

$$= \frac{\partial^2 \varphi}{\partial r^2} + \frac{1}{r}\frac{\partial \varphi}{\partial r} + \frac{1}{r^2}\frac{\partial^2 \varphi}{\partial \theta^2}$$

Thus the basic equation may be transformed to:

$$\nabla^4 \varphi = \left(\frac{\partial^2}{\partial r^2} + \frac{1}{r}\frac{\partial}{\partial r} + \frac{1}{r^2}\frac{\partial^2}{\partial \theta^2}\right)\left(\frac{\partial^2 \varphi}{\partial r^2} + \frac{1}{r}\frac{\partial \varphi}{\partial r} + \frac{1}{r^2}\frac{\partial^2 \varphi}{\partial \theta^2}\right) = 0 \qquad (3.16)$$

3.4 Stress analysis around the corner

In polar coordinate the analysis of the corner admits separable solution with bonded velocities at the corner. *Local solutions,* those satisfy all local boundary conditions, and *partial local solutions,* those, that when free surfaces are present, satisfy all local boundary conditions with the exception of the normal stress boundary conditions (Anderson and Davis, 1993).

Figure (3.1) shows the stress components in polar coordinates as used in the basic derivation. The various stress components may be derived using the following transformation:

$$\begin{bmatrix} \sigma_{rr} & \sigma_{r\theta} \\ \sigma_{r\theta} & \sigma_{\theta\theta} \end{bmatrix} = \begin{bmatrix} \cos\theta & \sin\theta \\ -\sin\theta & \cos\theta \end{bmatrix}\begin{bmatrix} \sigma_{xx} & \sigma_{xy} \\ \sigma_{xy} & \sigma_{yy} \end{bmatrix}\begin{bmatrix} \cos\theta & -\sin\theta \\ \sin\theta & \cos\theta \end{bmatrix} \qquad (3.17)$$
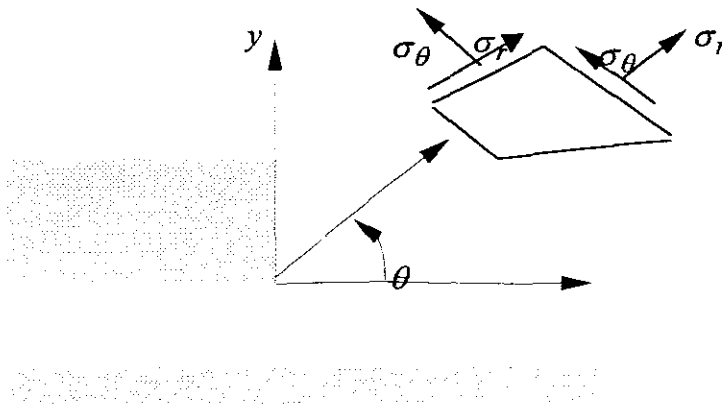
Figure 3.1 Stress components in polar coordinates

However, this study is concentrated on the Non-Newtonian flow in thin two-dimensional L-shaped cavities as shown in Figure (3.2). It is very important to show that the solution of Equation (3.16) which is an elliptic differential equation, will have singular components in the neighborhoods of each of the vertices A, B, C, D, and

_O_ with the worst singularity occurring at _O_, the vertex with the largest interior angle (Babuska and Miller 1994).
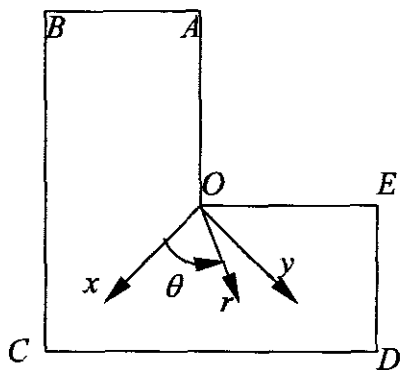
Figure 3.2 The L-shaped cavity

If the cavity has three dimensional, the problem will be more complex (Babuska and Miller 1994).

3.5 Formulation

The formulation of the problem is started by discussing the definition of the domain where the stream function has singularity (see for instance Yosibash, 1997; Szabo and Yosibash, 1996; Yosibash and Szabo, 1995). Consider a domain around the point _O_ as in Figure 3.3. Let $\partial\Omega = \cup_i \Gamma_i$ where Γ_i are analytic simple arcs curves called edges. These edges intersect at point called vertices to form a corner. The straight boundaries, which intersect in the singular point O, will be denoted by Γ_1 and Γ_2. On Γ_1 and Γ_2 the boundary conditions are assumed to be homogenous. In the remaining boundaries, $\varphi{=}0$ on Γ_i^D, $\varphi_n = 0$ on $\partial\Omega{-}\Gamma_i^D$ where _n_ denotes the outward normal vector to the boundary.
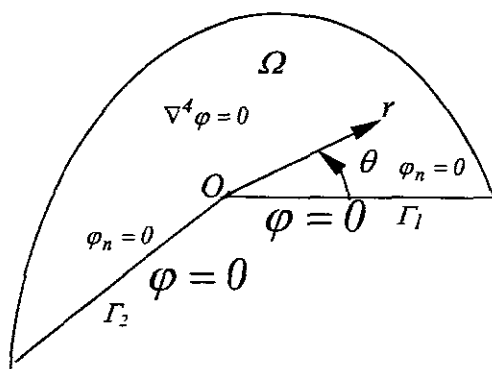
Figure 3.3 Domain with re-entrant corner and notation

The problem therefore becomes that of finding φ the solution satisfies the biharmonic equation given in Equation (3.16), which has the general solution given by Tomoshenko and Goodier (1970):

$$\varphi = C_0 r^2 + \left(C_1 + C_2 r^2 \right) \ln r + \left(C_3 + C_4 r^2 \right) \theta$$
$$+ \left[\left(C_5 \sin\theta + C_6 \cos\theta \right) r\theta + C_7 r \ln r \right] \tag{3.18}$$
$$+ \sum r^\lambda F_\lambda (\theta)$$

3.6 Asymptotic analysis of the singularity

The analysis of Micheal (1958) and Moffat (1964) gives the complete picture of the asymptotic behaviour of a fluid flow near a corner. This analysis is the cornerstone to approach the Non-Newtonian fluids. In this section, the detail of this approach is given. Micheal(1958) and Moffatt (1964) showed that the expression for the stream function in Equation (3.18) after neglecting the first four terms can be written as:

$$\varphi = r^\lambda F_\lambda (\theta) \tag{3.19}$$

Where λ is any number, real or complex, which may conveniently be called the exponent of the corresponding solution. Substitution of Equation (3.19) into Equation (3.16) yields an ordinary differential equation for $F_\lambda(\theta)$ as;

$$\left[\frac{d^2}{d\theta^2} + \lambda^2 \right] \left[\frac{d^2}{d\theta^2} + (\lambda - 2)^2 \right] F_\lambda = 0 \tag{3.20}$$

Equation (3.20) has the solution of the form

$$F_\lambda(\theta) = A \cos\lambda\theta + B \sin\lambda\theta + C \cos(\lambda - 2)\theta + D \sin(\lambda - 2)\theta \tag{3.21}$$

Here, A, *B, C,* and *D* are real constants to be determined, along with the exponent λ.

3.7 Boundary conditions

Boundary conditions along the two boundaries determine the constants in Equation (3.21) and may also impose certain restrictions on the values of λ and the corner angle α. In Figure 3.4, along a rigid surface, both velocity components must vanish. Along a planar free surface, the shear and normal stresses must vanish. The azimuthal (tangential) component of the velocity must vanish on the free surface. All the boundary conditions can be summarised as follows:

on the rigid boundary

$$\varphi = 0, \quad\quad v_\theta = 0 \text{ on } \theta = \pm\alpha \tag{3.22a}$$
$$v_r = 0 \text{ on } \theta = \pm\alpha \tag{3.22b}$$

on the free surface

$$\sigma_{r\theta} = 0 \qquad \text{on } \theta = 0 \qquad\qquad\qquad (3.23a)$$

$$\sigma_{\theta\theta} = 0 \qquad \text{on } \theta = 0 \qquad\qquad\qquad (3.23b)$$

The general expressions for $\sigma_{r\theta}$ and $\sigma_{\theta\theta}$ along $\theta = 0$ can be simplified, when use

is made of conditions $v_\theta = 0$ and $\dfrac{\partial v_\theta}{\partial r} = 0$ along $\theta = \pm\alpha$

The simplified expressions, in physical component form are given by Huilgol, (1977):

$$\sigma_{r\theta} = \eta A\langle r\theta\rangle$$

$$\sigma_{\theta\theta} = -p + \eta A\langle\theta\theta\rangle \qquad\qquad\qquad (3.24)$$

Here along $\theta = 0$

$$A\langle r\theta\rangle = r^{\lambda-2}F_\lambda''(\alpha)$$

$$A\langle\theta\theta\rangle = -2\lambda r^{\lambda-2}F_\lambda'(\alpha) \qquad\qquad\qquad (3.25)$$
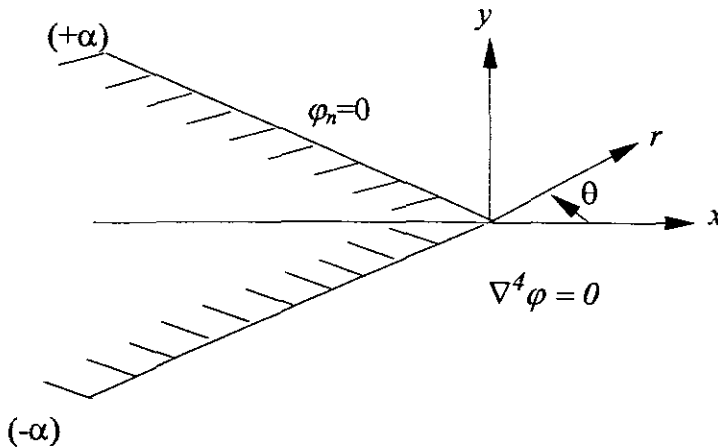
Figure 3.4 Corner boundary conditions

In Equation (3.24), p is the pressure and η the coefficient of viscosity.

Clearly to get a non-zero solution that satisfies the above conditions, which are homogeneous in the constants, A, B, C, D, this required satisfying two conditions between the coefficients, *i.e.* between α and the index λ. These conditions will thus serve to find pairs of values (α, λ) each of which will give a possible mode of separation. Imposing the non-slip boundary condition $v_r = v_\theta = 0$ At $\theta = \pm\alpha$ This

means that $F_\lambda(\pm\alpha) = F'_\lambda(\pm\alpha) = 0$. From $F_\lambda(\theta)$, these become four equations involving the constants A, B, C and D.

By simple additions and subtractions there are easily seen to be equivalent to:

$$A\cos\lambda\alpha + C\cos(\lambda-2)\alpha = 0 \tag{3.26a}$$
$$A\lambda\sin\lambda\alpha + C(\lambda-2)\sin(\lambda-2)\alpha = 0 \tag{3.26b}$$
$$B\sin\lambda\alpha + D\sin(\lambda-2)\alpha = 0 \tag{3.26c}$$
$$B\lambda\cos\lambda\alpha + D(\lambda-2)\cos(\lambda-2)\alpha = 0 \tag{3.26d}$$

Each pair of equations is homogeneous, and therefore if the index λ is chosen arbitrarily, the four constants will be zero.

3.8 Eigenfunctions solution

3.8.1 Antisymmetrical Flow

Figure (3.5) shows this type of the flow. In this case the values of λ are odd and the corresponding eingenfunction is also odd.
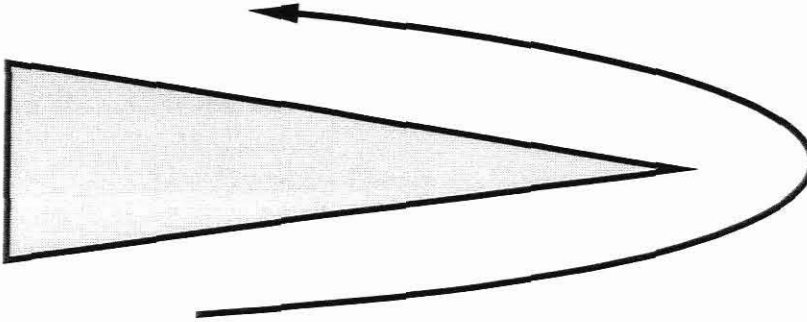
Figure 3.5 Antisymmetrical flow

The both velocity components vanish on $\theta = \pm\alpha$ provided $F_\lambda(\pm\alpha) = F'_\lambda(\pm\alpha) = 0$ so that B, $D = 0$

$$F_\lambda(\theta) = A\cos\lambda\theta + C\cos(\lambda-2)\theta \tag{3.27}$$

and $F(\alpha)$ given by

$$A\cos\lambda\alpha + C\cos(\lambda-2)\alpha = 0 \tag{3.28}$$

and $F'_\lambda(\alpha)$ is given by

$$A\lambda\sin\lambda\alpha + C(\lambda-2)\sin(\lambda-2)\alpha = 0 \tag{3.29}$$

The values of A and C in Equation (3.28) and Equation (3.29) can be non-zero if the determinant of the coefficient vanishes, i.e., if

$$(\lambda-2)\sin(\lambda-2)\alpha\cos\lambda\alpha - \lambda\sin\lambda\alpha\cos(\lambda-2)\alpha = 0 \tag{3.30}$$

Let $\mu = \lambda - 1$, Equation (3.30) reduces to the form:

$$sin\, 2\mu\alpha = -\mu\, sin\, 2\alpha \qquad (3.31)$$

3.8.2 Symmetrical flow

For this type of flow $F_\lambda(\theta)$ is odd, the both velocity components vanish on $\theta = \pm\alpha$ provided $F_\lambda(\pm\alpha) = F'_\lambda(\pm\alpha) = 0$. In this case $A=C=0$ and $F_\lambda(\theta)$ is given by:

$$F_\lambda(\theta) = B\, sin\, \lambda\theta + D\, sin(\lambda - 2)\theta \qquad (3.32)$$

and $F_\lambda(\alpha)$ given by:

$$B\, sin\, \lambda\alpha + D\, sin(\lambda - 2)\alpha = 0 \qquad (3.33)$$

and $F'_\lambda(\alpha)$ is given by:

$$B\lambda\, cos\, \lambda\alpha + D(\lambda - 2)cos(\lambda - 2)\alpha = 0 \qquad (3.34)$$

The values of B, D in Equation (3.33) and Equation (3.34) can be zero if the determinant of the coefficient vanishes, i.e., if

$$(\lambda - 2)cos(\lambda - 2)\alpha\, sin\, \lambda\alpha - \lambda\, cos\, \lambda\alpha\, sin(\lambda - 2)\alpha \qquad (3.35)$$

This reduce

$$sin\, 2\mu\alpha = +\mu\, sin\, 2\alpha \qquad (3.36)$$

Where $\mu = \lambda - 1$
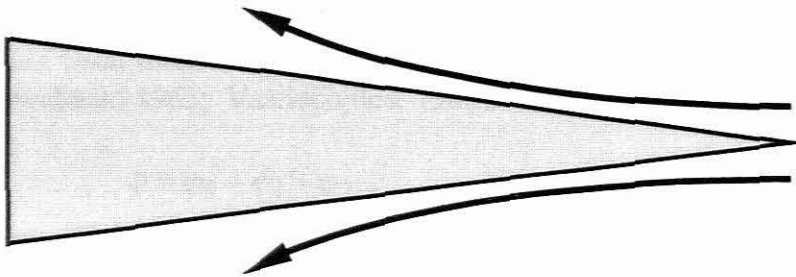
Figure 3.6 Symmetrical flow

The characteristic Equations (3.31) and (3.36) are solved numerically using iterative methods. For a given separation angle α Equations (3.31) and (3.36) give the

distribution of the eigenvalues μ. In this study, the cavity has a re-entrant corner with an angle $\alpha = \dfrac{3\pi}{4}$.

The first eigenvalues from Equations (3.31) and (3.36) ordered by increasing real part, for antisymmetrical and symmetrical flow are listed in Table 3.1 see Georgiou et al., (1990).

Antisymmetric	Symmetric
0,54448	0,90853
$1,62926 \pm 0,23125i$	$2,30133 \pm 0,31584i$
$2,97184 \pm 0,37393i$	$3,64148 \pm 0,41879i$
$4,31038 \pm 0,45549i$	$4,97890 \pm 0,48663i$
$5,64711 \pm 0,51368i$	$6,31508 \pm 0,53763i$
$6,98287 \pm 0,55911i$	$7,65051 \pm 0,57859i$
$6,31803 \pm 0,59642i$	$8,98546 \pm 0,61285i$

Table 3-1 Eingenvalue for asymptotic solution

It is worthwhile to note the following:

- Although $\mu = 1$ is a solution to (3.31) and (3.36), it is not an eigenvalue for this problem.
- There is an infinite number of eigenvalues for both sets of solutions.
- There is only one real eigenvalue for each solution and it is less than unity.
- The real parts of the complex eigenvalues are always greater than unity.

The velocities and stresses are obtained by differentiating Equation (3.19). Since $Re(\mu) > 0$, the velocities and the integrated stresses, which are $O(r^\lambda)$, approach to zero at the corner $(r \to 0)$. The stresses at the corner, however, are $O(r^{\mu-1})$ and become more singular as α increases.

3.9 Higher order solutions

In the case of the two-dimensional Navier-Stokes equations in the plane, the singularities has been treated by expanding the stream functions φ in the form (Lugt and Schwiderski 1965; Vasilopoulos, 1988).

$$\varphi = \varphi_0 + \varphi_1 + \varphi_2 \ldots \tag{3.36}$$

where φ_0 is the Stokes solution. The term φ_1 corrects for the mis-match in the inertial terms when φ_0 substituted into the full equations, while φ_2 corrects for the mis-match for $\varphi_0 + \varphi_1$ and so on. They assume that in the Stokes regime the stream function can be expanded in a series of the form

$$\varphi_0 = \sum_{n=1}^{\infty} A_n r^{\lambda_n} F_{\lambda_n}(\theta) \tag{3.37}$$

where the λ_n are suitably chosen and ordered so that

$$1 \langle Re(\lambda_1) \rangle \langle Re(\lambda_2) \rangle ... \tag{3.38}$$

The A_n are constants. The general flow is mixture symmetrical and antisymmetrical flow but it is convenient and permissible in view of the linearity of the Stokes equation to consider the types separately.

Taking the antisymetrical case Equation (3.27) is satisfied, and from Equation (3.28):

$$\frac{C}{A} = -\frac{\cos \lambda \alpha}{\cos(\lambda - 2)\alpha} \tag{3.39}$$

The stream function (3.37) becomes:

$$\varphi_{01} = r^{\lambda_1} A \left[\frac{\cos(\lambda_1 - 2)\alpha \cos \lambda_1 \theta - \cos \lambda_1 \alpha \cos(\lambda_1 - 2)\theta}{\cos(\lambda_1 - 2)\alpha} \right] \tag{3.40}$$

Taking the converse symmetrical case Equation (3.32) is satisfied, and from Equation (3.33):

$$\frac{D}{B} = -\frac{\sin \lambda \alpha}{\sin(\lambda - 2)\alpha} \tag{3.41}$$

The stream function becomes

$$\varphi_{02} = r^{\lambda_2} B \left[\frac{\sin(\lambda_2 - 2)\alpha \sin \lambda_2 \theta - \sin \lambda_2 \alpha \cos(\lambda_2 - 2)\theta}{\sin(\lambda_2 - 2)\alpha} \right] \tag{3.42}$$

but the stream function is given by:

$$\varphi_0 = \varphi_{01} + \varphi_{02} \tag{3.43}$$

Finally, the stream function takes the form

$$\begin{aligned} = r^{\lambda_1} A &\left[\frac{\cos(\lambda_1 - 2)\alpha \cos \lambda_1 \theta - \cos \lambda_1 \alpha \cos(\lambda_1 - 2)\theta}{\cos(\lambda_1 - 2)\alpha} \right] \\ + r^{\lambda_2} B &\left[\frac{\sin(\lambda_2 - 2)\alpha \sin \lambda_2 \theta - \sin \lambda_2 \alpha \sin(\lambda_2 - 2)\theta}{\sin(\lambda_2 - 2)\alpha} \right] \end{aligned} \tag{3.44}$$

$$\varphi_0 = r^{\lambda_1} F_{\lambda_1}(\theta) + r^{\lambda_2} F_{\lambda_2}(\theta) \tag{3.45}$$

There is only two real roots which satisfy the characteristic Equation (3.31) and (3.36) when $\alpha = \frac{3\pi}{4}$, these roots are $\lambda_1 = 1.544$ and $\lambda_2 = 1.908$ corresponding to antisymmetric and symmetric flow.

The pressure field in the neighbordhood of the corner is given by Weinbaum, (1968).

$$p = 4(\lambda_1 - 1)A\left(\frac{\cos \lambda_1 \alpha}{\cos(\lambda_1 - 2)\alpha}\right) r^{\lambda_1 - 2} \sin(\lambda_1 - 2)\alpha -$$
$$-4(\lambda_2 - 1)B\left(\frac{\sin \lambda_2 \alpha}{\sin(\lambda_2 - 2)\alpha}\right) r^{\lambda_2 - 2} \cos(\lambda_2 - 2) + c$$

(3.46)

where c is constant.

Finally, the stream function can be written on this form:

$$\varphi = Ar^{1.5445} F_1(\theta) + Br^{1.985} F_2(\theta)$$

(3.47)

giving rise to algebraic singularities in second derivatives, i.e. in pressure and stress, at the corner in both antisymmetric and symmetric parts of the flow. An interesting characteristics of the local asymptotic solution of the corner problem is that both the antisymmetrical and symmetrial solutions contribute one singular term that causes the stresses to become infinite such as:

$$\sigma_{nn} \sim c_1 r^{-0,456} + c_2 r^{-0,091}.$$

(3.48)

Along the bisector $\theta = 0$, the leading order symmetrical contributions to the radial velocity component and the pressure vanish; the contributions to the circumferential velocity component also vanishes. Therefore, at $\theta = 0$ and close to the singular point, the radial velocity component is proportional to $r^{0,544}$ and the circumferential velocity to $r^{0,909}$. The antisymmetrical contribution to the stress also vanishes at $\theta = 0$ and the stress is determined by the less singular symmetrical contribution.

The corner flow problems in this study is considered to be the flow between a rigid boundary and free surface which is equivalent to the die swell problem. Micheal (1958) showed that for zero surface tension on a planar free surface the angle α must be equal to π. Schultz and Gervasio (1990) suggested that either the slope is zero or the mean curvature is infinite. The first two roots for various angles up to $\frac{3\pi}{4}$ are listed in Sturges (1979). However, in this study, it is assumed that the radial form for the local solution is not very different from the solution for $\alpha = \pi$. Therefore, the local solution is the same as that for the die swell or the stick-slip problems. The problem of this study is antisymmetrical flow problem, the symmetrical flow is ignored from the formulation and the stream function for the antisymmtrical flow becomes

$$\varphi = r^{\lambda+1} A\left[cos(\lambda+1)\theta - cos(\lambda-1)\theta\right] \text{ for } \lambda = \tfrac{1}{2}, \tfrac{3}{2}, \tfrac{5}{2}, \dots \tag{3.49}$$

The asymptotic behaviour of stream function, velocity, pressure and stress simply:

$$\varphi \sim r^{\lambda+1}, \quad v \sim r^{\lambda}, \quad p, \ \sigma_{ij} \sim r^{\lambda-1}$$

so the most singular behaviour of the velocity and stress components are

$$v_i \sim r^{0.54448}, \sigma_{ij} \sim r^{-0.454}$$

there are two important consequences of these results. Although the stress field is singular at the corner, i.e. $\sigma_{ij} \rightarrow \infty$ as the force F exerted by the fluid on the boundary is finite. This fact is verified by computing

$$F = \iint_S \sigma_{ij} dS \tag{3.50}$$

where n is the unite normal pointing into the fluid and noting that the integral is finite as long as $\lambda + 1 > 1$.

The local solution will used to construct the singular element that will be discussed in Chapter 5. Note that the singular elements require only the knowledge of the radial form of the local solution Georgiou et al, (1990).

3.10 Closure

In this Chapter the local analysis of the stress singularity due to the abrupt change in the geometry of the cavities has been discussed. The analysis is carried out using the stream function concept, the polar co-ordinate is used to solve the biharmonic elliptic partial differential equation. The solution is based on an idea used to solve solid mechanics problems (fracture). The goal of the solution is to find how the stress and the velocity behave. This analysis will be used in Chapter 5 to derive the shape functions for the singular element.

CHAPTER 4

THE FINITE ELEMENT METHOD FORMULATION

4.1 Introduction

The conservation laws described in Chapter 2 results in partial differential equations (PDE) which are the continuity and momentum equation. The analytic or the exact solution of these equations is impossible due to the complexity of the boundary conditions as well as the boundary of the cavities, which is irregular. While insight has been gained from many analytic analyses, the approximations is necessary to obtain a solution often limit the applicability of the solution to generalities or qualitative assessment. For a realistic, detailed study a numerical method must introduced to explains the necessary transformations of the partial differential equations (PDE) to discrete formulation of the problem, that can be finally be solved numerically.

In this Chapter, one of the most power full methods to deal with these types of problems has been introduced. This method is called the finite element method (FEM). Through this Chapter all the steps of this method are discussed. In this study, also a special finite element method have to be implement, this issue will be discussed in detail in Chapter 5.

4.2 Weak variational formulation

The first step that must be undertaken in use of the finite element method is to write the variational formulation of the problem. Equation such as (2.16) and (2.32) are called the strong or classical formulation of the problem. These differential equations must be satisfied at every point within the domain of the flow. Solution for this type of formulation are often impossible because of irregularities and discontinuities in the data describing the problem. Hence, it is necessarily to look for a ``weaker" variational formulation of the problem. That will allow for irregularities in the data.

Here the formulation is based on the *Galerkin's weighted residual* approach. In this approach the basic equation is *weighted* with appropriate discrete weighting functions and the resulting equation integrated over the region of interest is equal to zero.

$$\int_\Omega (weighting\ function) \times (differential\ equation) d\Omega = 0 \qquad (4.1)$$

The weighted function in this study is the velocity and the differential equation is the momentum equation.

Let $L^2(\Omega)$ the Hilbert space of square-integrable functions, and $H^1(\Omega)$ the Sobolev space of functions which are square integrable up to its first derivative. We denote by $U \subset H^1(\Omega)$ the space of admissible velocities, defined by:

$$U = \left\{ u = (u_1, u_2) : u_1, u_2 \in H^1(\Omega), u = 0 \text{ on } \Gamma_e \cup \Gamma_w \right.$$

That is the weighting functions u satisfy the essential boundary conditions. To formulate the weighted residual statement, we approximate the solution by taking the product of momentum Equation (2.32) by the weighting function u, and integrating over the domain.

It is important to note that, the notation employed in this section is very powerful, yet very simple. The convention is used whereby ANY repeated subscript is assumed to imply a summation over its appropriate range (i and j over coordinates x and y), and k and l over 1 to 8 for a 2-D 4-node quadrilateral element. When a comma appears in a subscript list, this implies partial differentiation with respect to appropriate coordinate. Thus $v_{i,i}$ has an implied summation over the coordinates, and represent $\partial v_x / \partial x + \partial v_y / \partial y$. Using this notation the momentum equation can be written as:

$$\left(\delta_{ij} P + 2\eta \, \dot{\epsilon}_{ij} \right)_{,j} = 0 \tag{4.2}$$

Doing the variational and substituting for $\dot{\epsilon}_i$, the weighted residual form of Equation (4.2) is then:

$$\iint_{\Omega} u_i \left\{ \delta_{ij} P + \eta \left(v_{i,j} + v_{ji} \right) \right\}_{,j} d\Omega = 0 \tag{4.3}$$

We have the vector identity:

$$\left[u_i \left\{ \delta_{ij} P + \eta \left(v_{i,j} + v_{ji} \right) \right\} \right]_{,j} =$$
$$u_{i,j} \left\{ \delta_{ij} P + \eta \left(v_{i,j} + v_{ji} \right) \right\} + u_i \left\{ \delta_{ij} P + \eta \left(vv_{i,j} + v_{ji} \right) \right\}_{,j} \tag{4.4}$$

The Equation (4.4) can be used to expand the integral Equation (4.3) above, as well as the fact that the term in the integral can be simplified by the following:

$$\left(u_i \delta_{ij} P \right)_{,j} = u_{i,j} \delta_{ij} P = u_{i,i} P \tag{4.5}$$

and we obtain

$$\iint_{\Omega} \left\{ u_{i,i} P + u_{i,j} \eta \left(v_{i,j} + v_{ji} \right) \right\} d\Omega = \iint_{\Omega} u_i \left\{ \delta_{ij} P + \eta \left(v_{i,j} + v_{ji} \right) \right\}_{,j} d\Omega \tag{4.6}$$

The right hand side is an surface integral of a divergence, and so can be converted to line integral of the normal over the appropriate portion of the boundary. The above equation becomes:

$$\iint_{\Omega} \{ u_{i,i}P + u_{i,j}\eta(v_{i,j}+v_{ji}) \} d\Omega = \int_{\Gamma} u_i \sigma n_i d\Gamma \tag{4.7}$$

where

$$\sigma n_i = \{ \delta_{ij}P + \eta(v_{i,j}+v_{ji}) \} n \tag{4.8}$$

is the normal stress on the surface.

The normal stress on the surface can be neglected due the boundary conditions that made in Chapter 2, the variational formulation of the momentum equation becomes:

$$\iint_{\Omega} \{ u_{i,i}P + u_{i,j}\eta(v_{i,j}+v_{ji}) \} d\Omega = 0 \tag{4.9}$$

but $(v_{i,j}+v_{ji}) = 2\,\dot{\epsilon}_i$

Substituting into equation (4.9) lead to:

$$\iint_{\Omega} \{ u_{i,i}P + u_{i,j}2\eta\,\dot{\epsilon}_{ij} \} d\Omega = 0 \tag{4.10}$$

Separating the terms of Equation (4.10) gives:

$$\iint_{\Omega} u_{i,j}2\eta\,\dot{\epsilon}_{ij}\,d\Omega + \iint_{\Omega} u_{i,i}Pd\Omega \tag{4.11}$$

From the incompressibility condition for polymer melt, the continuity equation using the above notation is given by:

$$\dot{\epsilon}_{ii} = 0 \tag{4.12}$$

integrating $\dot{\epsilon}_{ii}$ over the area

$$\iint_{\Omega} \epsilon_{ii}\,d\Omega = 0 \tag{4.13}$$

and then substituting for $\dot{\epsilon}_{ii}$

$$\iint_{\Omega} v_{i,i} d\Omega = 0 \tag{4.14}$$

Equation (4.11) and Equation (4.14) are the variational form of the problem, it can be apply for the domain as a whole, but it also for particular subdomain, or element. Thus we would have only a set of element equations corresponding to the above, where only Ω and Γ would be changed to Ω^e and Γ^e for element e. To solve (4.11) special variation of the velocity and pressure must found. The first step is to subdivide the simulation domain into a number of subdomains called elements. Each element is associated with number of discrete points or nodes located within the element or its boundary. The variation of the velocity and the pressure within an element is then defined in terms of the values at the belonging node points. This issue will be discussed in the next section.

4.3 Isoparametric element

The domain occupied by the fluid is divided into simply shaped elements, and within each element, the dependent variables are interpolated from their values at set of nodal points. The interpolation function in the isoparametric formulation can be used to interpolate the solution, which is the vertical and the horizontal velocity, and the geometry of the element which is quadrilateral. Given that, the velocities and coordinates are interpolated as follows:

$$\begin{Bmatrix} v_x \\ v_y \end{Bmatrix} = [N]\{a_i\} \tag{4.15}$$

$$\begin{Bmatrix} x \\ y \end{Bmatrix} = [\tilde{N}]\{c\} \tag{4.16}$$

where

$$\{a_i\} = \begin{bmatrix} v_{1x} & v_{1y} & . & . & v_{nx} & v_{ny} \end{bmatrix}^T$$

$$\{c\} = \begin{bmatrix} x_1 & y_1 & . & . & x_n & y_n \end{bmatrix}^T$$

- if $[N]$ is higher order than $[\tilde{N}]$, the element is called *subparametric element*,
- if $[N] = [\tilde{N}]$, then the element is called *isoparametric element*,
- if $[N]$ is lower order than $[\tilde{N}]$, the element is called *superparametric element*.

In this study, the fluid domain is divided by quadrilateral isoparametric elements, the velocity has approximated by bilinear interpolation functions. The element has four nodes with two variables at each node (see Figure 4.1).
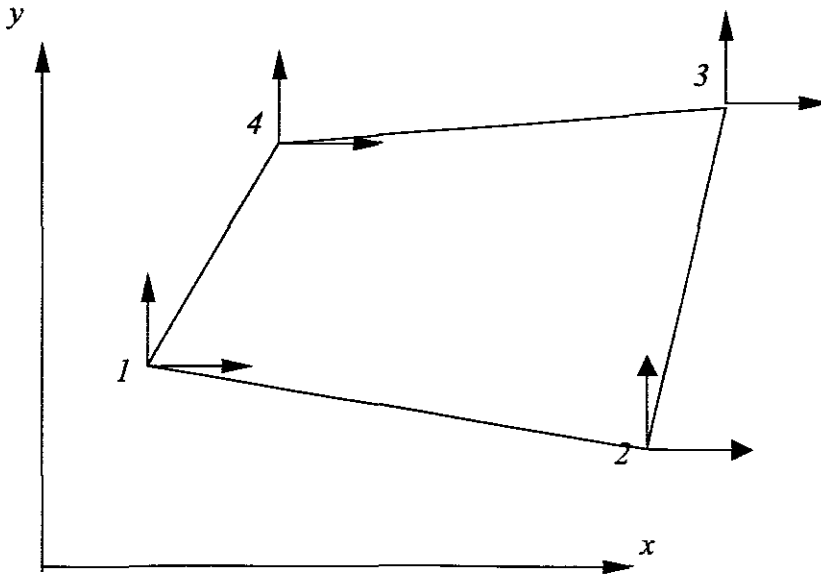
Figure 4.1 Four noded quadrilateral isoparametric element

The x component of the velocity at any point within the element can be expressed as a sum of values at the nodes times shape function evaluated at the point.

$$v_x = \sum_{i=1}^{4} N_i v_{xi} \qquad (4.17)$$

where v_i are the value of v at the node i in the element e. Similarly for the y-component of the velocity:

$$v_y = \sum_{1}^{4} N_i v_{y_i} \qquad (4.18)$$

Here the N's are shape functions or interpolating polynomials, and are defined such that each N_i is equal to one at the ith node , and equal to zero at all the other nodes in the element. With these substitutions for v_x and v_y it is apparent that the variational form depends only on the values of the velocity components at the nodes and the pressure in each element.

For convenience, let e for each node in the element the velocity vector to be defined as:

$$a_i = \begin{bmatrix} v_{xi} \\ v_{y_i} \end{bmatrix} \qquad (4.19)$$

Let similarly, the velocity vector v at any point within the element given by:

$$v = \begin{bmatrix} v_x \\ v_y \end{bmatrix} = \sum_{i=1}^{Ne} N_{iI} a_i \qquad (4.20)$$

this represented in matrix form as:

$$v = \begin{bmatrix} N_1 & 0 & N_2 & 0 & N_3 & 0 & N_4 & 0 \\ 0 & N_1 & 0 & N_2 & 0 & N_3 & 0 & N_4 \end{bmatrix} \{a_i\} \qquad (4.21)$$

where

$$\{a_i\} = \begin{bmatrix} v_{1x} & v_{1y} & v_{2x} & v_{2y} & v_{3x} & v_{3y} & v_{4x} & v_{4y} \end{bmatrix}^T \qquad (4.21)$$

Recall the expression for deformation rates

$$\dot{\epsilon}_{ij} = \frac{1}{2}\left(\frac{\partial v_i}{\partial x_j} + \frac{\partial v_j}{\partial x_i} \right)$$

The deformation rate can be expressed as a matrix product with the differential matrix operator L as follows:

$$\begin{bmatrix} \dot{\epsilon}_{xx} \\ \dot{\epsilon}_{yy} \\ \dot{\epsilon}_{xy} \end{bmatrix} = \begin{bmatrix} \dfrac{\partial}{\partial x} & 0 \\ 0 & \dfrac{\partial}{\partial y} \\ \dfrac{1}{2}\dfrac{\partial}{\partial y} & \dfrac{1}{2}\dfrac{\partial}{\partial y} \end{bmatrix} \begin{bmatrix} v_x \\ v_y \end{bmatrix} = LN\tilde{v} = B\tilde{v} \qquad (4.22)$$

here, the matrix $[B]$ is the deformation rate matrix. This matrix will be discussed on details in Appendix B

Recall the incompressibility condition here:

$$\dot{\epsilon}_{ii} = \dot{\epsilon}_{xx} + \dot{\epsilon}_{yy} = 0 \qquad (4.23)$$

which also can be expressed as a matrix product with the differential matrix operator M as follows:

$$\frac{\partial v_x}{\partial x} + \frac{\partial v_y}{\partial y} = \begin{bmatrix} \dfrac{\partial}{\partial x} & \dfrac{\partial}{\partial y} \end{bmatrix} \begin{bmatrix} v_x \\ v_y \end{bmatrix} = MN\tilde{v} = m^T C\tilde{v} \qquad (4.24)$$

where $m^T = \begin{bmatrix} 1 & 1 & 0 \end{bmatrix}$

Substitution of the approximation Equation (4.22) and Equation(4.24) back to the integral equations Equation(4.11) and Equation(4.14) yields:

$$[k_v]\begin{Bmatrix} v_x \\ v_y \end{Bmatrix} + [k_p]\{p\} = \{0\} \tag{4.25}$$

$$[k_p]^T \begin{Bmatrix} v_x \\ v_y \end{Bmatrix} = \{0\} \tag{4.26}$$

or

$$\begin{bmatrix} [k_v] & [k_p] \\ [k_p]^T & [0] \end{bmatrix} \begin{Bmatrix} \begin{Bmatrix} v_x \\ v_y \end{Bmatrix} \\ \{p\} \end{Bmatrix} = \begin{Bmatrix} \{0\} \\ \{0\} \end{Bmatrix} \tag{4.27}$$

4.4 Penalty method for eliminating the pressure

We apply a penalty method whereby the pressure, p is assumed to depend on the velocity gradients in the following form:

$$m^T Cv - \frac{p}{\Lambda} = 0 \tag{4.28}$$

where Λ is penalty parameter. Equation (4.28) allow p to be eliminated from the computation. As computationally it is advantageous to use the mixed form and introduce the penalty parameter only to eliminate the p values at the element levels, we shall presume such penalization to be done after mixed discretization.

The use of penalty forms in fluid mechanics was introduced early in the seventies by Zienkiewicz and Godbole (1975) and is fully discussed by Zienkiewicz and Vilotte (1985). The discretization equation will be:

$$\begin{bmatrix} [k_v] & [k_p] \\ [k_p]^T & \dfrac{I}{\Lambda} \end{bmatrix} \begin{Bmatrix} \begin{Bmatrix} v_x \\ v_y \end{Bmatrix} \\ p \end{Bmatrix} = \begin{Bmatrix} 0 \\ 0 \end{Bmatrix} \tag{4.29}$$

where I is the identity matrix. Equation (4.29) can be simplified to:

$$[[k_v] + \Lambda[k_p]^T[k_p]][v] = \{0\} \tag{4.30}$$

where

$$[k_v] = \iint_\Omega B^T DB d\Omega \tag{4.31}$$

$$[k_p] = -\iint_\Omega C d\Omega \tag{4.32}$$

The matrix $[D]$ contains the material properties is given by:

$$D = \begin{bmatrix} 2\eta & 0 & 0 \\ 0 & 2\eta & 0 \\ 0 & 0 & \eta \end{bmatrix}$$

For stable solution, it turns to be necessary that $[k_p]$ is singular. This can be accomplished by using integration in the numerical integration (see Fortin (1981)). This simply consists using a lower order Gaussian integration rule for evaluating of the integrals in $[k_p]$ will using a sufficiently higher order rule for $[k_v]$. This requirement actually reduces the computational load in generating the matrix equations.

In addition, we have also gained in the elimination of the additional unknown representing the pressure in each element. As an added benefit, the matrix is more closely banded as well as the elimination of the zeroes along the diagonal of the pressure equations which effectively eliminated the possibility of an iterative solution of the matrix equations.

The penalty constant, Λ, is typically chosen to be:

$$\Lambda = c\eta \tag{4.33}$$

where c is constant on the order of 10^7-10^{10} as in Zienkiewich and Vilotte (1985). This choice seems to yield reasonable results with regards compressibility and pressures, without producing numerical ill conditioning.

4.5 Conditions for the mixed formulation

In the solution of penalty formulation, four-noded quadrilateral elements are used with continuous bilinear velocity interpolation. The use of reduced (1-point) integration for the penalty term makes the penalty formulation equivalent to the mixed formulation. It is important to recall here that the mixed form allows only certain combinitions of N_v and N_p interpolations to be used without violating the convergence conditions. To ensure convergence in the solution, the interpolation functions for the velocity, N_v and the pressure, N_p, must be chosen such that dimension of N_p is one order less than that of N_v. The Q_1-P_0 element conforms to this requirement. Continuos bilinear interpolation is used for the velocity field and the pressure, or stress, field is constant over the element.

Owing to the incompressibility, or nearly incompressibility, condition present in the mixed formulation, mesh locking can occur. It is well known that the elements that satisfy the Babuska-Brezzi, or LBB, stability condition will not lock. Although the Q_1-p_0 elements does not satisfy the LBB condition, optimal rate of convergence can still be proven under certain conditions-nearly incompressible approximation and reduced integration. This was discussed in detail by Hughes (1987). Many other

elements useful in fluid mechanics are documented elsewhere, (Fortin, 1981; Englemen et al., 1982). It is of general interest to note that frequently elements with C_0 continuous pressure interpolations are used in fluid mechanics and indeed their performance is generally superior to those with discontinuous pressure interpolation on a given mesh, even though the cost of solution is marginally greater.

4.6   Shape functions

The essence of the finite element method, already stated above, is the approximation of the unknown by expression given as:

$$v = \sum_{i=1}^{k} N_i \cdot a_i = Na \tag{4.34}$$

where N_i are the interpolating shape functions prescribed in terms of linear independent functions and a_i are a set of unknown parameters. In the Galerkin method the variables are chosen to be identical with the values of the unknown function at the element nodes, thus making:

$$v_i \equiv a_i \tag{4.35}$$

Now consider to interpolate a constant function over the simulation domain. It is clear that a constant value of a_i specified at all nodes must result in a constant value of v which immediately implies that:

$$\sum_{i=1}^{k} N_i = 1 \tag{4.36}$$

At all the point of the domain. The so defined shape functions are referred to as standard shape functions.

In the simplest case (which is also the choice that is compatible with element to be developed in Chapter 5) a non-curved quadrilateral elements with a node in each corner have to be used. The shape functions N_i are taken as bilinear functions. They are given at each node by Zienkiewicz (1988):

$$N_1 = \frac{1}{4}(1-\xi)(1-\eta) \tag{4.37a}$$

$$N_2 = \frac{1}{4}(1+\xi)(1-\eta) \tag{4.37b}$$

$$N_3 = \frac{1}{4}(1+\xi)(1+\eta) \tag{4.37c}$$

$$N_4 = \frac{1}{4}(1-\xi)(1+\eta) \tag{4.37d}$$

In the isoparametric element the interpolation functions can be used to interpolate the coordinate of the element as well.

4.7 Coordinate Transformation

It is remarkable that two transformations are necessary to evaluate the integral in Equation (4.30) over the domain of interest:

Because the shape functions N_i are defined in terms of local coordinates (ξ, η), it is necessary to devise some means of expressing the global derivatives of the type occurring in the Equation (4.30) by local derivatives. The element of volume (or surface in case of boundaries) over which the integration has to be carried out need to be expressed in terms of the local coordinates with an appropriate change of integration limits.

To express these transformations, consider two dimensional local coordinates (ξ, η) and a corresponding two of global coordinates *(x, y)*. The following mathematical results based on the chain rules of differentiation is used:

Using the chain rule on $G = F_1(\xi, \eta) = F_2(x, y)$

$$dG = \frac{\partial G}{\partial x} dx + \frac{\partial G}{\partial y} dy$$

now the derivatives of the shape functions with respect to ξ and η have the form

$$\frac{\partial N_i}{\partial \xi} = \frac{\partial N_i}{\partial x}\frac{\partial x}{\partial \xi} + \frac{\partial N_i}{\partial y}\frac{\partial y}{\partial \xi} \tag{4.38}$$

$$\frac{\partial N_i}{\partial \eta} = \frac{\partial N_i}{\partial x}\frac{\partial x}{\partial \eta} + \frac{\partial N_i}{\partial y}\frac{\partial y}{\partial \eta} \tag{4.38}$$

or in matrix notation can be expressed as:

$$\begin{bmatrix} \dfrac{\partial N_i}{\partial \xi} \\ \dfrac{\partial N_i}{\partial \eta} \end{bmatrix} = \begin{bmatrix} \dfrac{\partial x}{\partial \xi} & \dfrac{\partial y}{\partial \xi} \\ \dfrac{\partial x}{\partial \eta} & \dfrac{\partial y}{\partial \eta} \end{bmatrix} \cdot \begin{bmatrix} \dfrac{\partial N_i}{\partial x} \\ \dfrac{\partial N_i}{\partial y} \end{bmatrix} = [J] \begin{bmatrix} \dfrac{\partial N_i}{\partial x} \\ \dfrac{\partial N_i}{\partial y} \end{bmatrix} \tag{4.39}$$

The left-hand side of the Equation (4.39) depends only on the shape functions N_i that are specified in the local coordinate system. Furthermore, as *(x, y)* are given explicitly, the matrix *J* can be found in terms of local coordinates. This matrix is known as the *Jacobian matrix*. Equation (4.39) represents a set of simultaneous equations in which $\partial N / \partial x$ and $\partial N / \partial y$ are the unknowns.

Since the point of interest is the definition of derivatives in terms of locally defined shape functions the remaining task is to convert the Jacobian matrix *J*. As a result the

derivatives of the shape functions in general coordinate system are found to be using Cramer's rule:

$$\begin{bmatrix} \dfrac{\partial N_i}{\partial x} \\[2mm] \dfrac{\partial N_i}{\partial y} \end{bmatrix} = [J]^{-1} \cdot \begin{bmatrix} \dfrac{\partial N_i}{\partial \xi} \\[2mm] \dfrac{\partial N_i}{\partial \eta} \end{bmatrix} = \dfrac{1}{|J|} \begin{bmatrix} \dfrac{\partial y}{\partial \eta} & -\dfrac{\partial y}{\partial \xi} \\[2mm] -\dfrac{\partial x}{\partial \eta} & \dfrac{\partial x}{\partial \xi} \end{bmatrix} \begin{bmatrix} \dfrac{\partial N_i}{\partial \xi} \\[2mm] \dfrac{\partial N_i}{\partial \eta} \end{bmatrix} \qquad (4.40)$$
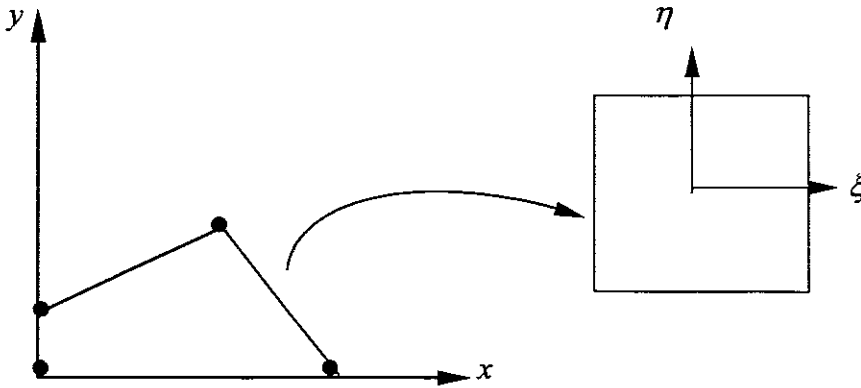
Figure 4.2 A transformation from a quadrilateral to master element

In Figure 4.2 a four noded element mapped onto local master element. For integration purposes a general located element defined in the plane coordinates (x, y) is mapped onto a *standard element* in the (ξ, η) coordinates system Figure 4.2.

Again the variation approach can be used but now interpolating the coordinates vectors itself instead of a distributed value. The variation approach can be written as:

$$x = X^T \cdot N(\xi, \eta) \qquad (4.41)$$

$$y = Y^T \cdot N(\xi, \eta) \qquad (4.42)$$

Where x and y are the coordinate vectors of the element points. Notice that (4.41) and (4.42) is the same formulation as (4.37) only applied to the global coordinate values. Using the Equations (4.41), (4.42) and (4.37) we find the values of J and $|J|$ at any point in any Ω_e. For instance;

$$J_{11} = \frac{\partial x}{\partial \xi} = \frac{\partial}{\partial \xi}\left[\frac{1}{4}(1-\xi)(1-\eta)x_1 + \frac{1}{4}(1+\xi)(1-\eta)x_2 + \frac{1}{4}(1+\xi)(1+\eta)x_3 + \frac{1}{4}(1-\xi)(1+\eta)x_4 \right]$$

$$= -\frac{1}{4}(1-\eta)x_1 + \frac{1}{4}(1-\eta)x_2 + \frac{1}{4}(1+\eta)x_3 + \frac{1}{4}(1+\eta)x_4$$

It can be written in matrix from as:

$$J_{11} = \frac{\partial x}{\partial \xi} = \begin{bmatrix} \dfrac{\partial N_1}{\partial \xi} & \dfrac{\partial N_2}{\partial \xi} & \dfrac{\partial N_3}{\partial \xi} & \dfrac{\partial N_4}{\partial \xi} \end{bmatrix} \begin{Bmatrix} x_1 \\ x_2 \\ x_3 \\ x_4 \end{Bmatrix}$$

(4.43)

$$= \begin{bmatrix} -\dfrac{(1-\eta)}{4} & \dfrac{(1-\eta)}{4} & \dfrac{(1+\eta)}{4} & -\dfrac{(1+\eta)}{4} \end{bmatrix} \begin{Bmatrix} x_1 \\ x_2 \\ x_3 \\ x_4 \end{Bmatrix}$$

or

$$[J] = \frac{1}{4} \begin{bmatrix} -(1-\eta) & (1-\eta) & (1+\eta) & -(1+\eta) \\ -(1-\xi) & -(1+\xi) & (1+\xi) & (1-\xi) \end{bmatrix} \begin{bmatrix} x_1 & y_1 \\ x_2 & y_2 \\ x_3 & y_3 \\ x_4 & y_4 \end{bmatrix}$$

(4.44)

Multiplying the two matrices gives:

$$[J] = \frac{1}{4} \begin{bmatrix} (x_2 - x_1)(1-\eta) + (x_3 - x_4)(1+\eta) & (y_2 - y_1)(1-\eta) + (y_3 - y_4)(1+\eta) \\ (x_4 - x_1)(1-\xi) + (x_3 - x_2)(1+\xi) & (y_4 - y_1)(1-\xi) + (y_3 - y_2)(1+\xi) \end{bmatrix} \quad (4.45)$$

And then the *Jacobian* is evaluated as:

$$|J| = \sum_{i=1}^{4} \sum_{j=1}^{4} \left[\left(\frac{\partial N_i}{\partial \xi} x_i \frac{\partial N_j}{\partial \eta} y_i \right) - \left(\frac{\partial N_i}{\partial \eta} x_i \frac{\partial N_j}{\partial \xi} y_i \right) \right]$$

$$= \sum_{i=1}^{4} \sum_{i=1}^{4} \left[x_i \left(\frac{\partial N_i}{\partial \xi} \frac{\partial N_j}{\partial \eta} - \frac{\partial N_i}{\partial \eta} \frac{\partial N_j}{\partial \xi} \right) y_i \right]$$

(4.46)

By setting $i = 1,2,3,4$ and $j = 1,2,3,4$ for each i, the summation in Equation (4.46) leads to $|J|$ in matrix notation as:

$$|J| = \frac{1}{8} \begin{bmatrix} x_1 & x_2 & x_3 & x_4 \end{bmatrix} \begin{bmatrix} 0 & 1-\eta & -\xi+\eta & -1+\xi \\ -1+\eta & 0 & 1+\xi & -\xi-\eta \\ \xi-\eta & -1-\xi & 0 & 1+\eta \\ 1-\xi & \xi+\eta & -1-\eta & 0 \end{bmatrix} \begin{Bmatrix} y_1 \\ y_2 \\ y_3 \\ y_4 \end{Bmatrix}$$

(4.47)

Expansion of $|J|$ in Equation (4.47) and omitting the tedious algebra gives:

$$|J| = \frac{1}{8} \left[(x_{13} y_{24} - x_{24} y_{13}) + \xi(x_{34} y_{12} - x_{12} y_{34}) + \eta(x_{23} y_{14} - x_{14} y_{23}) \right] \quad (4.48)$$

Where

$x_{ij} = x_i - x_j$ and $y_{ij} = y_i - y_j$

The inverse of the *Jacobian* is given by:

$$[J]^{-1} = \left| \frac{\partial(\xi,\eta)}{\partial(x,y)} \right| = \begin{vmatrix} \dfrac{\partial \xi}{\partial x} & \dfrac{\partial \eta}{\partial x} \\ \dfrac{\partial \xi}{\partial y} & \dfrac{\partial \eta}{\partial y} \end{vmatrix}$$

(4.49)

The computations of $\partial \xi / \partial x, \partial \eta / \partial x, \partial \xi / \partial y,$ and $\partial \eta / \partial y$ can be calculated as follows

$$\frac{\partial \xi}{\partial x} = \frac{1}{|J|} \left(\frac{\partial y}{\partial \eta} \frac{\partial \xi}{\partial \xi} - \frac{\partial y}{\partial \xi} \frac{\partial \xi}{\partial \eta} \right) = \frac{1}{|J|} \frac{\partial y}{\partial \eta} = \frac{1}{|J|} \left(\sum_{i=1}^{4} \frac{\partial N_i}{\partial \eta} y_i \right).$$

(4.50)

because $\partial \xi / \partial \eta = 0$

Similarly

$$\frac{\partial \xi}{\partial y} = -\frac{1}{|J|} \left(\sum_{i=1}^{4} \frac{\partial N_i}{\partial \eta} x_i \right)$$

(4.51)

$$\frac{\partial \eta}{\partial x} = -\frac{1}{|J|} \left(\sum_{i=1}^{4} \frac{\partial N_i}{\partial \xi} y_i \right)$$

(4.52)

$$\frac{\partial \eta}{\partial y} = \frac{1}{|J|} \left(\sum_{i=1}^{4} \frac{\partial N_i}{\partial \xi} x_i \right)$$

(4.53)

The inverse matrix of the *Jacobian* can be written on a special form, which is useful to evaluate the strain in terms of the local coordinate (see Appendix B).

$$[\Gamma] = [J]^{-1} = \frac{1}{J} \begin{bmatrix} J_{22} & -J_{12} \\ -J_{21} & J_{11} \end{bmatrix} = \begin{bmatrix} \Gamma_{11} & \Gamma_{12} \\ \Gamma_{21} & \Gamma_{22} \end{bmatrix}$$

(4.54)

With the help of parameter comparisons and simple transformations the global derivatives can be extracted.

To transform the variables and the region with respect to which the integration is made a standard process will be used that involves the determinant J. Thus the area element becomes

$$dxdy = |J| d\xi d\eta$$

(4.55)

Assuming that the inverse of J can be found the problem of general evaluation of an integral is reduced to element properties F of the form:

$$\int_{-1}^{1} \int_{-1}^{1} F(\xi,\eta) d\xi d\eta$$

(4.56)

The integration is carried out within a *standard element* in the local coordinate system and not in the complicated distorted shape, thus accounting for the simple integration limits.

4.8 Numerical Integration

The idea of numerical integration in finite element analysis is similar to integration by using well-known formulas such as the trapezoidal and Simpson rules. In finite element applications, the Gauss-Legendre formula is often used. In general terms, numerical integration can be expressed as:

$$\int_{x_1}^{x_2} F(x)dx = \sum_{i=1}^{m} F(x_i)W_i \tag{4.57}$$

where i denotes an integration point, m is the number of such points at which the function is evaluated and summed, and W_i are the weighting function. That is, an approximate values of the integral in Equation (4.57) is obtained by finding the summation of the values of the function at a number of points multiplied by a weighting function at each point.

To integrate over the x-y plane, first, it is important to transform x-y coordinate to $\xi - \eta$ coordinates by an appropriate transformation. The advantage of the transformation of any element onto a standard element offers the possibility to use standarized integration methods. Thus, a set of sampling points has to be chosen with the aim of the best accuracy. To integrate (4.57) a discrete formulation like:

$$I = \int_a^b \int_c^d F_1(x,y)dxdy = \int_{-1}^{1} \int_{-1}^{1} F_2(\xi,\eta)d\xi d\eta \tag{4.58}$$

Because the above integration would be over a rectangular domain in the x-y plane, to transform x and y we take the advantage of the shape functions

$$x = \frac{1-\xi}{2}x_1 + \frac{1+\xi}{2}x_2 \tag{4.59}$$

$$y = \frac{1-\eta}{2}y_1 + \frac{1+\eta}{2}y_2 \tag{4.60}$$

Next, integrating twice, as illustrated below:

$$I = \int_{-1}^{1} \int_{-1}^{1} F_2(\xi,\eta)d\xi d\eta \approx \int_{-1}^{1} \left[\sum_{i=1}^{n} F_2(\xi_i,\eta)W_i\right]d\eta \approx \sum_{j=1}^{n}\sum_{i=1}^{n} F_2(\xi_i,\eta_j)W_jW_i \tag{4.61}$$

where n is the order of integration, ξ_i, η_i are sampling points or the so-called *Gaussian points* within the standard element and W_i are belonging weighting functions. The accuracy of integration is described by the order of a polynomial, which integrated exactly. For Gaussian Quadrature, the order of polynomial exactly integrated is *2n-1*,

where n is the order of Quadrature used. The following table relates the sampling points and the weighting functions.

Order	Location of sampling point	Weight function
1	0	2
2	-0.577350269	1
	0.577350269	1
3	-0.77459667	0.5555555
	0	0.8888888
	0.77459667	0.5555555

Table 4-1 Sampling point related to weight function

In the case of our model the integration can be calculated using (4.61). With the values for sampling points and weighting functions taken from Table 4-1.

With the numerical integration used to substitute the exact integration, an additional error is introduced and the first impression is, that it should be reduced as much as possible. Therefore, it is for interest to determine:

- The minimum integration requirements permitting convergence
- The integration requirements necessary to preserve the rate of the convergence which would result in case of exact integration.

In turned out, that the minimum order for the numerical integration must be the same or higher than the order of the interpolation chosen by the shape functions. To preserve the accuracy of the results it is normally enough to increase the integration order by one in comparison to the interpolation order of the shape functions.

4.9 Solve for the primary unknowns: Nodal velocities

Equation (4.30) is a set of algebraic simultaneous equations. This set of equation is *nonlinear* because the coefficients K_{ij} in the matrix $[K_v]$, which are composed of material properties *(viscosity η)* is not constant and depend on the magnitude of the deformation rate and other loading conditions like temperature and the pressure. The unknowns in Eq.(4.30) are the nodal velocities given by the assemblage vector,

$\{v_i\}^T = \begin{bmatrix} v_{1x} & v_{1y} & v_{2x} & v_{2y} & v_{3x} & v_{3y} & v_{4x} & v_{4y} \end{bmatrix}$. Theses are called primary unknowns because they appear as the first quantities sought in the Equation (4.30). Very often additional or secondary quantities must be computed from the primary quantities. In our case the secondary quantities are the stresses and the deformation rate. It is relatively straightforward to find the secondary quantities once the primary quantities are known, since we can make use of the relations between the deformation rate and the velocities and the stress and deformation rate.

The equations can be solved by using iterative methods. One of the well known iterative methods to treat these types of equations is called The *Newton-Raphson method*.

Twenty-two points, plus triple-word-score, plus fifty points for using all my letters. Game's over. I'm outta here.

CHAPTER 5

SINGULAR FINITE ELEMENT METHOD

5.1 Introduction

To achieve maximal accuracy of the flow field near the corner of the cavity, special finite element analysis have to be used. Elements with special properties are required to treat this special domain of the cavity. The geometric features of the special domain may give to highly singular response in the solution of a field problem. In Chapter 3, the eigenfunctions analysis derived to characterize the asymptotic strength of the singularity to the solution field. However, the actual solution depends upon the nature of the loading and there are situations when the singularity does not contribute significantly. For this reason, it has been suggested that, ideally, singular finite elements (SFEM) should strike some balance between being able to represent smooth behavior and potential singular behavior.

In Chapter 3, the local asymptotic solution of two dimensional corner problem has been presented. This solution gives the stress distribution field near the singular point. The stresses exhibit behavior of the form $r^{\lambda-1}$, and the velocity at the corner varies as r^{λ} (λ is real number), where r is the distance from the corner and λ is the order of the singularity. The value of $\lambda (0 < \lambda < 1)$ depends on the geometry of the problem. In the case of antisymmetrical flow $\lambda = 0.544$ and in the case of symmetrical flow $\lambda = 0.9$.

In this Chapter, the singular finite element (SFEM) approach is reported in attempt to deal with singularity in injection moulding arising from the sudden change in the geometry of the cavities. The singular element interpolation functions are constructed from the eingenfunctions described in Chapter 3, and has a variation of the velocities of r^{λ} (λ is real number) from the singular point and hence a variation of the derivatives of $r^{\lambda-1}$.

The singular finite element technique has been developed and used extensively in solid mechanics (Dutta, 1993; Abdel Wahab and De Roeck 1996, 1995(a), 1995(b)), and introduced also for Newtonian fluid mechanics by Gergiou et al., (1989), (1990), but received limited attention for the non-Newtonian fluid. Here, this approach is introduced to simulate the Non-Newtonian fluid in injection moulding with corner singularity. The types of singular finite element, the construction of field shape functions and numerical integration over the singular element will be addressed in the next sections of this Chapter.

5.2   Types of singular finite elements

The desirability of using a special element with the proper singular behavior is almost self-evident. A properly constructed special element strictly speaking should observe the inter-element continuity required between the special element and its neighbors. Two singular finite elements approaches have been review it in Kermode et al., (1985).

5.2.1 Singular basis function approach

A set of supplementary basis functions chosen to reproduce the leading terms of the singularity solution is added to the standard finite element solution expansions (Srang and Fix 1973; Morley 1973). The singular functions are usually defined over several elements and can span the entire domain.

Two difficulties arise in applying this approach to an actual computation, even after the form of the singularities is known (see Srang and Fix 1973). The first is the evaluation of inner product involving singular functions, and the second is the inversion of the stiffness matrix. For the former there are a variety of tricks which exploit the special form of the singular functions. Generally speaking the most singular part-the radial dependence in the energy integrals-must be done analytically. The integration in θ, and if absolutely necessary, also the energy integrals involving only one singular function can be done by high-order numerical integration. A fixed quadrature rule of low accuracy is totally inappropriate.

The inversion of the stiffness matrix is a more serious problem. The addition of the singular functions destroys the band structure of the matrix and may lead to extra operations in elimination as well as extra storage requirements. In additions, the conditioning of the stiffness matrix is very much in question.

5.2.2 Singular Element Approach

In which special elements incorporating at least the radial form of the local solution (by means of special basis functions or singular geometric transformations) are employed in small region around the singularity while ordinary elements are used in the rest of the domain. The various proposed elements can be classified in three categories:

Embodied singularity elements
Special elements are employed around the singular point, and the corresponding field shape functions embody the form of the singularity (Tracey, 1971; Tracey and Cook 1977; Askar, 1987).

Embedded singularity elements
The leading terms of the singularity expansion are used to describe the full solution over multinode element surrounding the singular point, and conventional elements are used elsewhere (see Sih 1973).

Singular isoparametric elements

Singular geometric transformations, defined on the elements surrounding the singular point, can provide finite element approximations with the desired singular behaviour. The transformation becomes singular by properly changing the position of the midnodes, e.g. quarter point elements(Henshell and Shaw 1975; Bersoum, 1977; Horvath, 1994; Benzely, 1974). Even though the singular isoparametric elements have been successful in dealing with crack problems in fracture mechanics(Henshell and Shaw 1975; Bersoum, 1977) and are equivalent to the embodied singularity elements in some cases. The singular isoparametric element is not appropriate for fluid flow problems for the following reasons:

- Singular isoparametric elements cannot handle singular primary variables. The proposed elements can be constructed with no node at the singular point for the singular primary variables.

- Singular isoparametric elements with curved sides are difficult to use without loss of accuracy. Consequently, they are not effective as the embodied singularity elements for free surface problems.

- In order to describe general power- type singularities with isoparametric elements, one has either to increase the number of nodes per element or to construct special field shape functions which combination with the distortion of the physical element will yield the desired behavior. With the embodied singularity elements one has to modify only the field shape functions.

5.3   Element description

In the finite element discretization, we use singular triangular shaped elements in a small core around the singularity to capture the abrupt change in the geometry and ordinary rectangular elements in the rest of the domain, as illustrated in Figure 5.1.
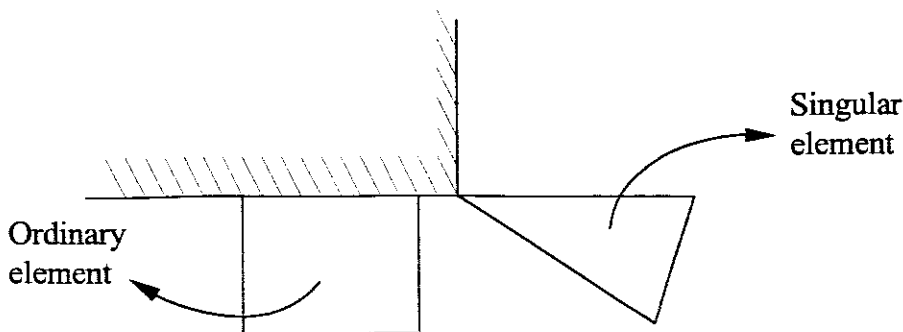
Figure 5.1 Ordinary and singular element

The singular element described here is a generalization of the singular element suggested by Tracey, (1971) for elastic crack tip singularity. The element is five nodes triangle, and has one of its nodes at the singular point, which is node 1 as in Figure 5.2. The power form variation is chosen in the direction away from the singular point low order smooth variation is chosen in the angular directions. Figure5.2 illustrates the triangular singular element that we are going to

implemented in this study. The shape functions is developed in terms of the oblique-co-ordinates ξ, η which vary over the range $[-1, 1]$ with in the element.

The radial edges correspond to $\eta = -1, 1$. The edge $\xi = -1$ is actually a point- the singular point, and the far transverse edge is $\xi = 1$.
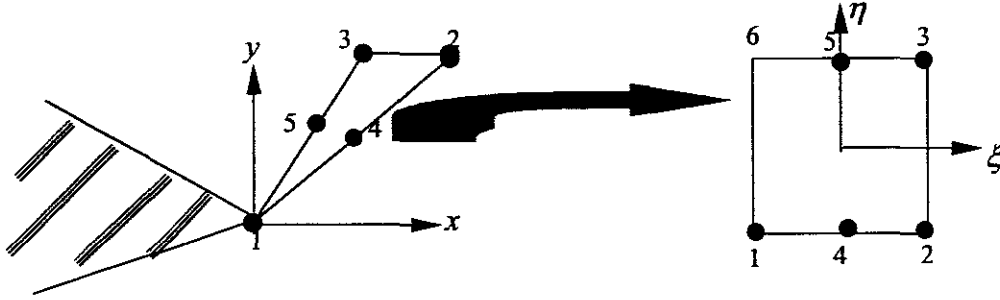
Figure 5.2 General triangle terminating singular point 1

5.4 The velocity shape function

The construction of the field shape functions, describing derivative singularities of the general form r^{n-1} $(0 < n < 1)$, has been the central subject of various works (Bersoum, 1976; Hughes and Akin, 1980). Hughes and Akin (1980) presented an algorithm for generating shape functions from an arbitrary starting set of independent functions. Unfortunately, this algorithm is not capable to achieve satisfactory result when few nodes added to the element. Dydo and Busby, (1997) developed a new equivalent algorithm to circumvent these difficulties. For the present work, the previous algorithm has been used to derive the shape functions.

The algorithm for constructing the interpolation functions is:

Step1:
$$M_{m+1}(r) \leftarrow \frac{M_{m+1}(r) - \sum_{a=1}^{m} M_{m+1}(r_a)M_a(r)}{M_{m+1}(r_{m+1}) - \sum_{a=1}^{m} M_{m+1}(r_a)M_a(r_{m+1})}$$

Step 2: $M_a(r) \leftarrow M_a(r) - M_a(r_{m+1})M_{m+1}(r)$

Step 3:   If $m+1 < n$, replace m by m+1 and repeat step 1-3
            If $m+1 = n$ Stop

In the above, $M_a(r)$ is the ath shape function of the coordinates r. $M_a(r_{m+1})$ is the nodal value of M_a evaluated at the r_{m+1} nodal point. The arrow $\leftarrow$ means 'is replaced by'. Each shape function that is added to the set of the existing shape functions requires;

Each previous shape function to be evaluated at each of the new nodal locations, $M_{m+1}(r_a)$. The subscript m is the original number of the shape functions, and n is the total number of shape functions after the set expanded. The subscript a is simply a counter-index.

Remark: we should note that $r = r(\xi)$, and this will proved next sections.

The shape function M construct by considering one dimensional tree nodes elements with nodes given by $r_1 = 0$, $r_2 = 1/2$ and $r_3 = 1$ as in Figure 5.3. We wish to construct shape functions capable of exactly representing $1, r,$ and r^λ singularity.
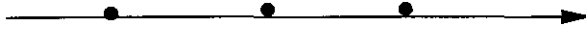
Figure 5.3 One dimensional three- node element

The algorithm start by using preliminary shape functions, in our case we begin with the following shape functions.

$$M_1 = 1 - 2r$$
$$M_2 = 2r \tag{5.1}$$
$$M_3 = r^\lambda$$

Observe that $M_a(r_b) = \delta_{ab}$ $1 \le a, b \le 2$ in terms of algorithm $m=2$ and $n=3$. Using the above algorithm we get.

$$M_3(r) \leftarrow \frac{M_3(r) - M_3(1)M_2(r)}{M_3(2) - M_3(1)M_2(2)} = \frac{r^\lambda - 2\left(\frac{1}{2}\right)^\lambda r}{1 - 2\left(\frac{1}{2}\right)^\lambda} \tag{5.2}$$

$$M_1(r) \leftarrow M_1(r) - M_1(2)M_3(r) = 1 - 2r + \left[\frac{r^\lambda - 2\left(\frac{1}{2}\right)^\lambda r}{1 - 2\left(\frac{1}{2}\right)^\lambda}\right] \tag{5.3}$$

$$M_2(r) \leftarrow M_2(r) - M_2(2)M_3(r) = 2r - 2\left[\frac{r^\lambda - 2\left(\frac{1}{2}\right)^\lambda r}{1 - 2\left(\frac{1}{2}\right)^\lambda}\right] \tag{5.4}$$

The field shape functions must embody the singularity and be compatible with the adjacent ordinary elements. Therefore, for the five nodes Lagrange types element, the shape functions shall be constructed from the products of the tree node-one dimensional shape functions by the linear shape function in the η direction. Hence the shape functions for the velocities

$$\phi^i = M^i(\xi)P^i(\eta) \tag{5.6}$$

To maintain the compatibility with adjoining elements, two velocity nodes are needed in the η direction. At $\xi = -1$, $P = 1$ and the two velocity nodes of the master element in Figure 5.2 collapse to one node with only two degrees of freedom for the two velocity components.

The two dimensional shape functions for the velocity may then defined as follow.

$$\phi_1(\xi,\eta) = M_1(\xi) \tag{5.7a}$$

$$\phi_2(\xi,\eta) = M_2(\xi)P_1(\eta) \tag{5.7b}$$

$$\phi_3(\xi,\eta) = M_2(\xi)P_2(\eta) \tag{5.7c}$$

$$\phi_4(\xi,\eta) = M_3(\xi)P_1(\eta) \tag{5.7d}$$

$$\phi_5(\xi,\eta) = M_3(\xi)P_2(\eta) \tag{5.7e}$$

For more detail see Appendix C for the shape function and its derivatives

5.5 Geometry shape function

5.5.1 Degenerate linear triangular elements

Now in pure isoparametric formulation the element geometry would be defined by the same form as Equation (5.7) and have an arbitrary shape. But in the singular finite element methods the geometry has deferent interpolation function. In this case the element is not isoparametric, the interpolation function for the geometry is lower order than the interpolation function for the field and the element is called subparametric element as we have seen in Chapter 4.

We shall derive the geometry interpolation for the singular element from the bilinear four node quadrilateral master element by closing node 1 and 4 (see Figure 5.4). Specifically we set $x_4 = x_1$, and define new shapes functions for triangle.
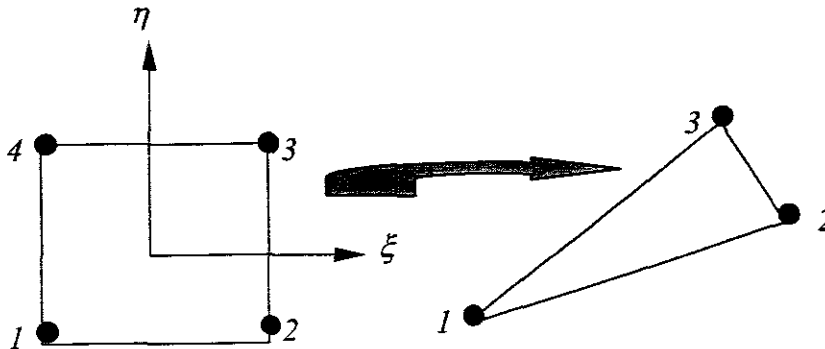
Figure 5.4 Geometry of triangular element

$\widetilde{N}_a$, $a=1, 2, 3$ as follows.

$$x = \sum_{a=1}^{4} \widetilde{N}_a x_a \qquad (5.8)$$

$$= \left(\widetilde{N}_1 + \widetilde{N}_4\right)x_1 + \widetilde{N}_2 x_2 + \widetilde{N}_3 x_3 = \sum_{a=1}^{3} \widetilde{N}_a x_a \qquad (5.9)$$

We derive the shape function for the geometry of the element by using the following Lagrange formula:

$$L_a(\xi) = \frac{\displaystyle\prod_{\substack{b=1 \\ b \neq a}}^{m}(\xi - \xi_b)}{\displaystyle\prod_{\substack{b=1 \\ b \neq a}}^{m}(\xi_a - \xi_b)} \qquad (5.10)$$

Omitting the tedious algebra we can write directly the interpolation function for quadrilateral four nodes element.

$$\widetilde{N}_1(\xi,\eta) = \frac{1}{4}(1-\xi)(1-\eta)$$

$$\widetilde{N}_2(\xi,\eta) = \frac{1}{4}(1+\xi)(1-\eta)$$

$$\widetilde{N}_3(\xi,\eta) = \frac{1}{4}(1+\xi)(1+\eta) \qquad (5.11)$$

$$\widetilde{N}_4(\xi,\eta) = \frac{1}{4}(1-\xi)(1+\eta)$$

And then we can write the interpolation function in the following form

$$\widetilde{N}_a = \begin{cases} \widetilde{N}_1 + \widetilde{N}_4 = \dfrac{1}{2}(1-\xi) \\ \widetilde{N}_i = (1+\xi\xi_i)(1+\eta\eta_i) \quad \text{For} \quad i=2,3 \end{cases} \qquad (5.12)$$

and therefore,

$$x = \sum_{i=1}^{3} \widetilde{N}_i x_i \qquad (5.13)$$

$$y = \sum_{i=1}^{3} \widetilde{N}_i y_i \qquad (5.14)$$

5.5.2 Isosceles triangle

We consider a isosceles triangle with vertices $v_1(x_1,y_1), v_2(x_2,y_2)$ and $v_3(x_3,y_3)$ shown in Figure 3.4 where x, y are Cartesian co-ordinates. This triangle can be described by local coordinates (ξ,η) or by the polar coordinate (r,θ). The triangle has the following dimension, R and base h. The relations between the various coordinates are given by Yiang, (1982).
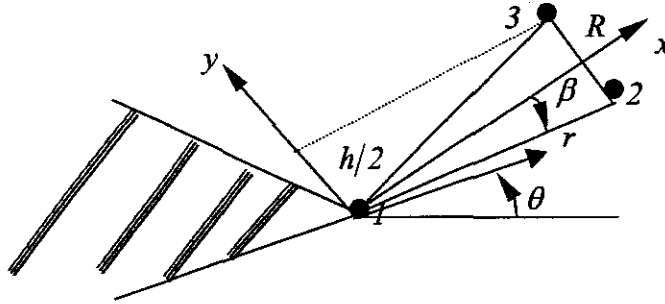
Figure 5.5 Isosceles triangle at the singularity.

$$x = (1+\xi)\frac{R}{2} \qquad\qquad (5.15a)$$

$$y = (1+\xi)\eta\frac{h}{2} \qquad\qquad (5.15b)$$

It is straight forward to show that $(\xi+1)$ is always a linear function of r times a trigonometric function of angular orientation within the element and that η is solely a trigonometric function of angle.

From the Equation (5.15a) we have

$$(1+\xi) = \frac{2x}{R} \qquad\qquad (5.16)$$

but $x = r\cos\theta$, we substitute in the above equation we get

$$(1+\xi) = \frac{2}{R}r\cos\theta \qquad\qquad (5.17)$$

From the second equation of Equation (5.15) we have

$$\eta = \frac{2y}{(1+\xi)h} \qquad\qquad (5.18)$$

using a little algebra we can show that

$$\eta = \frac{y}{x} \bigg/ \frac{h}{R} = \frac{\tan\theta}{\tan\beta} \tag{5.19}$$

It is clear also to show

$$(1+\xi) = r f(\theta) \text{ and } \eta = \eta(\theta) \tag{5.20}$$

With $(1+\xi)$ being a linear function of r, and therefore $(1+\xi)^\lambda$ vary as r^λ

5.6 The Jacobian transformation for the geometry

In this section, the *Jacobian* transformation for the geometry is introduced. The transformation was discussed in details in Chapter 4 for the ordinary four node elements here will be applied directly to singular element.

$$[J] = \begin{bmatrix} J_{11} & J_{12} \\ J_{21} & J_{22} \end{bmatrix} = \begin{bmatrix} \dfrac{\partial x}{\partial \xi} & \dfrac{\partial y}{\partial \xi} \\ \dfrac{\partial x}{\partial \eta} & \dfrac{\partial y}{\partial \eta} \end{bmatrix} = \begin{bmatrix} \displaystyle\sum_{i=1}^{3} \dfrac{\partial \tilde{N}_i}{\partial \xi} x_i & \displaystyle\sum_{i=1}^{3} \dfrac{\partial \tilde{N}_i}{\partial \xi} y_i \\ \displaystyle\sum_{i=1}^{3} \dfrac{\partial \tilde{N}_i}{\partial \eta} x_i & \displaystyle\sum_{i=1}^{3} \dfrac{\partial \tilde{N}_i}{\partial \eta} y_i \end{bmatrix} \tag{5.21}$$

Using Equation (5.13) and Equation (5.14) gives:

$$x = \tilde{N}_1 x_1 + \tilde{N}_2 x_2 + \tilde{N}_3 x_3$$
$$y = \tilde{N}_1 y_1 + \tilde{N}_2 y_2 + \tilde{N}_3 y_3 \tag{5.22}$$

Substituting the interpolation functions into Equation (5.22) gives:

$$x = \frac{1}{2}(1+\xi)x_1 + \frac{1}{4}(1+\xi)(1-\eta)x_2 + \frac{1}{4}(1+\xi)(1+\eta)x_3 \tag{5.23}$$

$$y = \frac{1}{2}(1+\xi)y_1 + \frac{1}{4}(1+\xi)(1-\eta)y_2 + \frac{1}{4}(1+\xi)(1-\eta)y_3 \tag{5.24}$$

Referring to Figure 5.5, if the element has the global angle β and global radice R then:

$$x_1 = 0, \quad x_2 \approx x_3 = R\cos\beta$$
$$y_1 = 0, \quad y_2 = -y_3 = R\sin\beta \tag{5.25}$$

$$if \ \alpha \cong 0 \quad \cos\beta = 1$$
$$if \ \alpha \cong 0 \quad \sin\beta = \beta$$

After certain manipulation gives:

$$x = \frac{R}{2}(1+\xi)$$

$$y = \frac{R}{2}\beta(1+\xi)\eta \tag{5.26}$$

Any point p on the radial line is at distance r from the singularity.

$$r = \sqrt{x^2 + y^2}$$

$$r = \frac{R}{2}(1+\xi)\sqrt{1+\beta^2\eta^2} \tag{5.27}$$

or

$$(1+\xi) = \frac{2r}{R\sqrt{1+\beta^2\eta^2}} \tag{5.28}$$

$$\frac{\partial x}{\partial \xi} = \frac{R}{2} \tag{5.29}$$

$$\frac{\partial x}{\partial \eta} = 0 \tag{5.30}$$

$$\frac{\partial y}{\partial \xi} = \frac{R\beta}{2}\eta \tag{5.31}$$

$$\frac{\partial y}{\partial \eta} = \frac{R\beta}{2}(1+\xi) \tag{5.32}$$

Substituting the above equations into Equation (5.21) the *Jacobian* becomes:

$$[J] = \begin{bmatrix} \dfrac{R}{2} & \dfrac{R\beta}{2}\eta \\ 0 & \dfrac{R\beta}{2}(1+\xi) \end{bmatrix} = \begin{bmatrix} J_{11} & J_{12} \\ J_{21} & J_{22} \end{bmatrix} \tag{5.33}$$

And its determinant

$$|J| = \frac{\partial x}{\partial \xi}\frac{\partial y}{\partial \eta} - \frac{\partial x}{\partial \eta}\frac{\partial y}{\partial \xi}$$

$$|J| = \frac{R^2\beta}{4}(1+\xi) \approx (1+\xi) \tag{5.34}$$

The inverse of $[J]$ is obtained as:

$$[J]^{-1} = \frac{1}{|J|}\begin{bmatrix} J_{22} & -J_{12} \\ -J_{21} & J_{11} \end{bmatrix} = \begin{bmatrix} \dfrac{2}{R} & -\dfrac{2\eta}{R(1+\xi)} \\ 0 & \dfrac{2}{R\beta(1+\xi)} \end{bmatrix} = \begin{bmatrix} \Gamma_{11} & \Gamma_{12} \\ \Gamma_{21} & \Gamma_{22} \end{bmatrix} \tag{5.35}$$

5.7 Deformation rate

To evaluate the deformation rate matrix, we need first to calculate the derivatives of v_x and v_y with respect to ξ and η

$$\frac{\partial v_x}{\partial \xi} = \sum_{i=1}^{5} \frac{\partial \phi_i}{\partial \xi} v_{xi}, \quad \frac{\partial v_x}{\partial \eta} = \sum_{i=1}^{5} \frac{\partial \phi_i}{\partial \eta} v_{xi}$$

$$\frac{\partial v_y}{\partial \xi} = \sum_{i=1}^{5} \frac{\partial \phi_i}{\partial \xi} v_{yi}, \quad \frac{\partial v}{\partial \eta} = \sum_{i=1}^{5} \frac{\partial \phi_i}{\partial \eta} v_{yi}$$

$$\text{(5.36)}$$

$$\frac{\partial v_x}{\partial \xi} = \left[-1 - 4X + 4X\lambda(1+\xi)^{\lambda-1} \right] v_{x1} - \left\{ 2X\left[1 - \lambda(1+\xi)^{\lambda-1} \right] \right\} \left\{ (1-\eta)v_{x2} + (1+\eta)v_{x3} \right\}$$

$$\left\{ \left(4X + \frac{1}{2} \right) - 4X\lambda(1+\xi)^{\lambda-1} \right\} \left\{ (1-\eta)v_{x4} + (1+\eta)v_{x5} \right\}$$

$$\text{(5.37)}$$

$$\frac{\partial v_x}{\partial \eta} = [0]v_{x1} + 2X\left[(1+\xi) - (1+\xi)^{\lambda} \right] v_{x2} - 2X\left[(1+\xi) - (1+\xi)^{\lambda} \right] v_{x3}$$

$$- \left[\left(4X + \frac{1}{2} \right)(1+\xi) - 4X(1+\xi)^{\lambda} \right] v_{x4} + \left[\left(4X + \frac{1}{2} \right)(1+\xi) - 4X(1+\xi)^{\lambda} \right] v_{x5}$$

$$\text{(5.38)}$$

$$\frac{\partial v_y}{\partial \xi} = \left[-1 - 4X + 4X\lambda(1+\xi)^{\lambda-1} \right] v_{y1} - \left\{ 2X\left[1 - \lambda(1+\xi)^{\lambda-1} \right] \right\} \left\{ (1-\eta)v_{y2} + (1+\eta)v_{y3} \right\}$$

$$\left\{ \left(4X + \frac{1}{2} \right) - 4X\lambda(1+\xi)^{\lambda-1} \right\} \left\{ (1-\eta)v_{y4} + (1+\eta)v_{y5} \right\}$$

$$\text{(5.39)}$$

$$\frac{\partial v_y}{\partial \eta} = [0]v_{y1} + 2X\left[(1+\xi) - (1+\xi)^{\lambda} \right] v_{y2} - 2X\left[(1+\xi) - (1+\xi)^{\lambda} \right] v_{y3}$$

$$- \left[\left(4X + \frac{1}{2} \right)(1+\xi) - 4X(1+\xi)^{\lambda} \right] v_{y4} + \left[\left(4X + \frac{1}{2} \right)(1+\xi) - 4X(1+\xi)^{\lambda} \right] v_{y5}$$

$$\text{(5.40)}$$

The equations derivative of the velocity with respects to the local coordinates for any point along the line θ=constant (η=constant), will depend on ξ, and can be written in the form:

$$\frac{\partial v_x}{\partial \xi} = a_0(\eta) + a_1(\eta)(1+\xi)^{\lambda-1}$$

$$\text{(5.41)}$$

$$\frac{\partial v_x}{\partial \eta} = b_0(\eta)(1+\xi) + b_1(\eta)(1+\xi)^{\lambda}$$

$$\text{(5.42)}$$

$$\frac{\partial v_y}{\partial \xi} = c_0(\eta) + c_1(\eta)(1+\xi)^{\lambda-1}$$

$$\text{(5.43)}$$

$$\frac{\partial v_y}{\partial \eta} = d_0(\eta)(1+\xi) + d_1(\eta)(1+\xi)^{\lambda}$$

$$\text{(5.44)}$$

where $a_0, a_1, b_0, b_1, c_0, c_1, d_0, d_1$ are constants for any given set of nodal velocities and along any line θ =constant

The deformation rate vector $\{\dot{\epsilon}\}$ is expressed in terms of the nodal velocities as follows:

$$\{\dot{\epsilon}\} = \begin{Bmatrix} \dot{\epsilon}_{xx} \\ \dot{\epsilon}_{yy} \\ \dot{\epsilon}_{xy} \end{Bmatrix} = \begin{Bmatrix} \dfrac{\partial v_x}{\partial x} \\ \dfrac{\partial v_y}{\partial y} \\ \dfrac{\partial v_x}{\partial y} + \dfrac{\partial v_y}{\partial v_x} \end{Bmatrix} \begin{bmatrix} 1 & 0 & 0 & 0 \\ 0 & 0 & 0 & 1 \\ 0 & 1 & 1 & 0 \end{bmatrix} \begin{Bmatrix} v_{x,x} \\ v_{x,y} \\ v_{y,x} \\ v_{y,y} \end{Bmatrix} \qquad (5.45)$$

$$\begin{Bmatrix} v_{x,x} \\ v_{x,y} \\ v_{y,x} \\ v_{y,y} \end{Bmatrix} = \begin{bmatrix} \Gamma_{11} & \Gamma_{12} & 0 & 0 \\ \Gamma_{21} & \Gamma_{22} & 0 & 0 \\ 0 & 0 & \Gamma_{11} & \Gamma_{12} \\ 0 & 0 & \Gamma_{21} & \Gamma_{22} \end{bmatrix} \begin{Bmatrix} v_{x,\xi} \\ v_{x,\eta} \\ v_{y,\xi} \\ v_{y,\eta} \end{Bmatrix} \qquad (5.46)$$

$$\begin{Bmatrix} v_{x,\xi} \\ v_{x,\eta} \\ v_{y,\xi} \\ v_{y,\eta} \end{Bmatrix} = \begin{bmatrix} \phi_{1,\xi} & 0 & \phi_{2,\xi} & 0 & \phi_{3,\xi} & 0 & \phi_{4,\xi} & 0 & \phi_{5,\xi} & 0 \\ \phi_{1,\eta} & 0 & \phi_{2,\eta} & 0 & \phi_{3,\eta} & 0 & \phi_{4,\eta} & 0 & \phi_{5,\xi} & 0 \\ 0 & \phi_{1,\xi} & 0 & \phi_{2,\xi} & 0 & \phi_{3,\xi} & 0 & \phi_{4,\xi} & 0 & \phi_{5,\xi} \\ 0 & \phi_{1,\eta} & 0 & \phi_{2,\eta} & 0 & \phi_{3,\eta} & 0 & \phi_{4,\eta} & 0 & \phi_{5,\eta} \end{bmatrix} \begin{Bmatrix} v_{x1} \\ v_{y1} \\ v_{x2} \\ v_{y2} \\ v_{x3} \\ v_{y3} \\ v_{x4} \\ v_{y4} \\ v_{x5} \\ v_{y5} \end{Bmatrix} \qquad (5.47)$$

Equation (5.46) and Equation (5.47) can be simplified in the following form:

$$\begin{Bmatrix} \dot{\epsilon}_{xx} \\ \dot{\epsilon}_{yy} \\ \dot{\epsilon}_{xy} \end{Bmatrix} = \begin{bmatrix} \Gamma_{22} & -\Gamma_{12} & 0 & 0 \\ 0 & 0 & -\Gamma_{21} & \Gamma_{11} \\ -\Gamma_{21} & \Gamma_{11} & \Gamma_{22} & -\Gamma_{12} \end{bmatrix} [D\phi]\{v_i\} \qquad (5.48)$$

The matrix $[D\phi]$ contains the derivatives of the shape functions ϕ with respect to ξ and η i.e.,

$$[D\phi] = \begin{bmatrix} \phi_{1,\xi} & 0 & \phi_{2,\xi} & 0 & \phi_{3,\xi} & 0 & \phi_{4,\xi} & 0 & \phi_{5,\xi} & 0 \\ \phi_{1,\eta} & 0 & \phi_{2,\eta} & 0 & \phi_{3,\eta} & 0 & \phi_{4,\eta} & 0 & \phi_{5,\eta} & 0 \\ 0 & \phi_{1,\xi} & 0 & \phi_{2,\xi} & 0 & \phi_{3,\xi} & 0 & \phi_{4,\xi} & 0 & \phi_{5,\xi} \\ 0 & \phi_{1,\eta} & 0 & \phi_{2,\eta} & 0 & \phi_{3,\eta} & 0 & \phi_{4,\eta} & 0 & \phi_{5,\eta} \end{bmatrix} \quad (5.49)$$

The derivatives of v_x and v_y with respect to x and y are obtained by multiplying $[J]^{-1}$ by their derivatives with respect to ξ and η. From Equations (5.46) and (5.48)

$$\frac{\partial v_x}{\partial x} = \Gamma_{11} \frac{\partial v_x}{\partial \xi} + \Gamma_{12} \frac{\partial v_x}{\partial \eta}$$

$$= \frac{2a_0}{R} + \frac{2a_1}{R}(1+\xi)^{\lambda-1} - \frac{2b_0}{R}(1-\eta) - \frac{2b_1}{R}(1-\eta)(1+\xi)^{\lambda-1} \quad (5.50)$$

Collecting the terms containing the same powers of $(1+\xi)$, noting that η=constant on any line θ=constant gives:

$$\frac{\partial v_x}{\partial x} = A_0(\eta) + A_1(\eta)(1+\xi)^{\lambda-1} \quad (5.51)$$

Similarly

$$\frac{\partial v_x}{\partial y} = \Gamma_{21} \frac{\partial v_x}{\partial \xi} + \Gamma_{22} \frac{\partial v_x}{\partial \eta} \quad (5.52)$$

In this case $\Gamma_{21} = 0$

$$\frac{\partial v_x}{\partial y} = \Gamma_{22} \frac{\partial v_x}{\partial \eta}$$

$$= \frac{2}{R\beta(1+\xi)}\left[b_0(\eta)(1+\xi) + b_1(\eta)(1+\xi)^{\lambda}\right] \quad (5.53)$$

Multiplying inside the bracket we have

$$\frac{\partial v_x}{\partial y} = B_0(\eta) + B_1(\eta)(1+\xi)^{\lambda-1} \quad (5.54)$$

The derivatives for v_y are similar and can be written as:

$$\frac{\partial v_y}{\partial x} = \Gamma_{11} \frac{\partial v_y}{\partial \xi} + \Gamma_{12} \frac{\partial v_y}{\partial \eta} \quad (5.55)$$

$$\frac{\partial v_y}{\partial x} = C_0(\eta) + C_1(\eta)(1+\xi)^{\lambda-1} \quad (5.56)$$

and

$$\frac{\partial v_y}{\partial y} = \Gamma_{21}\frac{\partial v_y}{\partial \xi} + \Gamma_{22}\frac{\partial v_y}{\partial \eta} \qquad (5.57)$$

but $\Gamma_{21} = 0$ therefore,

$$\frac{\partial v_y}{\partial y} = \Gamma_{22}\frac{\partial v_y}{\partial \eta} \qquad (5.58)$$

$$\frac{\partial v_y}{\partial y} = D_0(\eta) + D_1(\eta)(1+\xi)^{\lambda-1} \qquad (5.59)$$

$$\frac{\partial v_x}{\partial y} + \frac{\partial v_y}{\partial x} = \Gamma_{21}\frac{\partial v_x}{\partial \xi} + \Gamma_{22}\frac{\partial v_x}{\partial \eta} + \Gamma_{11}\frac{\partial v_y}{\partial \xi} + \Gamma_{12}\frac{\partial v_y}{\partial \eta} \qquad (5.60)$$

Omitting the tedious algebra it is straightforward to show that terms in the deformation rate matrix described in Chapter 4 $[B]$ take the form:

$$\{\dot{\in}\} = \begin{Bmatrix} \dot{\in}_{xx} \\ \dot{\in}_{yy} \\ \dot{\in}_{xy} \end{Bmatrix} = \begin{Bmatrix} \dfrac{\partial v_x}{\partial x} \\[2mm] \dfrac{\partial v_y}{\partial y} \\[2mm] \dfrac{\partial v_y}{\partial x} + \dfrac{\partial v_x}{\partial y} \end{Bmatrix} = \sum_i [B_i]\{\bar{v}_i\} = [B]\{\bar{v}\}, \quad \{\bar{v}_i\} = \begin{Bmatrix} \bar{v}_{xi} \\ \bar{v}_{yi} \end{Bmatrix} \qquad (5.61)$$

where

$$[B] = [B_a(\eta)] + (1+\xi)^{\lambda-1}[B_b(\eta)] \qquad (5.62)$$

Here *[B$_a$]* is linear and *[B$_b$]* is polynomial of $n+1$ order. The exponent $(\lambda-1)$ to the non-dimensional term $(1+\xi)$ in Equation (5.62) represents the deformation rate singularity in this analysis. It is noted that the modification is only pertinent to the term multiplied by λ in the deformation rate nodal velocities matrix $[B]$, compared to the conventional non-singular case when λ equals unity.

5.8 Numerical integration

A variety of numerical schemes integration exist e.g. the midpoint rule, the trapezoidal rule, Simpson's rule, other, higher open and closed Newton-cotes formulae, composite version of these, Romberg integration and Gaussian integration. Gaussian integration has a distinct advantage over other methods in that no error arises when an n or more Gauss point formula is used to integrate a

polynomial of degree *2n-1*. This is essentially twice the order of Newton-Cotes formula involving an equivalent number of function evaluations. This higher order translates into high accuracy where the integrand is smooth in the sense that it is well approximated by a polynomial, alternatively where it can be written as the product of a function well approximated by a polynomial and a known weight function containing an integrable singularity.

Thus quadratures rules that integrates the stiffness matrix accurately would vary with λ either by sampling points, weights, or both.

$$[K_e(\lambda)] = \int_{-1}^{1}\int_{-1}^{1}[B]^T[D][B]det[J]d\xi d\eta + \Lambda\int_{-1}^{1}\int_{-1}^{1}[C]^T[C]det[J]d\xi d\eta \qquad (5.63)$$

Substituting Equation (5.62) into the first integral of Equation (5.63) gives:

$$\int_{-1}^{1}\int_{-1}^{1}\left([B_a(\eta)]^T + (1+\xi)^{\lambda-1}[B_b(\eta)]^T\right)[D]*$$

$$* \left([B_a(\eta)] + (1+\xi)^{\lambda-1}[B_b(\eta)]\right)det[J]d\xi d\eta \qquad (5.64)$$

by using normal multiplication we get

$$H_3(1+\xi)^{2\lambda-2} + H_2(1+\xi)^{\lambda-1} + H_1$$

where

$$H_3 = \int_{-1}^{1}\int[B_b(\eta)]^T[D][B_b(\eta)][J]d\xi d\eta \qquad (5.65)$$

$$H_2 = \int_{-1}^{1}\int\left([B_a(\eta)]^T[D][B_b(\eta)] + [B_b(\eta)]^T[D][B_a(\eta)]\right)[J]d\xi d\eta \qquad (5.66)$$

$$H_1 = \int_{-1}^{1}\int[B_a(\eta)]^T[D][B_a(\eta)][J]d\xi d\eta \qquad (5.67)$$

Using Equation (5.34) for the *Jacobian* $[J] = \dfrac{R^2\beta}{4}(1+\xi) \approx (1+\xi)$ and holding η constant in the integral in Equation (5.64) we are lead to integral of the form:

$$\int_{-1}^{1}d\eta\int_{-1}^{1}\left[H_1 + H_2(1+\xi)^{\lambda-1} + H_3(1+\xi)^{2(\lambda-1)}\right](1+\xi)d\xi$$

$$I = \int_{-1}^{1}d\eta\int_{-1}^{1}\left[H_1(1+\xi) + H_2(1+\xi)^{\lambda} + H_3(1+\xi)^{2\lambda-1}\right]d\xi \qquad (5.68)$$

$$I = \int_{-1}^{1}\left[H_1(1+\xi) + H_2(1+\xi)^{\lambda} + H_3(1+\xi)^{2\lambda-1}\right]d\xi$$

Stern (1979) approximate the integral as:

$$I' = \sum_{i=1}^{2} W_i \left[H_1(1+\xi_i) + H_2(1+\xi_i)^\lambda + H_3(1+\xi_i)^{2\lambda-1} \right] \qquad (5.69)$$

For the ξ integration the two points rules have been used;

$$I_m = \int_{-1}^{1} x^m dx = \frac{2^{m+1}}{m+1} = W_1 x_1^m + W_2 x_2^m \qquad (5.70)$$

Exact for tree values of $m=1$, $m=\lambda$, and $m=2\lambda-1$, for $0<\lambda<1$, and

$$x_1 = (1+\xi_1) \qquad\qquad\qquad\qquad (5.71)$$
$$x_2 = (1+\xi_2) \qquad\qquad\qquad\qquad (5.72)$$

For $m=1$, $m=\lambda$, $m=2\lambda-1$

$$W_1(1+\xi_1) + W_2(1+\xi_2) = 2$$

$$W_1(1+\xi_1)^\lambda + W_2(1+\xi_2)^\lambda = \frac{2^{\lambda+1}}{(1+\lambda)} \qquad (5.73)$$

$$W_1(1+\xi_1)^{2\lambda-1} + W_2(1+\xi_2)^{2\lambda-1} = \frac{2^\lambda}{2\lambda}$$

In the set of Equation (5.73), we have more unknowns than equations. We place the first sampling point near the singular point of the element at $\xi_1 = -7/9$ and solve the set of equation for given value of λ. Duhaman (1979) chose $\xi_2 = 1$ where there is no loss of continuity of displacement gradient. The advantages of this choice is that it gives direct expressions for ξ_1, W_1, W_2 as a function of λ For special case where $\lambda=1/2$ and after the solution of Equation (5.73) we have the following sampling point and weighting function given by Solecki and Swelow (1984);

$$\xi_1 = -0.7777778, \qquad\qquad \xi_2 = 0.38888889$$
$$W_1 = 0.6666667, \qquad\qquad W_2 = 1.33333333$$

Other values for the sampling point and the weighting functions are possible by chousing other value for λ and solving again the set of Equation (5.73).

5.9 Closure

A two dimensional five noded singular finite element was presented. The element is compatible with the quadrilateral four noded isoparametric elements. This advantages leads to simplifying the modeling of the corner by reducing the number of elements required for accurate solution. The elements also satisfy the constant strain condition. Therefore, its application has wide applications. The interpolation function for the field and the geometry has been developed. Special quadrature has been presented this rule vary with the sampling point or weight or both.

COMPUTER SIMULATION AND NUMERICAL RESULTS

6.1 Introduction

To accurately simulate the processes of the injection moulding, a simulation code must include a variety of Non-Newtonian models and the variety of the numerical methods. Considerable progress has recently been made in developing finite element routines and programming techniques for 2-D and 3-D free surface flows. **CRATMOLD** (Mahomed, 1998) is one of the best codes based on the FEM, is best suited for low Reynolds number flows as well as for complex free surface problems. **CRATMOLD** provides the facility to translates a mathematical formulation of nonlinear discretized coupled partial differential equation system into a highly optimized model which will then be passed to a nonlinear numerical solver that can handle different mathematical models on quadrilateral grid.

In this study, the **CRATMOLD** code has been used to understand certain aspects of Non-Newtonian fluid behavior around a singular point as encountered in the injection moulding filling process. The following sections gave a general overview of **CRATMOLD** and the results obtained using **CRATMOLD.**

6.2 General overview

The core of **CRATMOLD** code is a simulation system, which can handle non-linear partial differential equation systems in time and space in either one or two dimension for the incompressible Stokes formulation. It's designed to automatically generate and regenerate of the finite element mesh. The non-linear (Non-Newtonian) solution of the finite element flow formulation. The adaptive refinement of the finite element mesh, the iterative solution of the melt front position based on the extermination of the free surface functional and finally the explicit advancement of the melt front and the tracking of the solid boundaries.

Four-noded isoparametric quadrilateral elements, which are automatically generated by the mesh generation routines for selected domain, are used to interpolate the finite element solution. Higher order interpolation and integration routines are available. The mesh generator is limited to four-noded bilinear elements and it can not generate the singular element. The objective of this study is to modify or to add a routine to generate

special finite elements to be used around sharp corner in a cavity to solve the problem of singularities.

6.2.1 Program implementation

CRATMOLD starts by reading input data required generating the mesh from the files prepared by the user. This data specifies the boundary of the fluid domain and material properties, and the background mesh used for interpolating the mesh density distribution. The data specifying the boundary of the fluid domain and material properties is written in the file IMESH while the background mesh information is written in the file BMESH. Once the input has been read from these files, the process of automatic mesh generation is performed. The output of this module, i.e. the generated mesh, is written to the file GMESH. Since the generated mesh is going to be used as the background mesh for the next time step, the mesh is also written to BMESH. In this case nodal mesh densities are included.

When the mesh generation process is over, the finite element analysis module is executed. Input data to this module is the generated mesh in GMESH, the time step information in IMOLD and the cavity mesh in CMESH. The cavity mesh provides information about the cavity of the mould. The finite element module solves the Stokes flow problem presented in Chapter 2 to calculate the nodal velocities across the fluid domain. The output of this module, i.e. the velocity field, is written to the file OMOLD.

Owing to uneven distribution of the velocity through the domain, it becomes important to adjust the mesh such that small elements are distributed in areas where the velocity gradient is higher and conversely. Once the nodal velocities are determined, the melt front nodes are advanced to a displacement vector equal to the velocity times the time step taken. The melt front is advanced such that it does not intersect the boundary of the cavity specified in CMESH. The melt front position together with the mold boundary in contact with the fluid outlines the boundary of the fluid domain for the next time step. Data specifying the new domain is stored in IMESH. The process is repeated until the cavity is filled. The program will inform the user that the mold is completely filled.

6.2.2 Input data

CRATMOLD required a total of four input files CMESH, BMESH, IMESH and IMOLD. The file CMESH provides the topological and material data for the cavity. It used for tracking the melt front. Generally, the materials properties will not vary the cavity but the geometrical data, such as may vary.

Each region is then divided into a number of four noded elements according to standard finite element topological conventions. This information is stored in CMESH.

The file BMESH is identical to CMESH at the start of the filling process. Thereafter, it is self-generated. It contains the background mesh information, which is used for mesh density interpolation during the mesh generation process. The background mesh data does not necessarily need to represent the cavity of the mold since the mesh density information is interpolated.

The file IMESH contains the input mesh data of the current boundaries of the fluid domain. This input file must prepared be the user for the initial state of the flow domain. For the next step, the boundary segments describing the domain occupied by the fluid, after advancing the position of the melt front, are copied automatically to this file to form the input mesh. The boundary of the fluid domain is divided into number of segments, each segment being described by a number of points and having a particular boundary condition. Boundary segments are indicated as either a free surface (constant stress boundary) or a solid liquid interface (constant velocity boundary). Constant velocity boundary values are taken as polymer entrance lines.

The last input file required is IMOLD and this file contains the user-specified fill-time, the time at which the mesh is initiated and the time increment explicit advancement of the melt front.

All these input files are given in Appendix D.

6.2.3 Output data

The output file is the generated mesh GMESH this file contains the topological data for the generated finite element mesh. In addition to this, the material data sets are also specified as well as the boundary nodes and corresponding boundary values. It serves as an input file for the finite element analysis module. The mesh generated by the mesh generation module using the domain specified in IMESH is written to this file automatically.

6.3 Results and discussion

In this section the numerical results obtained for the flow around a right angle corner is presented. The geometry and the boundary conditions are depicted in Figure 6.1. The inlet is taken at $x=0$, the singularity is positioned at $x=10$ and $y=8$. The centerline is placed at $y=4$, and the upper boundary is located at $y_1=8$ and $y_2=18$.The variation of the velocity components will be given at the section AA where $x=9$, BB $x=11$, CC, $y=4$, also along the line PQ and PS . The stresses will be computed along the horizontal wall at $y=8$ and along the vertical wall at $x=10$ as in Figure 6.1.
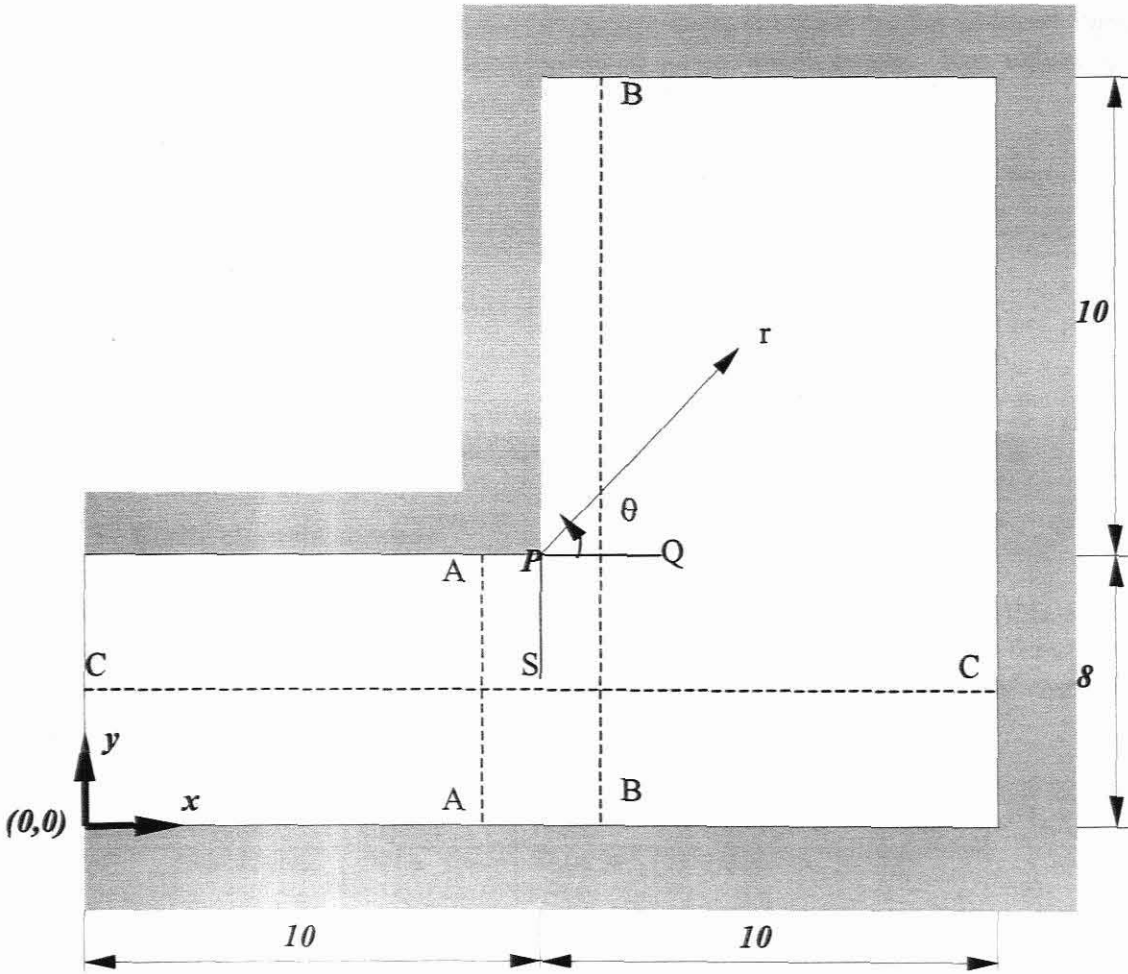
Figure 6.1 Geometry of the mould cavity.

6.4 Material properties

The polymer used in this study is Polystyrene grade Dow Styron 678 D, which is modelled by the Cross-Exponential viscosity model given by:

$$\eta(\dot{\varepsilon}, T, P) = \frac{\eta_0(T, P)}{1 + \left(\dfrac{\eta_0 \, \bar{\dot{\varepsilon}}}{\tau^*}\right)^{1-n}} \tag{6.1}$$

with

$$\eta_0(T, P) = B \exp\left(\frac{T_b}{T}\right) \exp(\beta) \tag{6.2}$$

Where η represent the shear viscosity, η_0 the zero shear rate viscosity, $\bar{\dot{\varepsilon}}$ shear rate, τ^* transition stress, n power law index, T_b temperature constant, T temperature, B material constant, β pressure dependent coefficient in viscosity model and p the pressure. These

five constants for this model are taken from the resin database of the C-Mold injection moulding simulation code, and are presented in the table below. The values of the physical constants that were used are all in SI units.

n	0.2799
$\tau^*(Pa)$	1.484×10^4
$B(Pa.s)$	5×10^{-8}
$T_b(K)$	13520
$\beta(Pa^{-1})$	3.5×10^{-8}

Table 6-1 Summary of the Cross-Exponential viscosity model constants

6.5 Finite element meshes

The finite element meshes used for the calculations of the flow field in this study are generated by the CRATMOLD Non-Newtonian flow simulation code. The first mesh *M1* was used to calculate the velocity and the stresses. All the information of mesh *M1* is summarized in Table 6.2.

Cavity Volume	Filled volume	Time elapsed	Percentage filled	Mesh density	Number of nodes	Number of elements
520 mm³	504.72 mm³	.971 s	97.06 %	1 mm	293	256

Table 6-2 Data for mesh *M1*

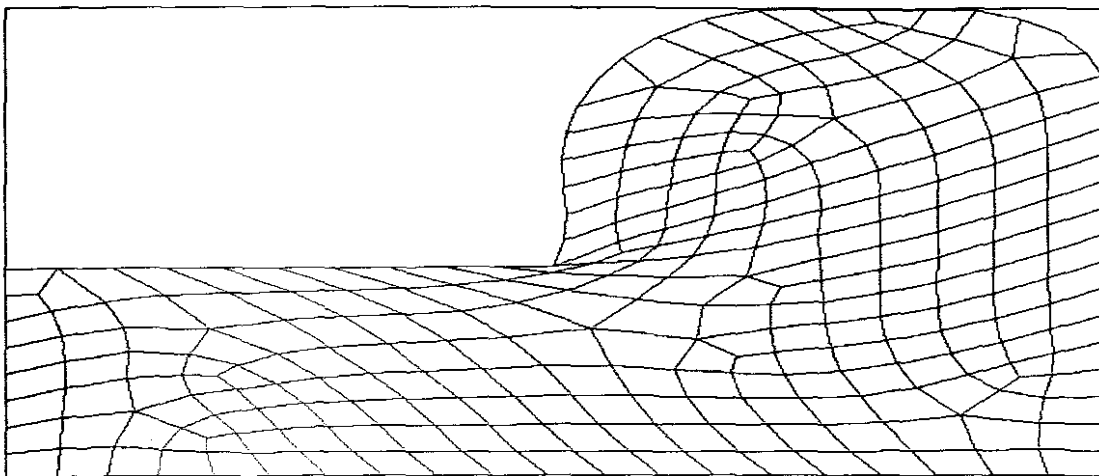The mesh *M1* is showed in Figure 6.2.

Figure 6.2 Finite element mesh *M1*

6.6 Velocity field

The simulation of Non-Newtonian flow around corner can be analyzed in terms of the velocity components. It is not understood how the velocities behave around the corner where we have the sudden change in the geometry of the mould. In this section we show how the velocity behaves in certain section of the mould cavity. We have two velocity components, the horizontal and the vertical velocity. These velocities are computed in the following sections:

- The section AA at $x=9$ before the corner, the section BB at $x=11$ after the corner.
- The centerline of the mould $y=4$ or in section CC,
- In the radial direction along the line PQ and PS.

All these sections are shown in Figure 6.1.

6.6.1 Velocity profiles

In Figures 6.3 and 6.4 there are plotted velocities profiles. The horizontal and the vertical velocity are computed along the section AA just before the corner at $x=9$, and along the section BB after the corner at $x=11$. The polymer was injected with constant velocity $V_e=200mm/s$ from small region in the cavity mould.

As expected, the maximum of the horizontal velocity profile just before the corner is of the centre of the cavity mould and it is higher in this region as in Figure 6.3. (a). When the fluid passes the corner at $x=11$, the horizontal velocity reaches the maximum value as shown in Figure 6.4.(a) and then starts to decrease gradually due to the deceleration of the flow. In this case the vector velocity and vector acceleration have different directions and therefore the velocity has a negative sign, thus the flow stops and the velocity becomes zero.
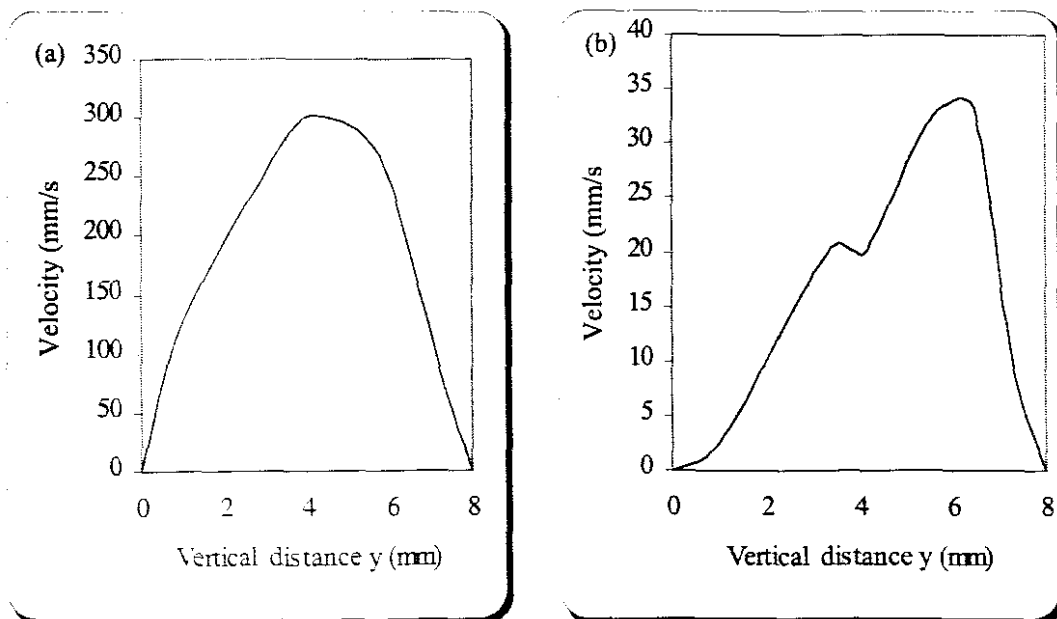
Figure 6.3 The velocity profile at $x=9$, (a) Horizontal velocity v_x, (b) Vertical velocity v_y
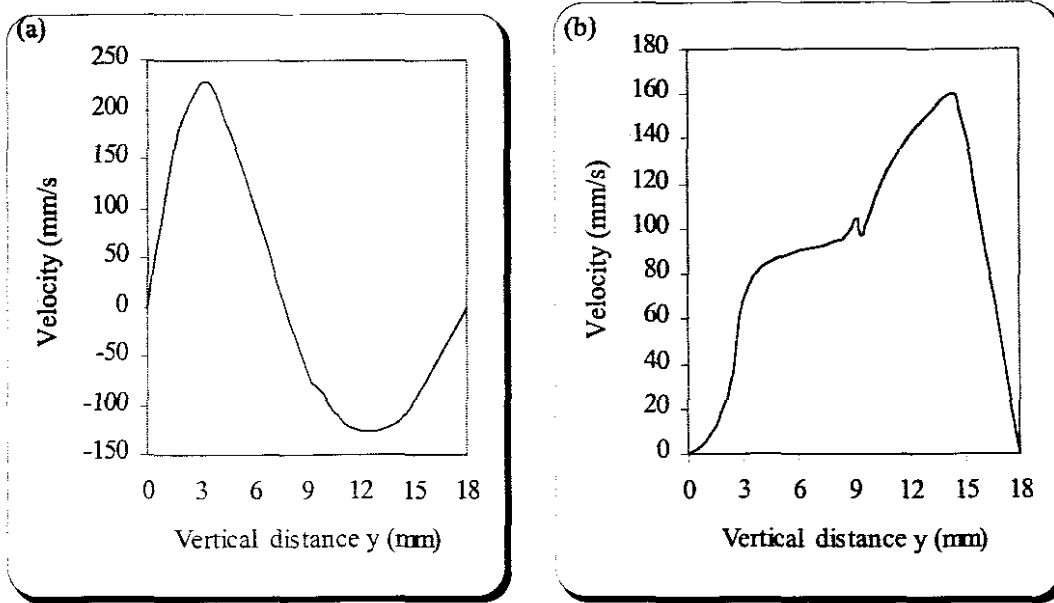
Figure 6.4 The velocity profiles at $x=11$, Horizontal velocity v_x, (b) Vertical velocity v_y

The vertical velocity was also computed. In Figure 6.3.(b) and Figure 6.4 (b), we plotted the vertical velocity as a function of the vertical distance y. At $x=9$, the vertical velocity take the maximum value at $y=8$ which is next the singular point and starts to decrease due to the deceleration of the flow.

6.6.2 Centerline velocity

The velocities along the section CC at $y=4$, are plotted in Figures 6.5.
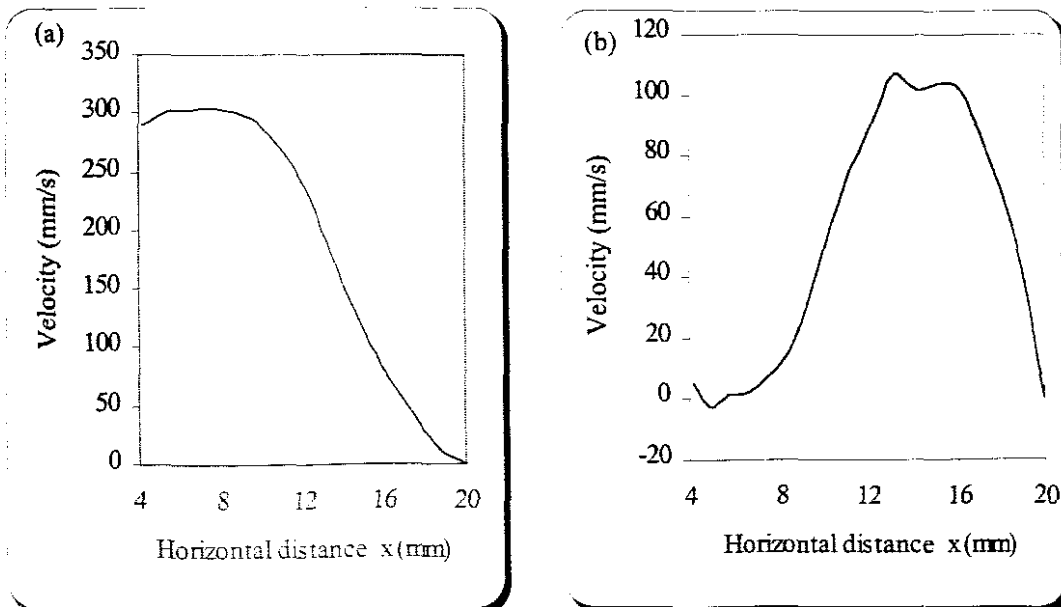
Figure 6.5 The centerline velocity, (a) Horizontal velocity v_x, (b) Vertical velocity v_y

As expected, the velocity in the small region in the mould cavity before the corner is high and reaches the maximum value in the section across the corner, then will decrease gradually in the largest region after the corner.

6.6.3 Velocity near the corner

From the analytical solution that has been given in Chapter 3, the velocity exhibits behavior of the form $r^{0.544}$. In Figure 6.6 this function is presented and gives a smooth curve for the velocity.
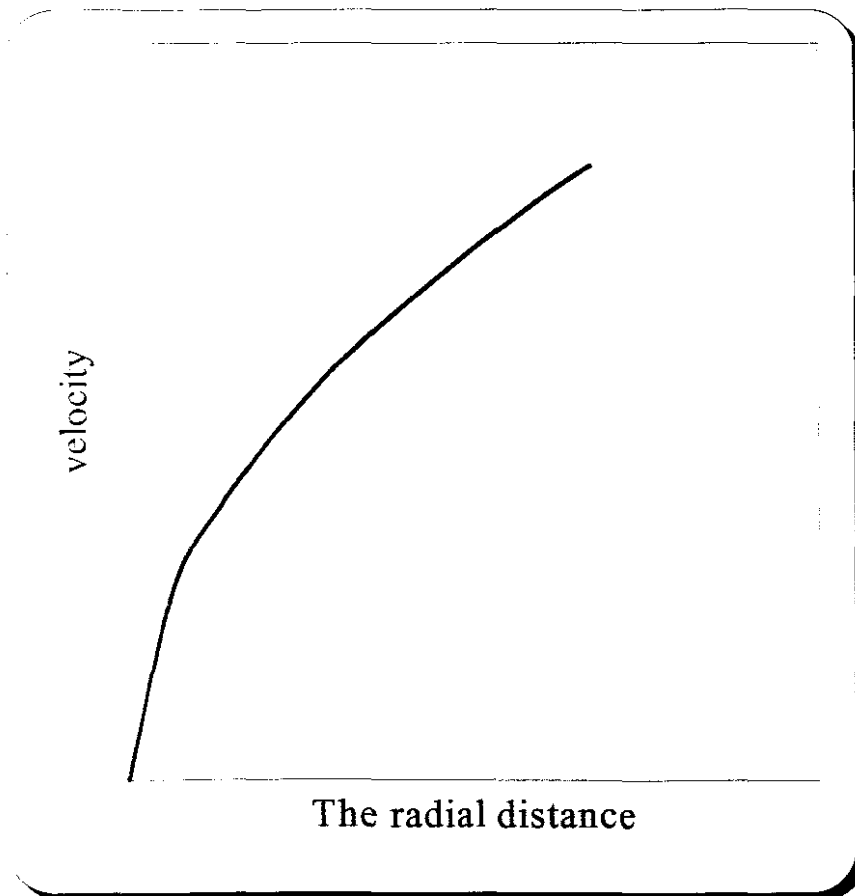
Figure 6.6 Velocity analytical solution

In order to evaluate the results, we computed both the vertical and horizontal velocity from the singular point in the x and y directions. Let us now examine in Figure 6.7 the results obtained along the horizontal and the vertical distance from the corner using the mesh given in Table 6.2.

In Figure 6.7. the horizontal and the vertical velocities have been plotted along the line *PS* as shown in Figure 6.1.
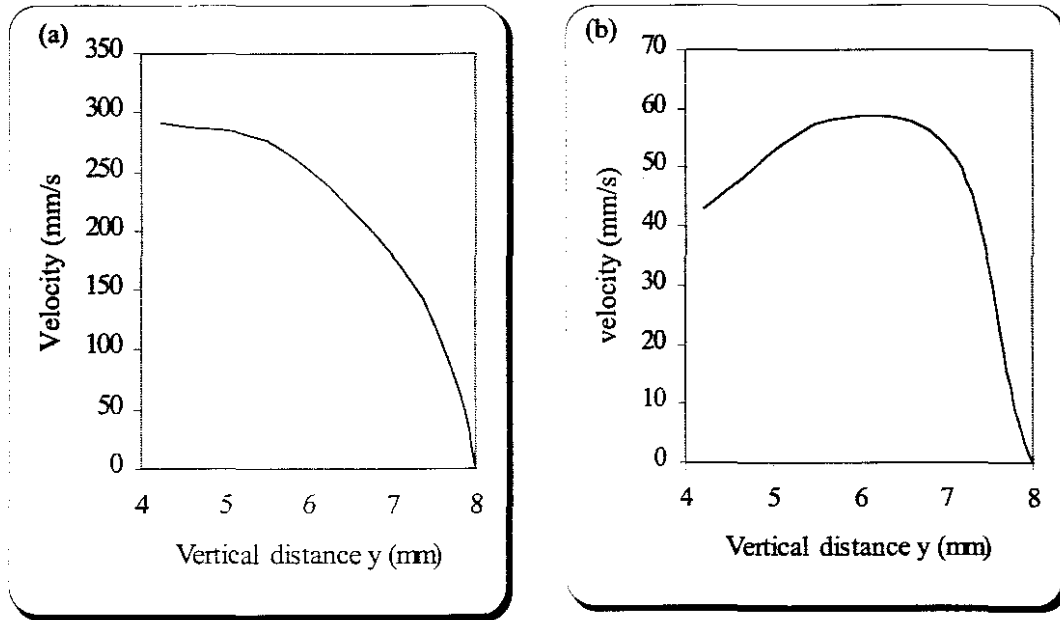
Figure 6.7 The velocity, along the line *PS*, (a) Horizontal velocity, (b) Vertical velocity

The curve representing the horizontal velocity is shown in Figure 6.7. (a). This curve is smooth and is free of oscillations. The vertical velocity has been plotted in Figure 6.7.(b). The curve is not smooth enough and is different from the analytical solution shown in Figure 6.6.

Finally the velocity components in the horizontal distance along the line *PQ* as shown in Figure 6.1 were also computed. Here, the vertical velocity is free of oscillations and the curve is smooth. Some oscillations has been noticed for the horizontal velocity as shown in Figure 6.8 (a).
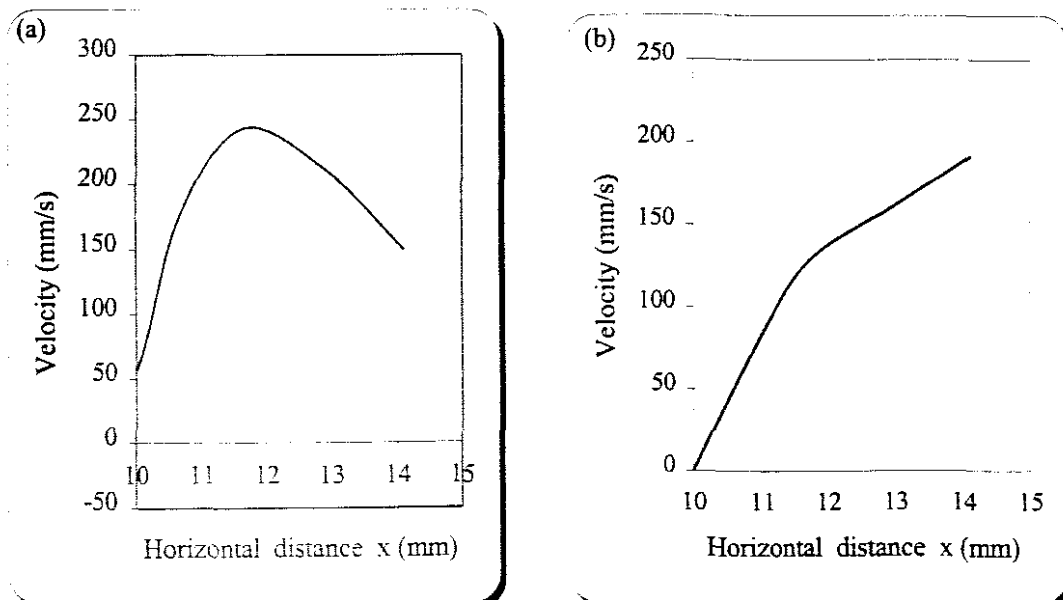
Figure 6.8 The velocity, along the line *PQ*, (a) Horizontal velocity, (b) Vertical velocity

Compared with the analytical solution, the finite element mesh gives reasonable results for the velocity even without mesh refinement.

6.7 Qualitative description of the stress fields

From the analytical solution given in Chapter 3, the stress varies as $\sigma_{ij}^v \approx r^{-0.456}$, where r is the radial distance from the corner. This is an asymptotic solution of the stresses. In Figure 6.9 the stress is plotted as a function of the radial distance. From the graph, the stress behaves smoothly and asymptotically, and tends to infinity as r approaches to zero, which is the singular point.
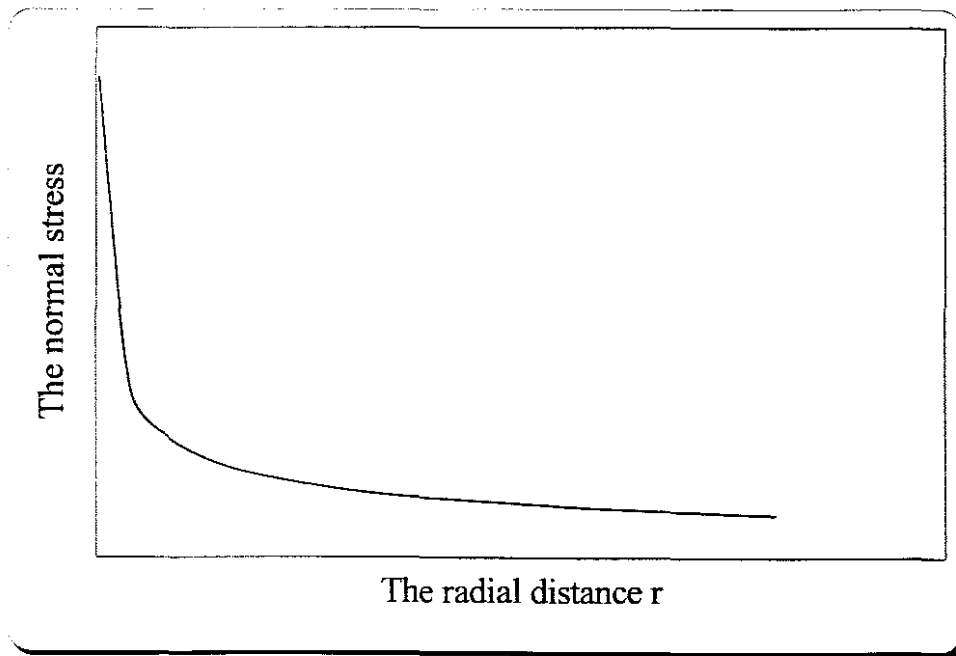
Figure 6.9 The asymptotic stress solution

The computation for the viscous stresses σ_{xx}^v, σ_{yy}^v and the shear stress σ_{xy}^v along the two walls forming the corner at $y=8$ and $x=10.$, started by plotting the graph of the stress components as a function of the horizontal distance x along the wall $y=8$ using the finite element mesh $M1$.

The distance x represents a small interval near to the singular point before and after the corner. It should be remembered the corner or the singular point is located at $(x,y) = (10,8)$.

Figures (6.10), (6.11), and (6.12) illustrate the Normal viscous stress $\sigma_{xx}^v, \sigma_{yy}^v$, and the shear stress σ_{xy}^v respectively. All the stresses are characterized by spurious oscillations

around the singular point at $x=10$. The graphs representing the stresses are not smooth and they are not in agreement with the analytical solution.
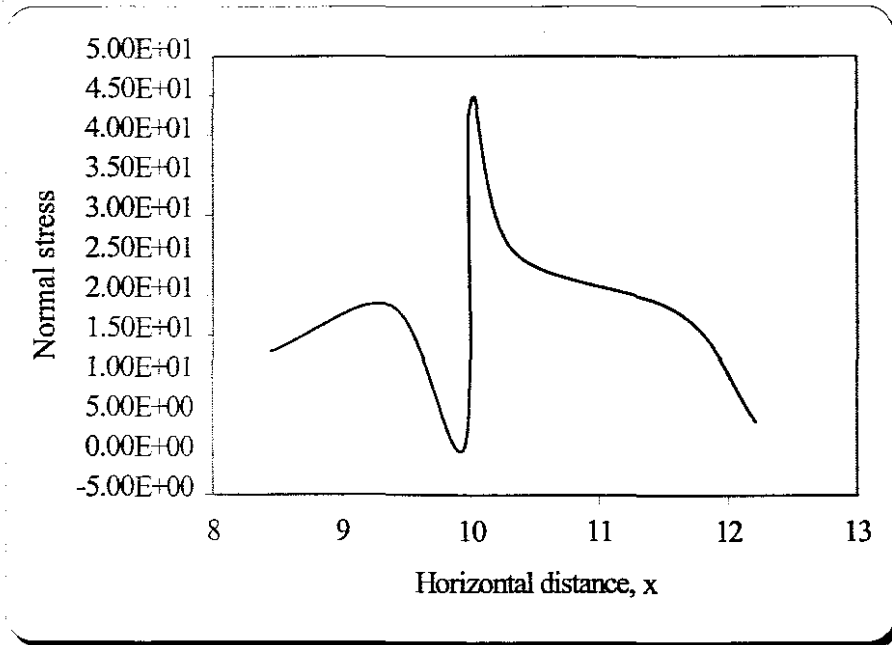
Figure 6.10 The Normal stress σ_{xx}^v along the wall $y=8$
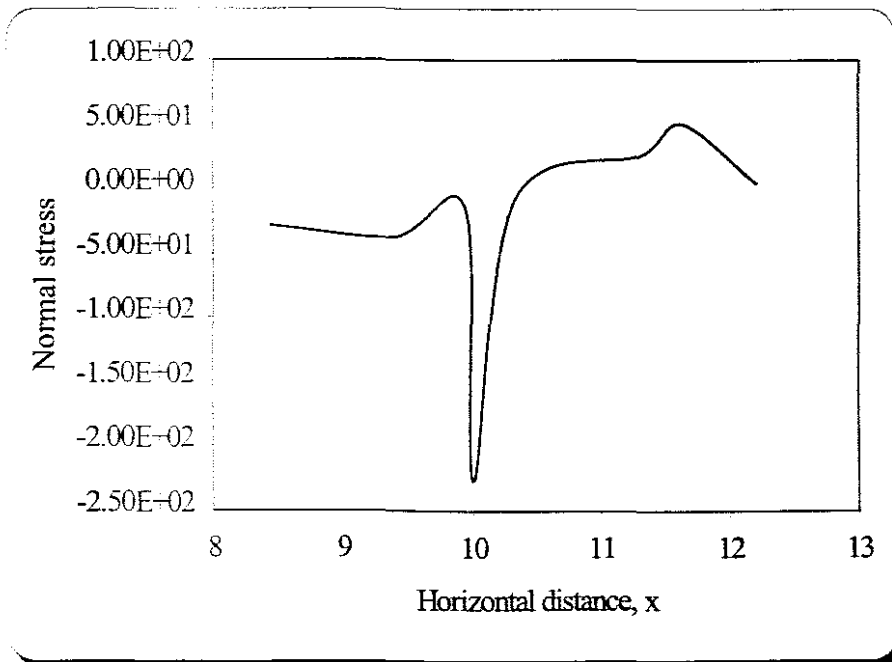
Figure 6.11 The Normal stress σ_{yy}^v a long the wall $y=8$
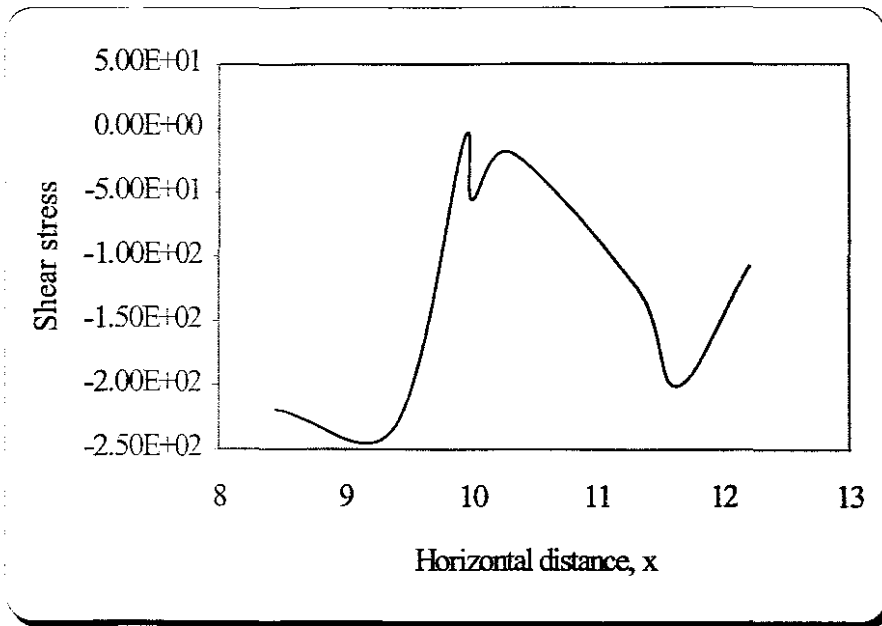
Figure 6.12 The shear stress σ_{xy}^{V} along the wall $y=8$

The computation for the different stresses along the vertical wall at $x=10$ is also presented. All the stresses are shown in Figures (6.13), (6.14) and (6.15).
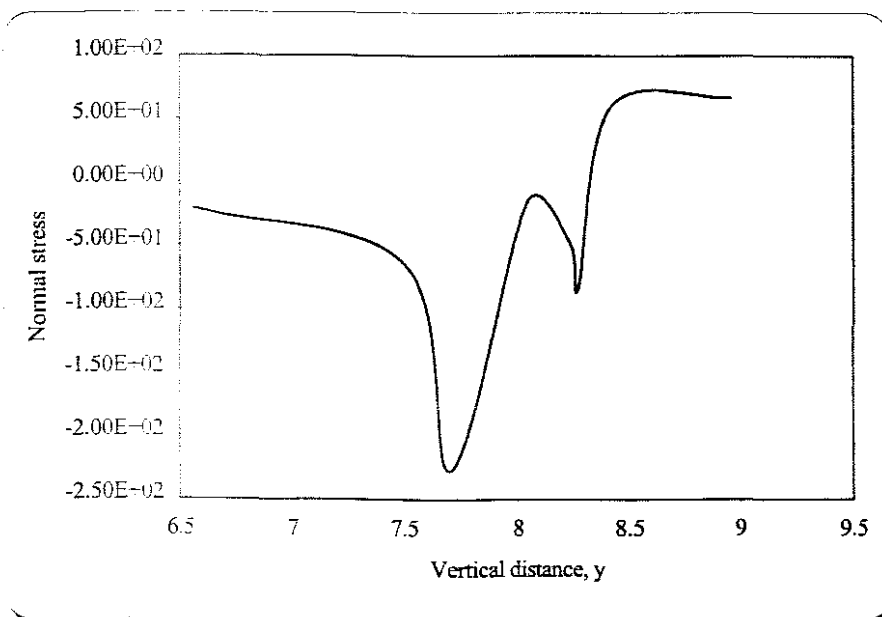
Figure 6.13 The Normal stress σ_{xx}^{V} along the wall $x=10$
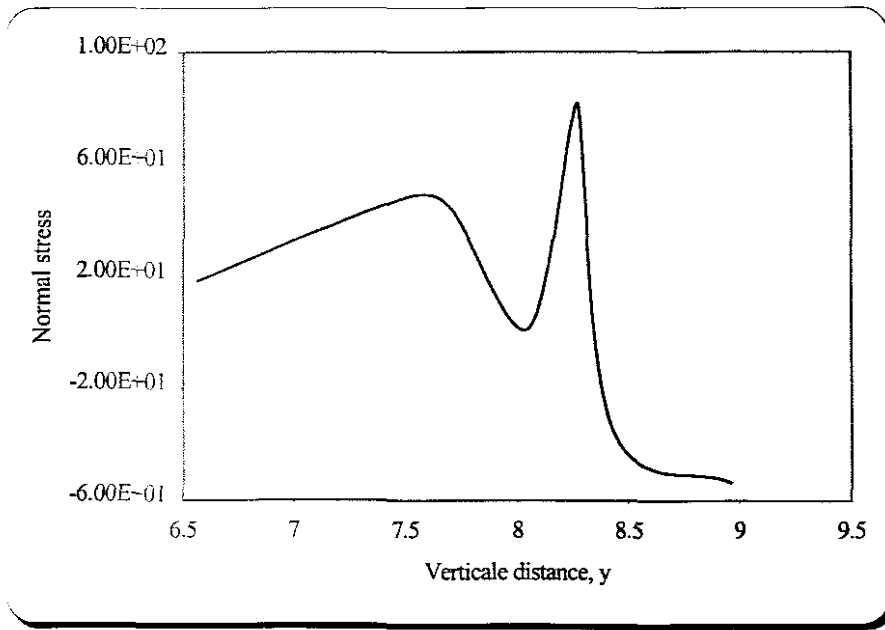
Figure 6.14 The normal stress σ_{yy}^{v} a long the wall $x=10$
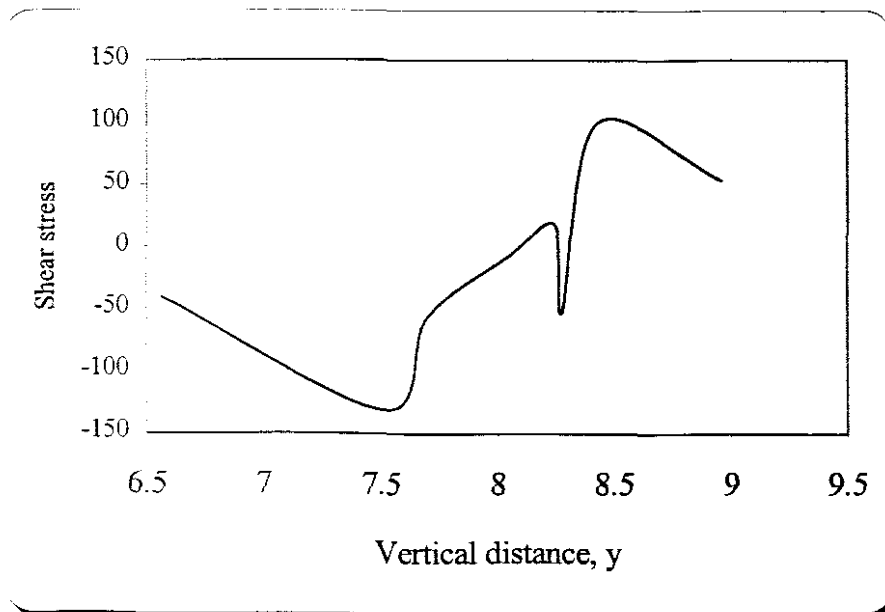
Figure 6.15 The shear stress σ_{xy}^{v} along the wall $x=10$

Using the mesh $M1$ the stresses exhibit also some oscillations around the singular point. This oscillations take a maximum amplitude exactly at $x =10$ which is the singular point. The oscillations are due to the discontinuity in the geometry, giving rise to a jump in the values of the stresses

In order to obtain reasonable results and to eliminate the oscillations in the stress fields around the corner, the mesh refinement approach has been introduced. This approach is

based on the h version of the finite element method, where h is the size of the element. In this version the accuracy can be achieved by refining the mesh (small h) while the degree of the polynomial p remain fixed. In this study a mesh M2 with a smaller density (small size) of *0.5 mm* was generated. The information of mesh M2 and the corresponding filling simulation is summarized in Table 6.3.

Cavity volume	Filled volume	Time elapsed	Percentage filled	Mesh density	Number of nodes	Number of elements
520 mm³	*504.72 mm³*	*.861 s*	*86.15 %*	*0.5 mm*	1014	946

Table 6-3 Data for mesh M2

Figure 6.16 shows the finite element mesh that used in this simulation.
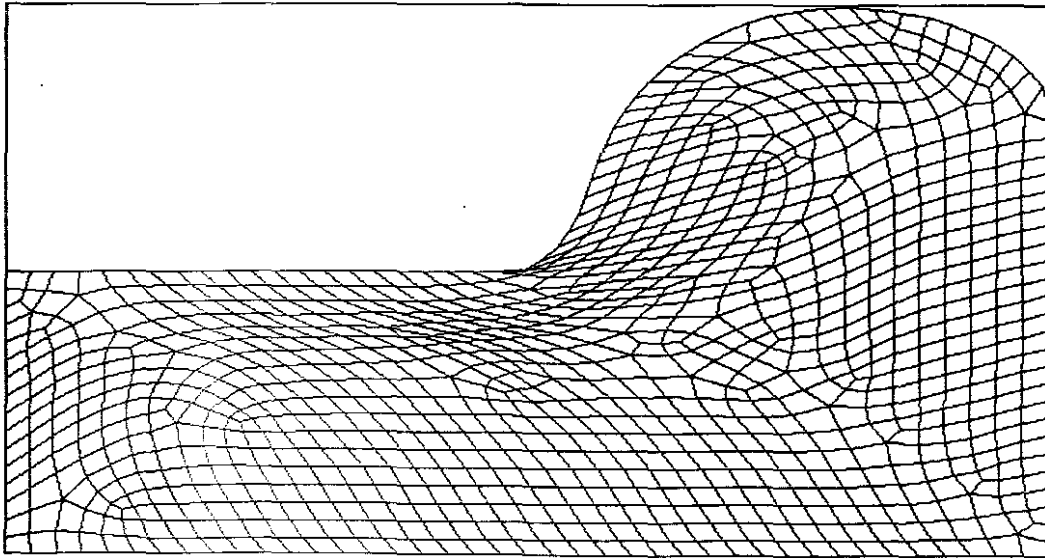
Figure 6.16 Finite elements mesh M2

Computing first the stresses along the wall *y=8* this computation gives the real values of the stress around the corner. In Figures (6.17), (6.18) and (6.19) the stress fields along the horizontal distance x are plotted, just before and after the corner. As expected the stresses exhibit singular behavior around the corner. The same behavior is noticed here compared with that of the first computation when the mesh M1 was used, but the results are more agreeable with the real behavior.

Figure 6.17 shows the curve of viscous normal stress σ_{xx}^v. The curve starts to increase smoothly from a position indicating a very small stress value. From this position the curve oscillates between a maximum and a minimum values for the stress. The normal viscous stress σ_{yy}^v curve is signifecally different to the stress σ_{xx}^v curve. This is showed in Figure 6.18. the behavior of the stress in this case is comprise the value of the stress

decrease just before the corner and then the curve change its direction at the corner down and starts to increase.
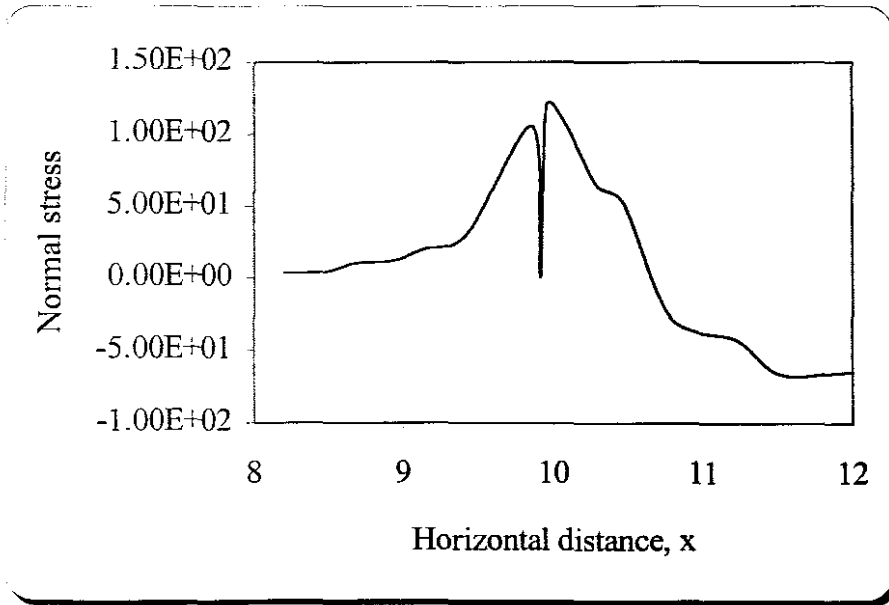
Figure 6.17 The Normal stress σ_{xx}^{v} along the wall y=8
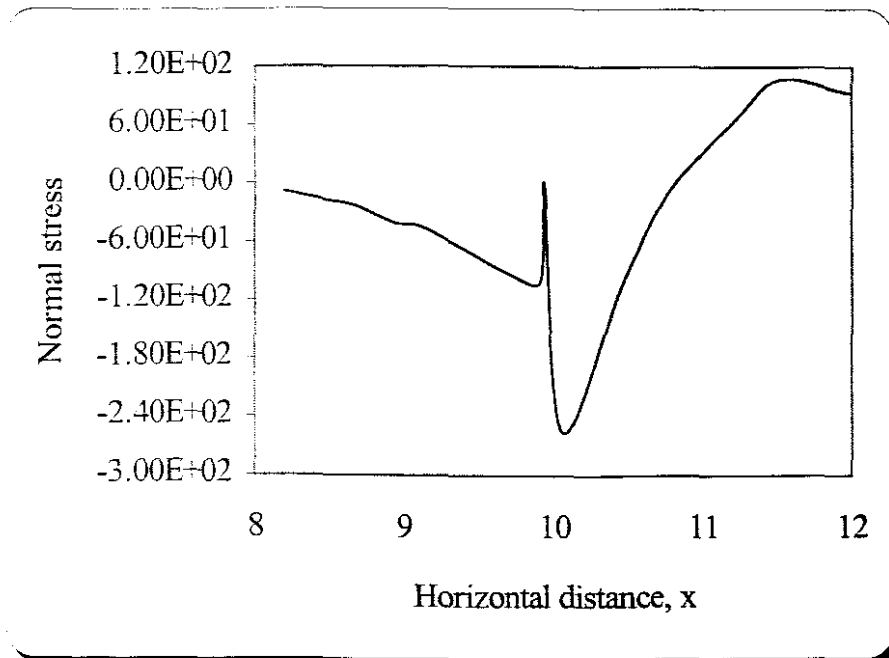
Figure 6.18 The Normal stress σ_{yy}^{v} along the wall y=8 for mesh M2
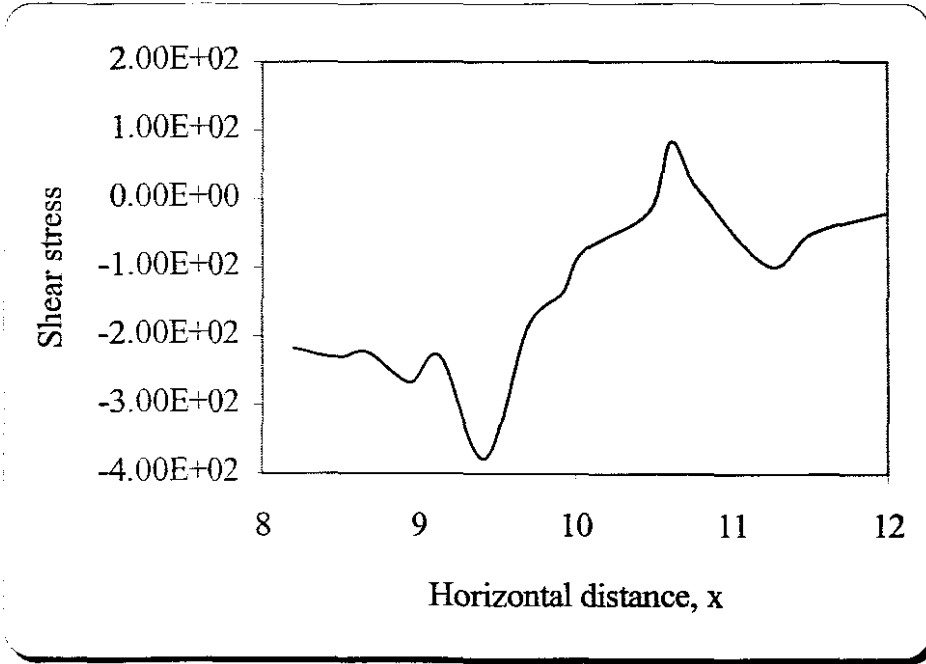
Figure 6.19 The Normal stress σ_{xy}^v along the wall y=8 for mesh *M2*

In Figures (6.20), (6.21) and (6.22) the different components of the stresses computed along the wall *x=10*.
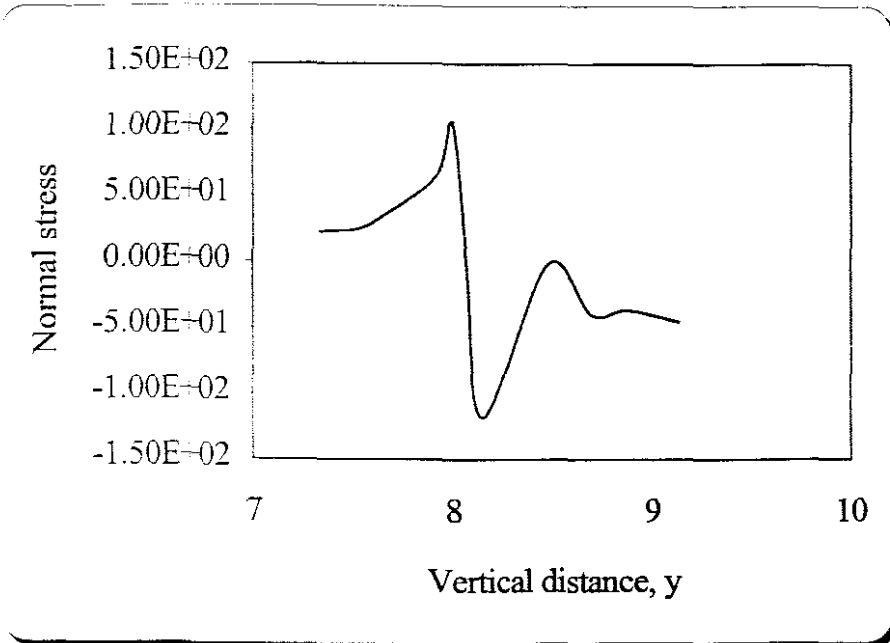
Figure 6.20 The Normal stress σ_{xx}^v along the wall *x=10* for mesh M2

The results can not superimpose due to the location of the corresponding Gauss point.
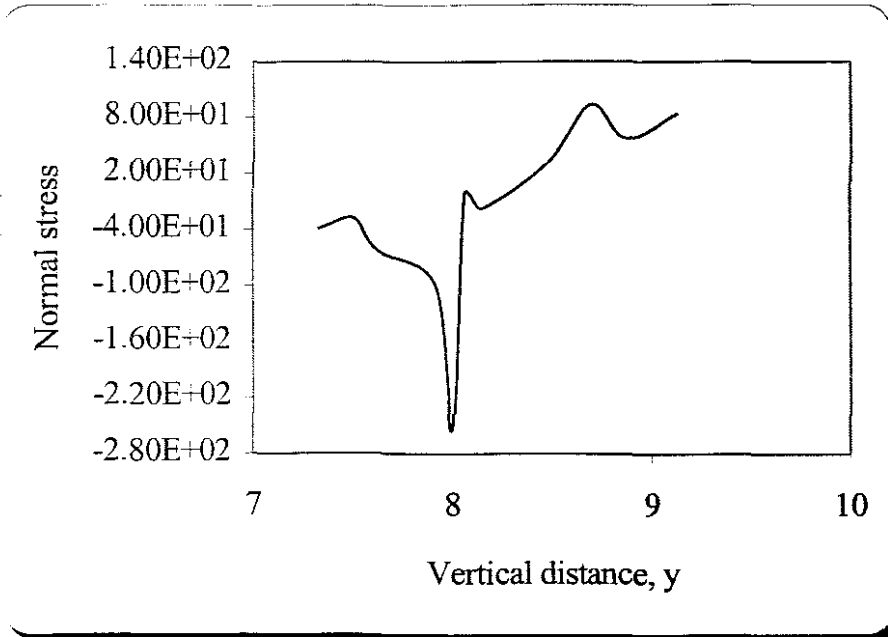
Figure 6.21 The Normal stress σ_{yy}^v along the wall $x=10$ for mesh $M2$
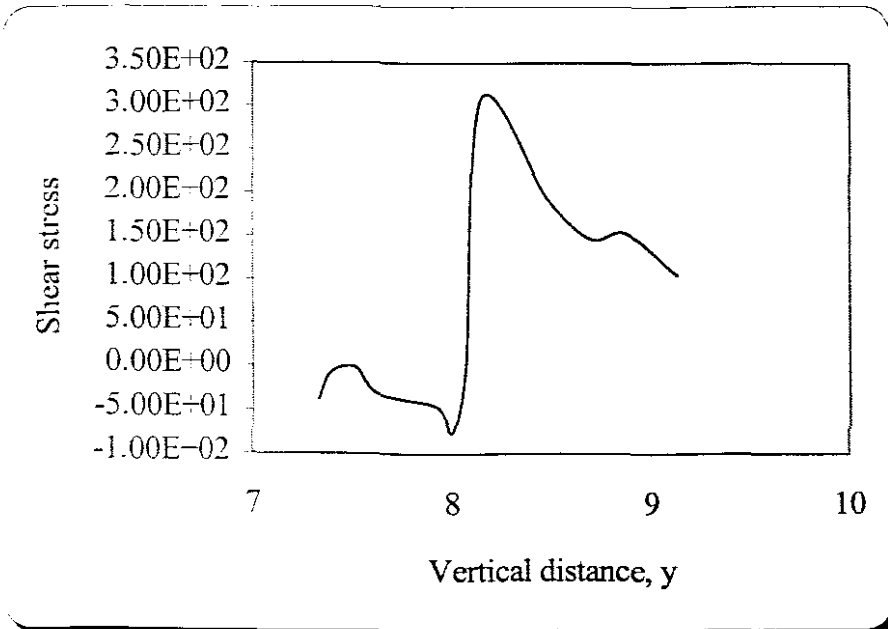
Figure 6.22 The Normal stress σ_{xy}^v along the wall $x=10$ for mesh $M2$

Generally, the singular behavior of Non-Newtonian fluid (polymer melt) can be interpreted as follows:

The flow of polymer melt during injection moulding filling is predominantly shear flow, which layers of material elements slide over each other. When the melt passes the area of

the corner the material elements undergo elongation and the flow becomes an extensional flow. Here, there will be some disentanglement, slippage chains over each other, and molecular alignment in the direction of applied stress. As a result, the resistance exhibited by polymer to flow decreases with deformation rate, due to the evolution of its microstructure (which tends to align in the flow direction). This is often referred to as shear-thinning behaviour, which translates to lower viscosity with a higher shear rate. This sudden change of the type of the flow due to the sudden change in the geometry of the mould cavity is partially responsible for the oscillations in the stresses and the singular behaviour.

CHAPTER 7

CONCLUSIONS AND RECOMMENDATIONS

7.1 Conclusions

The overall goal of this dissertation has been to understand certain aspects of Non-Newtonian fluid behavior around a singular point in as encountered in the injection moulding filling process. The study focused on the stress singularity that arises from the abrupt change in the geometry of the cavities.

The research philosophy in this dissertation has been to approach these complex issues in a very basic generic way. A numerical approach based on the analytical approach was taken, since the more complex problems defy closed-form or analytical solutions. The simulation to help interpret the data and prevailing mechanisms was used. The regions of validity of the best existing simplified analytical and numerical models of other works have been explored as well.

A numerical simulation code called **CRATMOLD** for the solution of plane transient free surface flow has been used to achieve the above goal. The problem to implement the proposed method, which is the singular finite element method (SFEM) into the code, was very complex. It was too difficult to generate a mesh for the singular element automatically due to the code. The code has been written to generate only four noded quadrilateral elements for each time step. It was attempted to generate a singular element mesh manually around the corner by modifying the original quadrilateral mesh. The idea is to replace the three quadrilateral elements around the singular point by six triangular elements by splitting each element into two, or into four, to get twelve triangular elements. Due to the distortion of the quadrilateral elements around the corner it was not possible to use this idea and to introduce the singular element into the code. Since the singular finite element method (SFEM) was too complex to implement at the present time, a standard finite element method with mesh refinement to deal with stresses and the velocity around the singular point was used.

The stresses and the velocities along the two walls forming the corner have been computed by using two finite element meshes. The first mesh was of 1mm density. The results obtained using this mesh density were not satisfactory for the stresses. A mesh refinement has been made by decreasing the density to a 0.5mm, these results were more reasonable. It was not possible to refine the mesh further in this study due to the shortage of computer memory.

A special singular element to deal with the corner problem has been developed. This singular element has a special shape function for the velocity and for the geometry, and special integration quadrature. Future workers should be able to take this element and implement it into **CRATMOLD** if a capability can be generated, or implement it into another code.

Thus, in this dissertation, we have attained about two major goals as set forth in our original objectives:

- The full understanding of fluid mechanics, for both Newtonian and non-Newtonian fluids and the causes of the singular behavior of non-Newtonian fluids;
- The full understanding of the finite element method and the singular finite element. This represents a powerful tool for treating singularity problems.

7.2 Recommendations for future work

7.2.1 Physical issues

The development of numerical methods for simulating the steady state and transient flows of non-Newtonian fluids is not sufficient to give a real behavior of the flow, especially in situations when the singularities are present. Experiments should be set up to measure the flow fields, which are the velocity and the stresses, for comparison with the simulations.

The challenge in these experiments will be the simultaneity of measurement of the stresses and the velocity. The velocity field can be measured by laser-Doppler velocimetry (LDV). Fluid stress is determined by measurement of flow-induced birefringence (FIB) by using a two-colour FIB system. These issues necessitate a study beyond this dissertation.

7.2.2 Numerical method issues

The main drawback of the current numerical method is the work required to carry out the full simulation of the singularities of the Non-Newtonian fluid in the injection moulding process. A code to deal with a variety of the singularities in this process is very important. The code should include the singularity due to the multicorner mould, singularity due to the interface of the melt front and the air trap, and singularity due to the interface of two different melts front, as well as the singularity in the temperature. Also the simulation should be extended to three-dimensional moulds by developing special singular elements. The code should be written to generate different types of element simultaneity. However, this is suited for a Ph.D. study.

REFERENCES

1. Abdel Wahab, M. M., and De Roeck, G., (1995a), ' A 2-D five-noded finite element to model power singularity', *Int. J. Fract.*, **74**, 89-97.

2. Abdel Wahab, M. M., and De Roeck, G., (1995b), ' A 3-D six-noded finite element containing a λ singularity', *Int. J. Fract.*, **70**, 347-356.

3. Abdel Wahab, M. M., and De Roeck, G., (1996), ' A family of elements with λ singularity', *Advances in Engineering Software.*, **26**, 23-28.

4. Anderson, D. M., and Davis, S. H., (1993), ' Two-fluid viscous in a corner', *J. Fluid Mech.*, **257**, 1-31.

5. Aris, R., (1989), *Vector, Tensor and the Basic Equations of Fluid Mechanics*, Dover, New York.

6. Askar, H. G., (1987), ' special elements for point singularities', *Comput. Methods. Appl Mech. Eng.*, **63**, 271-280.

7. Babuska, I., and Miller, V., (1994), 'The P and h-p versions of the finite element method, basics principles and properties', *SIAM Review*, **36(4)**, 578-632.

8. Babuska, I., and Rheinboldt, W. C., (1978), 'Error estimates for adaptive finite element computations', *SIAM J. Num. Analysis*, **15(4)**.

9. Baker, J., (1983), *Finite element computational fluid dynamics*, Hemisphere, New York.

10. Benzely, S. E., (1974), ' Representation of singularities with isoparametric elements', *Int. J. Numer. Methods Eng.*, **8**, 537-544.

11. Bersoum, R. S., (1976), ' on the use of isoparametric elements in linear fracture mechanics', *Int. J. Numer. Methods Eng.*, **10**, 25-37.

12. Bersoum, R. S., (1977), 'Triangular quarter point elements as elastic and perfectly-plastic crack-tip elements', *Int. J. Numer. Methods Eng.*, **11**, 85-98.

13. Bird, R. B., Armstrong, R., and Hassager, O., (1987), *Dynamics of Polymeric Liquids*, Vol. 1, Fluid Mechanics, 2nd revised ed., Wiley.

14. Bloch, A., Townsend, P., and Webster, M. F., (1994), ' Extensional effects in flows through contractions with abrupt or rounded corners', *J. Non-Newt.Fluid Mech.*, **54**, 285-302.

15. Broyer, E., Gutfinger, C., and Tadmor, Z., (1975), ' A theoretical model for the cavity filling process in injection molding', *Trans. Soc. Rheology.*, **19(3)**, 423-444.

16. Bulletin for the International Association for Computational Mechanics (BIACM) No 4, (1997).

17. Cai, W., Lee, H. C., and Oh, H.S., (1993),' Coupling of spectral method and the p version of the finite element method for elliptic boundary value problems containing singularities.' *J. Comp. Phys.*, **108**, 314-326.

18. Chung, T. G., (1988), *Continuum Mechanics*, Prentice-Hall, Englewood Cliffs, N. J.

19. Crochet, M. G., Davies, A. R., and Walters, K., (1984), *Numerical Simulation of Non-Newtonian Flow*, Elsevier, Amsterdam.

20. Crochet, M. G., and Walters, K., (1983), 'Numerical methods in Non-Newtonian fluid mechanics', *Ann. Rev. Fluid. Mech.*, **15**, 241-260.

21. Davies, R., (1988), 'Re-entrant corner singularities in Non-Newtonian flow. Part 1: Theory', *J. Non-Newt. Fluid Mech.*, **29**, 269-293.

22. Davies, R., and Delvin, J., (1993), 'On corner flow of Oldroyd-B fluids', *J. Non-Newt. Fluid Mech.*, **50,** 173-191.

23. Davies, R., Walters, K., and Webster, M. F., (1979),'Long- range memory effects in flows involving abrupt change in geometries. Part 3: Moving boundaries', *J. Non-Newt. Fluid Mech.*, **4,** 325-344.

24. Dunham, R. S., (1979),' A quadrature rule for conforming quadratic crack tip elements', *Int. J. Numer. Methods Eng.*, **14,** 287-312.

25. Dutta, B., (1993), ' A six noded element for analysing power type singularities under thermal loads', *Int. J. Numer. Methods Eng.*, **36,** 2287-2303.

26. Dydo, J. R., and Busby, H. R., (1997), ' An improved algorithm for developing special finite element shape functions', *Comm. Numer. Methods. Eng.*, **13,** 687-693.

27. Emanal, G., (1994), *Analytical Fluid Dynamics*, CRC Press, Inc.

28. Englemen, M. S.,. Sani, R. L., Gresho, P. M., and Bercovier, H., (1982),' Consistent v. reduced integration penalty methods for incompressible media using several old and new elements', *Int. J. Num. Meth. Fluids*, **4,** 25-42.

29. Fortin, M., (1981) ,' Old and new finite elements for incompressible flow', *Int. J. Num. Meth. Fluids*, **1,** 374-64.

30. Friedrichs, B., and Guceri, S. I., (1993), ' A novel hybrid numerical technique to model 3D fountain flow in injection molding processes', *J. Non-Newtonian. Fluid. Mech.*, **49,** 141-173.

31. Garcia, M. A., Macosko, C. W., Subbiah, S., and Guceri, S. I., (1991), ' Modelling of reactive filling in complex cavities: Comparison of fountain flow approximations', *Int. Polym. Proc.*, **6(1),** 73-82.

32. Georgiou, G. C., Olson, L. G., and Schultz, W., (1991), ' The integrated singular basis function method for the stick-slip and the die swell problems', *Int. J. Numer. Methods. Fluids.*, **13,** 1251-1265.

33. Georgiou, G. C., Olson, L. G., and Smyrlis, Y.S., (1996), ' A singular function boundary integral method for the Laplace equation', *Commi. Numer. Methods. Eng.*, **12,** 127-134.

34. Georgiou, G. C., Olson, L. G., Schultz, W. W., and Sagan, S., (1989), ' A singular finite element for Stokes flow: the stick-slip peroblem', *Int. J. Numer. Methods Fluids.*, **9,** 1353-1367.

35. Georgiou, G. C., Schultz, W. W., and Olson, L. G., (1990), ' Singular finite element for the sudden expansion and the die swell problems', *Int. J. Numer. Methods Fluids.*,**10,** 357-372.

36. Hassager, O., (1988), ' Integral models and extensional flow', *International Conference on Extensional Flow*, Chamonix, France.

37. Hassanger, O., and Laurdissen, T., (1988), 'Singular behaviour of power law fluid in Hele- Shaw flow', *J. Non-Newtonian. Fluid. Mech.*, **29,** 337-346.

38. Henshell, R. D., and Shaw, K. J., (1975), ' Crack tip elements are unenecessary', *Int. J. Numer. Methods Eng.*, **9,** 495-507.

39. Hieber, and Shen, S. F., (1980), ' A finite element/finite difference simulation of the injection molding process', *J. Non-Newtonian. Fluid. Mech.*, **7,** 1-32.

40. Holsten, H., and Paddon, D. J., (1981), 'Singular finite difference for treatment of re-entrant corner flow part 1: Newtonian flow', *J. Non-Newtonian Fluid mech.*, **8,** 81-93.

41. Horvath, (1994), ' Higher order singular isoparametric elements for crack problems', *Comm. Numer. methods. Eng.*, **10,** 73-80.

42. Hughes, T. J. R. and Akin, J.E., (1980), ' Techniques for developing "special" finite element shape functions with particular reference to the singularities', *Int. J. Numer. Methods Eng.*, **15**, 733-751.

43. Hughes, T. J. R., (1987), *The Finite Element Method*, prentice-Hall, Englewood Cliffs, NJ.

44. Huilgol, R. R., (1977),' The separation of a second order fluid at a straight edge', *J. Non-Newtonian. Fluid. Mech.*, **2**, 89-96.

45. Isayev, (Ed.), (1987), *Injection and Compression Molding Fundamentals*, Marcel Dekker, New York.

46. Kamal, M. R., Goyal, S. K., and Chu, E., (1988),' Simulation of injection mold filling of viscoelastic polymer with fountain flow', *AIChE J.*, **34(1)**, 94-106.

47. Keiller, R. A., (1991), 'Corner flow of a suspesion of rigid rods', *J. Non-Newt. Fluid Mech.*, **40**, 323-335.

48. Kermode, M., Mc Karrell, A., and Delves, L. M., (1985), 'The calculation of singular coefficients', *Comput. Methods. Appl. Mech. Eng.*, **50**, 205-215.

49. Keunings, R., and Crochet, M. J., (1984), 'Numerical simulation of the flow of viscoelastic fluid through an abrupt contraction', *J. Non-Newt. Fluid Mech.*, **14**, 279-298.

50. Kim, M. E., Brown, E. R., and Armstrong, R. C., (1983), 'The role of inertia and shear thinning in flow of an inelastic liquid through an axisymmetric sudden contraction', *J. Non-Newt. Fluid Mech.*, **13**, 341-363.

51. Lee, N Y., Shultz, W. W., and Boyd, J. P., (1987), 'Spectral solutions for flows with corner singularities', *APS Division of Fluid Mechanics 40th Annual Meeting*, Eugene, OR.

52. Legat, V., and Oden, J. T., (1996), 'An adaptive h-p finite element method for incompressible free surface flows of generalized Newtonian fluids', *Zeitscurift fur Anewandte Mathemtik und phusik.*, **46**, 365-399.

53. Lipscomb, G. G., Keunings, R., and Denn, M. M., (1987), ' Implications of boundary singularities in complex geometries', *J. Non-Newt. Fluid Mech.*, **24**, 85-96.

54. Lucas, T. R., and Oh, H. S., (1993), 'The method of auxiliary mapping for the finite element solutions of elliptic problems containing singularities', *J Comp. Phys.*, **108**, 327-342.

55. Lugst, H. J., and Schwideski, M., (1965),' Flow around dihaderal angles-I. Eigenmotion analysis', *Proc. Roy. Soc.*, **A 285**, 382

56. Maders, H., Demay, Y., and Agassant, J. F., (1990),'Numerical and analytical study of the stress singularity in an isothermal Newtonian Stokes flow in a plane convergent geometry', *Eur. J. Mech., B/Fluids.*, **9**, (1), 75-92.

57. Mahomed, N., and Kleiber, M., (1998), ' An aspect ratio conditions for the buckling and floding of polymeric jets in injection mold filling', *Comput. Assi. Mech. Eng.*, **5**, 227-243.

58. Mahomed, N., (1998), *Computational modelling of injection mould filling with new treatment of free surface*, Ph.D. Thesis, Warsaw.

59. Mendelson, M A., Yeh, P. W., Brown, R. A., and Amstrong, R. C., (1982), ' Approximation error in finite element calculation of viscoelastic fluid flows', *J. Non-Newt. Fluid Mech.*, **10**, 31-54.

60. Micheal, D. H., (1958), ' The separation of a viscous liquid at straight edge', *Mathematika*, **5**, 82-84.

61. Moffatt, H. K., (1964), 'Viscous and resistive eddies near a sharp corner', *J. Fluid. Mech.*, **18**, 1-18.

62. Morley, L. S. D., (1973), ' Finite element solution of boundary value problem with non-removable singularities', *Phil. Trans. R. Soc. Lond.* A, **275**, 463-488.

63. Oden, J. T., Kennon, S. R., Tworzydlo, W. W., Bass, J. M., and Berry, C., (1993), 'Progress on adaptive h-p finite element methods for the incompressible Navier-Stokes equations', *J. Comp. Phys.*, (in press).

64. Olson, L. G., Gergiou, G. C. and Schultz, W. W., (1991), ' An efficient finite element method for treating singularities in Laplace's equation', *J. Comput. Phy.*, **96(2)**, 391-410.

65. Perera, M. G. N., and Walters, K., (1977), 'Long- range memory effects in flows involving abrupt change in geometries. Part 1: Flows associated with L-shaped and T-shaped geometries', *J. Non-Newt. Fluid Mech.*, **2**, 49-81.

66. Perera, M. G. N., and Walters, K., (1977),'Long- range memory effects in flows involving abrupt change in geometries. Part 2: The expansion/contraction/expansion problem', *J. Non-Newt. Fluid Mech.*, **2**, 191-204.

67. Pogu, M., and Tournemine, G., (1990),'Modeling and study of viscous flows in domains with corner', *Eur. J. Mech., B/Fluids.*, **9**, (2), 129-154.

68. Renardy, M., (1994), ' How to integrate the upper conveted Maxwell (UCM) stresses near a singularity (and maybe elsewhere, too)', *J. Non-Newt. Fluid Mech.*, 52, 91-95.

69. Rosenberg, J. R., and Keunings, R., (1988), 'Further results on the flow of Maxwell fluid trough an abrupt contraction', *J. Non-Newt. Fluid Mech.*, **29**, 295-302.

70. Sih, G. C., (ed.), (1973), *Method of fracture I. Method of Analysis and Solutions of Crack Problems*, Nordoff, Leyden.

71. Solecki, J. S., and Swelow, J. L., (1984), ' On quadrature and singular finite elements', *Int. J. Numer. Methods Eng.*, **20**, 395-408.

72. Song, J. H., and Yoo, J. Y., (1987), 'Numerical simulation of viscoelastic flow through a sudden contraction using a type dependent difference method', *J. Non-Newt. Fluid Mech.*, **24**, 221-243.

73. Srang, G., and Fix, G. J., (1973), *An analysis of the Finite Element Method*, prentice-Hall, Englewood Cliffs, NJ.

74. Sshultz, W. W., and Gervasio, C., (1990), ' The study of the singularity in the die swell problem', *Q. Jl. Mech. App. Math.*, 43 pt.3.

75. Stern, M., (1979), ' Families of consistent conforming elements with singular derivative fields', *Int. J. Numer. Methods Eng.*, **14**, 409-421.

76. Sturges, L. D., (1979), ' Die swell: the separation of the free surface', *J. Non-Newtonian. Fluid . Mech.*, 6, 155-.

77. Subbiah, S., Trafford, D. L., and Guceri, S. I., (1989), 'Non-isothermal flow of polymers into two dimensional thin cavity molds: A numerical grid generation approach', *Int. J. Heat Mass Transfer.*, **32(3)**, 415-434.

78. Szabo, B. A., and Yosibash, Z., (1996), ' Numerical analysis of singularities in two dimensions. Part2: Computation of generalized flux/intensity factors', *Int. J. Numer. Methods. Eng.*, **39** (3) 409-434.

79. Tanguy, P. A., and Lacroix, R., (1991), ' A 3D mold filling study with significant heat effects', *Int. Polym. Proc.*, **6(1)**, 19-25.

80. Tanner, R. I. and Huang, X., (1993), 'Stress singularities on Non-Newtonian stick-slip edge flows', *J. Non-Newtonian. Fluid. Mech.*, **50**,135-160.

81. Tomoshenko, S., and Goodier, J. N., (1970), *Theory of Elasticity*, 3rd ed., McGraw-Hill, New York.

82. Tracey, M., (1971),' Finite element for determination of crack tip elastic stress intensity factor', *Eng. Fract. Mech.*, **3**, 255-265.

83. Tracey, M., and Cook, T. S., (1977), ' Analysis of power type singularities using finite elements', *Int. J. Numer. Methods. Eng.*, **11**, 1225-1233.

84. Vasilopoulos, D., (1988), ' On the determination of higher order terms of singular elastic fields near corner.' *Numiri. Math*, **53**, 51-95.

85. Walters, K., and Webster, M. F., (1982), *Phil. Trans. R. Soc. London, ser.* **A, 308** 199-218.

86. Warichet, V., and Legat, V., (1996), ' Adaptive h-p finite element viscoelastic flow calculations', *Compu. Method. App. Mech. Eng.*, **136,** 95-110.

87. Weinbaum, S., (1968),' On the singular points in laminar two-dimensional near wake flow field', *J. Fluid Mech.*, **33(1),** 38-63.

88. White, F. M., (1991), *Viscous Fluid Flow*, 2nd edition McGraw-Hill International Edition.

89. White, S. A., Gotsis, A. D., and Baird, D. J., (1987), 'Review of entry flow problem: experimental and numerical', *J. Non-Newt. Fluid Mech.*, **24**, 121-159.

90. Wigley, N. M., (1988), ' An efficient method for subtracting of singularities at corners Laplace's equation', *J. Comput. Phy.*, **78**, 369-377.

91. Yiang, L., (1982), ' Some interpolation function formulae for triangular and quadrilateral elements', *Int. J. Numer. Methods Eng.*, **18**, 959-966.

92. Yosibash, Z., (1997) ,' Numerical analysis on singular solution of poison equation in two dimension', *Comput. Mech.*, **20** 320-330.

93. Yosibash, Z., and Szabo, B. A., (1995), ' Numerical analysis of singularities in two dimensions. Part1: Computation of eigenpairs', *Int. J. Numer. Metheds. Eng.*, **12**, 2055-2082.

94. Zienkiewicz, O. C., (1988), *The finite element method*, McGraw-Hill, New York.

95. Zienkiewicz, O. C., Liu, Y. C., and Huang, G. C., (1988), 'Error estimation and adaptivity in flow formulation for forming problems', *Int. J. Num. Methods. Eng.*, **25**, 23-42.

96. Zienkiewicz, O.C., and Godbole, P.N., (1975), 'viscous, incompressible flow with special reference to non-Newtonian (plastic) fluids', in *Finite Elements in Fluids* (eds J. T. Oden *et al.*), Vol.2, pp.25-55, Wiley, Chichester.

97. Zienkiewicz, O.C., Vilotte, J. P., Toyoshima, S., and Nakazawa, S., (1985),' Iterative method for constrained and mixed approximation. An inexpensive improvement of FEM performance', *Comp. Meth. Appl. Mech. Eng.*, **51**, 3-29.

APPENDIX A

The Hele Shaw Flow Formulation

Adopting the coordinate definition as shown in Figure 2.2 and following the assumptions of the Hele Shaw flow, the expressions govern the fluid motion become

x- momentum

$$\frac{\partial p}{\partial x} = \eta \frac{\partial^2 v_x}{\partial z^2}$$

(A.1)

y- momentum

$$\frac{\partial p}{\partial y} = \eta \frac{\partial^2 v_y}{\partial z^2}$$

(A.2)

From Figure 2.2, the boundary conditions in the z direction are:

$$v_x = 0 \qquad , \qquad v_{y=0} \qquad \text{at} \qquad z=h$$

(A.3)

$$\frac{\partial v_x}{\partial z} = 0 \qquad , \qquad \frac{\partial v_y}{\partial z} = 0 \qquad \text{at} \qquad z=0$$

(A.4)

For an incompressible, inelastic fluid, the equation of continuity is given by

$$\frac{\partial}{\partial x}\left(h\bar{v}_x\right) + \frac{\partial}{\partial y}\left(h\bar{v}_y\right) = 0$$

(A.5)

where $\bar{v}_x$ and $\bar{v}_y$ are the mean velocities averaged through the gape of with *2h*.

Integrating (A.1) and (A.2) in the gapwise direction and using boundary conditions (A4):

$$\eta \frac{\partial v_x}{\partial z} = \frac{\partial p}{\partial x} z$$

(A.6)

$$\eta \frac{\partial v_y}{\partial z} = \frac{\partial p}{\partial y} z$$

(A.7)

Integrating (A.6) using boundary condition (A.3)

$$v_x = \frac{1}{\eta} \int \frac{\partial p}{\partial x} z dz$$

$$\frac{1}{\eta} \frac{\partial p}{\partial x}\left[\frac{z^2}{2}\right] + C$$

$$C = -\frac{1}{\eta} \frac{\partial p}{\partial x}\left[\frac{h^2}{2}\right]$$

$$v_x = \frac{1}{\eta}\frac{\partial p}{\partial x}\left[\frac{z^2}{2}\right] - \frac{1}{\eta}\frac{\partial p}{\partial x}\left[\frac{h^2}{2}\right]$$

$$= \frac{1}{\eta}\int_0^z \frac{\partial p}{\partial x}z\,dz - \frac{1}{\eta}\int_0^h \frac{\partial p}{\partial x}z\,dz$$

$$v_x = -\frac{1}{\eta}\int_z^h \frac{\partial p}{\partial x}z\,dz \tag{A.8a}$$

Similarly

$$v_y = -\frac{1}{\eta}\int_z^h \frac{\partial p}{\partial y}z\,dz \tag{A.8b}$$

The mean velocities averaged through the gapwise direction are obtained as follows:

$$\bar{v}_x = \frac{1}{h}\int_0^h v_x\,dz$$

$$= \frac{1}{h}\int_0^h \left[-\frac{1}{\eta}\frac{\partial p}{\partial x}\left(\frac{h^2}{2} - \frac{z^2}{2}\right)\right]dz$$

$$= -\frac{1}{h}\frac{1}{\eta}\frac{\partial p}{\partial x}\left[\frac{h^2 z}{2} - \frac{z^3}{6}\right]_0^h$$

$$= -\frac{1}{h}\frac{1}{\eta}\frac{\partial p}{\partial x}\frac{h^3}{3}$$

$$\bar{v}_x = -\frac{1}{h}\frac{\partial p}{\partial x}\int_0^h \frac{z^2}{\eta}\,dz \tag{A.9a}$$

Similarly

$$\bar{v}_y = -\frac{1}{h}\frac{\partial p}{\partial y}\int_0^h \frac{z^2}{\eta}\,dz \tag{A.9b}$$

Substituting Equations (A.9) into the continuity equation (A.5)

$$\frac{\partial}{\partial x}\left[S\frac{\partial p}{\partial x}\right] + \frac{\partial}{\partial y}\left[S\frac{\partial p}{\partial y}\right] = 0 \tag{A.10}$$

where

$$S = \int_0^h \frac{z^2}{\eta}\,dz \tag{A.11}$$

APPENDIX B

The Deformation Rate Matrix

In this Appendix we present the detail of the deformation rate (strain matrix) [B], for two dimensional quadrilateral isoparametric element:

From equation (4.54) we have

$$[\Gamma] = [J]^{-1} = \frac{1}{J}\begin{bmatrix} J_{22} & -J_{12} \\ -J_{21} & J_{11} \end{bmatrix} = \begin{bmatrix} \Gamma_{11} & \Gamma_{12} \\ \Gamma_{21} & \Gamma 22 \end{bmatrix} \tag{B.1}$$

The strains are given by:

$$\epsilon_x = \frac{\partial v_x}{\partial x} = \Gamma_{11}\frac{\partial v_x}{\partial \xi} + \Gamma_{12}\frac{\partial v_x}{\partial \eta} \tag{B.2}$$

$$= \Gamma_{11}\begin{bmatrix} \dfrac{\partial N_1}{\partial \xi} & \dfrac{\partial N_2}{\partial \xi} & \dfrac{\partial N_3}{\partial \xi} & \dfrac{\partial N_4}{\partial \xi} \end{bmatrix}\begin{Bmatrix} v_{1x} \\ v_{2x} \\ v_{3x} \\ v_{4x} \end{Bmatrix} + \Gamma_{12}\begin{bmatrix} \dfrac{\partial N_1}{\partial \eta} & \dfrac{\partial N_2}{\partial \eta} & \dfrac{\partial N_3}{\partial \eta} & \dfrac{\partial N_4}{\partial \eta} \end{bmatrix}\begin{Bmatrix} v_{1x} \\ v_{2x} \\ v_{3x} \\ v_{4x} \end{Bmatrix}$$

$$\epsilon_y = \frac{\partial v_y}{\partial y} = \Gamma_{21}\frac{\partial v_y}{\partial \xi} + \Gamma_{22}\frac{\partial v_y}{\partial \eta} \tag{B.3}$$

$$= \Gamma_{21}\begin{bmatrix} \dfrac{\partial N_1}{\partial \xi} & \dfrac{\partial N_2}{\partial \xi} & \dfrac{\partial N_3}{\partial \xi} & \dfrac{\partial N_4}{\partial \xi} \end{bmatrix}\begin{Bmatrix} v_{1y} \\ v_{2y} \\ v_{3y} \\ v_{4y} \end{Bmatrix} + \Gamma_{22}\begin{bmatrix} \dfrac{\partial N_1}{\partial \eta} & \dfrac{\partial N_2}{\partial \eta} & \dfrac{\partial N_3}{\partial \eta} & \dfrac{\partial N_4}{\partial \eta} \end{bmatrix}\begin{Bmatrix} v_{1y} \\ v_{2y} \\ v_{3y} \\ v_{4y} \end{Bmatrix}$$

$$\epsilon_{xy} = \frac{\partial v_x}{\partial y} + \frac{\partial v_y}{\partial x} = \Gamma_{21}\frac{\partial v_x}{\partial \xi} + \Gamma_{22}\frac{\partial v_x}{\partial \eta} + \Gamma_{11}\frac{\partial v_y}{\partial \xi} + \Gamma_{12}\frac{\partial v_y}{\partial \eta} \tag{B.4}$$

Thus, the strain equations are summarized as the next three equations:

$$\{\epsilon\} = \begin{Bmatrix} \epsilon_x \\ \epsilon_y \\ \epsilon_{xy} \end{Bmatrix} = \begin{bmatrix} 1 & 0 & 0 & 0 \\ 0 & 0 & 0 & 1 \\ 0 & 1 & 1 & 0 \end{bmatrix}\begin{Bmatrix} v_{x,x} \\ v_{x,y} \\ v_{y,x} \\ v_{y,y} \end{Bmatrix} \tag{B.5}$$

$$\begin{Bmatrix} v_{x,x} \\ v_{x,y} \\ v_{y,x} \\ v_{y,y} \end{Bmatrix} = \begin{bmatrix} \Gamma_{11} & \Gamma_{12} & 0 & 0 \\ \Gamma_{21} & \Gamma_{22} & 0 & 0 \\ 0 & 0 & \Gamma_{11} & \Gamma_{12} \\ 0 & 0 & \Gamma_{21} & \Gamma_{22} \end{bmatrix}\begin{Bmatrix} v_{x,\xi} \\ v_{x,\eta} \\ v_{y,\xi} \\ v_{y,\eta} \end{Bmatrix} \tag{B.6}$$

$$
\begin{Bmatrix} v_{x,\xi} \\ v_{x,\eta} \\ v_{y,\xi} \\ v_{y,\eta} \end{Bmatrix} =
\begin{bmatrix}
N_{1,\xi} & 0 & N_{2,\xi} & 0 & N_{3,\xi} & 0 & N_{4,\xi} & 0 \\
N_{1,\eta} & 0 & N_{2,\eta} & 0 & N_{3,\eta} & 0 & N_{4,\eta} & 0 \\
0 & N_{1,\xi} & 0 & N_{2,\xi} & 0 & N_{3,\xi} & 0 & N_{4,\xi} \\
0 & N_{1,\eta} & 0 & N_{2,\eta} & 0 & N_{3,\eta} & 0 & N_{4,\eta}
\end{bmatrix}
\begin{Bmatrix} v_{x1} \\ v_{y1} \\ v_{x2} \\ v_{y2} \\ v_{x3} \\ v_{y3} \\ v_{x4} \\ v_{y4} \end{Bmatrix}
\tag{B.7}
$$

Multiplying the above 3 matrices together forms [B] for a linear quadrilateral element

$$
[B] =
\begin{bmatrix}
1 & 0 & 0 & 0 \\
0 & 0 & 0 & 1 \\
0 & 1 & 1 & 0
\end{bmatrix}
\begin{bmatrix}
\Gamma_{11} & \Gamma_{12} & 0 & 0 \\
\Gamma_{21} & \Gamma_{22} & 0 & 0 \\
0 & 0 & \Gamma_{11} & \Gamma_{12} \\
0 & 0 & \Gamma 21 & \Gamma_{22}
\end{bmatrix}
\begin{bmatrix}
N_{1,\xi} & 0 & N_{2,\xi} & 0 & N_{3,\xi} & 0 & N_{4,\xi} & 0 \\
N_{1,\eta} & 0 & N_{2,\eta} & 0 & N_{3,\eta} & 0 & N_{4,\eta} & 0 \\
0 & N_{1,\xi} & 0 & N_{2,\xi} & 0 & N_{3,\xi} & 0 & N_{4,\xi} \\
0 & N_{1,\eta} & 0 & N_{2,\eta} & 0 & N_{3,\eta} & 0 & N_{4,\eta}
\end{bmatrix}
$$

Multiplying the first two matrices gives:

$$
[B] =
\begin{bmatrix}
\Gamma_{11} & \Gamma_{12} & 0 & 0 \\
0 & 0 & \Gamma_{21} & \Gamma_{22} \\
\Gamma_{21} & \Gamma_{22} & \Gamma_{11} & \Gamma_{12}
\end{bmatrix}
\begin{bmatrix}
N_{1,\xi} & 0 & N_{2,\xi} & 0 & N_{3,\xi} & 0 & N_{4,\xi} & 0 \\
N_{1,\eta} & 0 & N_{2,\eta} & 0 & N_{3,\eta} & 0 & N_{4,\eta} & 0 \\
0 & N_{1,\xi} & 0 & N_{2,\xi} & 0 & N_{3,\xi} & 0 & N_{4,\xi} \\
0 & N_{2,\xi} & 0 & N_{2,\eta} & 0 & N_{3,\eta} & 0 & N_{4,\eta}
\end{bmatrix}
$$

The final matrix is:

$$
[B] =
\begin{bmatrix}
\left(\Gamma_{11}N_{1,\xi} + \Gamma_{12}N_{1,\eta}\right) & 0 & \left(\Gamma_{11}N_{2,\xi} + \Gamma_{12}N_{2,\eta}\right) & 0 \\
0 & \left(\Gamma_{21}N_{1,\xi} + \Gamma_{22}N_{1,\eta}\right) & 0 & \left(\Gamma_{21}N_{2,\xi} + \Gamma_{22}N_{2,\eta}\right) \\
\left(\Gamma_{21}N_{1,\xi} + \Gamma_{22}N_{1,\eta}\right) & \left(\Gamma_{11}N_{1,\xi} + \Gamma_{12}N_{1,\eta}\right) & \left(\Gamma_{21}N_{2,\xi} + \Gamma_{22}N_{2,\eta}\right) & \left(\Gamma_{11}N_{2,\xi} + \Gamma_{12}N_{2,\eta}\right)
\end{bmatrix}
$$

$$
\begin{bmatrix}
\left(\Gamma_{11}N_{3,\xi} + \Gamma_{12}N_{3,\eta}\right) & 0 & \left(\Gamma_{11}N_{4,\xi} + \Gamma_{12}N_{4,\eta}\right) & 0 \\
0 & \left(\Gamma_{21}N_{3,\xi} + \Gamma_{22}N_{3,\eta}\right) & 0 & \left(\Gamma_{21}N_{4,\xi} + \Gamma_{22}N_{2,\eta}\right) \\
\left(\Gamma_{21}N_{3,\xi} + \Gamma_{22}N_{3,\eta}\right) & \left(\Gamma_{11}N_{3,\xi} + \Gamma_{12}N_{3,\eta}\right) & \left(\Gamma_{21}N_{4,\xi} + \Gamma_{22}N_{4,\mu}\right) & \left(\Gamma_{11}N_{4,\xi} + \Gamma_{12}N_{4,\eta}\right)
\end{bmatrix}
$$

APPENDIX C

Interpolation Function for the Singular Element

The velocity interpolation functions for two-dimensional five nodes singular element and it derivative are given by:

$$\phi_1(\xi,\eta) = -\xi - 4X(1+\xi) + 4X(1+\xi)^\lambda \tag{C.1}$$

$$\phi_i(\xi,\eta) = -2X\Big[(1+\xi) - (1+\xi)^\lambda\Big](1+\eta\eta_i) \text{ for } i = 2,3 \tag{C.2}$$

$$\phi_i(\xi,\eta) = \Big[\Big(4X+\frac{1}{2}\Big)(1+\xi) - 4X(1+\xi)^\lambda\Big](1+\eta\eta_i) \text{ for } i = 4,5 \tag{C.3}$$

Where $X = 1/4\big(2^\lambda - 2\big)$

The derivative of the interpolation function with respect to ξ and η are:

$$\frac{\partial\phi_1(\xi,\eta)}{\partial\xi} = -1 - 4X + 4X\lambda(1+\xi)^{\lambda-1} \tag{C.4}$$

$$\frac{\partial\phi_i(\xi,\eta)}{\partial\xi} = -2X\Big[1 - \lambda(1+\xi)^{\lambda-1}\Big](1+\eta\eta_i) \text{ for } i = 2,3 \tag{C.5}$$

$$\frac{\partial\phi_i(\xi,\eta)}{\partial\xi} = \Big[\Big(4X+\frac{1}{2}\Big) - 4X\lambda(1+\xi)^{\lambda-1}\Big](1+\eta\eta_i) \text{ for } i = 4,5 \tag{C.6}$$

$$\frac{\partial\phi_1(\xi,\eta)}{\partial\eta} = 0 \tag{C.7}$$

$$\frac{\partial\phi_i(\xi,\eta)}{\partial\eta} = -2X\Big[(1+\xi) - (1+\xi)^\lambda\Big]\eta_i \text{ for } i = 2,3 \tag{C.8}$$

$$\frac{\partial\phi_i(\xi,\eta)}{\partial\eta} = \Big[\Big(4X+\frac{1}{2}\Big)(1+\xi) - 4X(1+\xi)^\lambda\Big]\eta_i \text{ for } i = 4,5 \tag{C.9}$$

Appendix D

INPUT AND OUTPUT FILES FOR THE CRATMOLD

BMESH: BACKGROUND MESH - USED FOR DENSITY INTERPOLATION

```
6                                   [nnode]
1       0.000      8.000      1.000  [n,xnode(1,n),xnode(2,n),bdelta(n)]
2      00.000      4.000      1.000
3      00.000      0.000      1.000
4       4.000      0.000      1.000
5       4.000      4.000      1.000
6       4.000      8.000      1.000
2                                   [nelem]
1    1    2    5    6    1          [e,inode(1,e),inode(2,e),inode(3,e),
2    2    3    4    5    1            inode(4,e),ireg(e)]
1                                   [nreg]
1 .1000E+01 .1000E+08 .4730E+03 .2799E+00 .1484E+05 .5000E-07 .13520+05 .3500E-07
 [r,  d(r,1),  d(r,2),  d(r,3),  d(r,4),  d(r,5),  d(r,6),  d(r,7),  d(r,8)]
```

nnode   -number of nodes in background mesh
xnode(1,n)   -x-coordinate of background mesh n
xnode(2,n)   -y-coordinate of background mesh n
bdelta(n)   -mesh density at background mesh n
nelem   -number of elements in background mesh n
inode(1,e)   -node1 1 of background element e
inode(2,e)   -node1 2 of background element e
inode(3,e)   -node1 3 of background element e
inode(4,e)   -node1 4 of background element e
ireg(e)   -region number of background element e
nreg   -number of regions in background mesh
d(r,1)   -half gape width for background region r
d(r,2)   -penalty parameter for background region r
d(r,3)   -injection temperature of melt for background region r
d(r,4)   -power law index for background region r
d(r,5)   -transition stress for background region r
d(r,6)   -Cross constant b for background region r
d(r,7)   -temperature constant for background region r
d(r,8)   -Cross constant beta for background region r

CMESH: CAVITY MESH-USED FOR MELT FRONT TRACKING

```
8                                   [nnodec]
1      00.000      8.000      1.000  [n,xnodec(1,n),xnodec(2,n),cdelta(n)]
2      00.000      0.000      1.000
3      10.000      0.000      1.000
4      20.000      0.000      1.000
5      20.000      8.000      1.000
6      20.000     18.000      1.000
7      10.000     18.000      1.000
8      10.000      8.000      1.000
3                                   [nelem]
1    1    2    3    8    1          [e,inodec(1,e),inodec(2,e),inodec(3,e),
2    8    3    4    5    1            inodec(4,e),iregc(e)]
3    8    5    6    7    1
1                                   [nregc]
1 .1000E+01 .1000E+08 .4730E+03 .2799E+00 .1484E+05 .5000E-07 .13520+05 .3500E-07
 [r,  d(r,1),  d(r,2),  d(r,3),  d(r,4),  d(r,5),  d(r,6),  d(r,7),  d(r,8)]
```

nnodec   -number of nodes in cavity
xnodec(1,n)   -x-coordinate of node n
xnodec(2,n)   -y-coordinate of node n

```
cdelta(n)        -mesh density at cavity node n
nelemc           -number of elements in cavity
inodec(1,e)      -node1 1 of cavity element e
inodec(2,e)      -node1 2 of cavity element e
inodec(3,e)      -node1 3 of cavity element e
inodec(4,e)      -node1 4 of cavity element e
iregc(e)         -region number of cavity element e
nregc            -number of regions in cavity
d(r,1)           -half gape width for background region r
d(r,2)           -penalty parameter for background region r
d(r,3)           -injection temperature of melt for background region r
d(r,4)           -power law index for background region r
d(r,5)           -transition stress for background region r
d(r,6)           -Cross constant b for background region r
d(r,7)           -temperature constant for background region r
d(r,8)           -Cross constant beta for background region r
```

IMESH: INPUT MESH DATA OF BOUNDARY SEGMENTS AND NODES

TO BE USED FOR QUADRILATERAL MESH GENERATION

```
4                                                    [nseg]
1    1    1   .20000+03   .0000E+00   2   1   2     [s,isegcurves(s),isegtype(s),
2    1    1   .0000E+00   .0000E+00   2   2   3      valuesegx(s),valuesegy(s),
3    1    2   .0000E+00   .0000E+00   2   3   4      npoinseg(s),ipoin(1,s),...
4    1    1   .0000E+00   .0000E+00   2   4   1      ipoin(npoinseg,s)]
4                                                    [npoin]
1    00.000    8.000                                [p,coor(1,p),coor(2,p)]
2    00.000    0.000
3     1.000    0.000
4     1.000    8.000
```

```
nseg             -number of boundary segments describing the fluid domain
isegcurve(s)     -curve type for boundary segment s: 1=linear, 2=cubic spline
isegtype(s)      -boundary coondition type for boundary segment: 1=const velocity
                   2=const stress
valuesegx(s)     -x-value of boundary condition boundary segment s
valuesegy(s)     -y-value of boundary condition boundary segment s
npoinseg(s)      -number of points on bpundary segment s
ipoin(1,s)       -point number 1 of boundary segment s, etc
coor(1,p)        -x-coordinate of point p
coor(2,p)        -y-coordinate of point p
```

IMOLD: DATA FOR TIME INTEGRATION

```
1.000    0.030    0.005                 [ftime,start,dt]
```

```
ftime            -filling time
start            -initial or restart time
dt               -time increment
```

OUTPUT FILE OMOLD

```
Cavity volume =     520.00 mm3    Filled volume =      16.00 mm3
 Time elapsed =      .031 secs    Percentage filled =  3.08%
 ELEMENT TOPOLOGICAL DATA

NEWTONIAN VELOCITY FIELD
    1      200.000         .000      [n, vnode(1,n),vnode(2,n)]
    2      200.000         .000
    3      200.000         .000
    4      200.000         .000
    5      200.000         .000
    6      200.000         .000
    7      200.000         .000
    8      200.000         .000
    9      200.000         .000
```

```
10          .000          .000
11       297.414       107.445
12       190.096        14.571
13       212.318        13.762
14       200.441         -.185
15       212.360       -11.795
16       189.786       -15.688
17       294.886       -95.104
18          .000          .000
```

```
n                -number of nodes
vnode(1,n)       -horizontal velocity of node n
vnode(2,n)       -vertical velocity of node n
```

STRESS FIELD . . . .
```
element no=,    1
    1     .2113     7.7909  -.19290E+03   .28596E+02  -.11726E+03   [ngaupoint,xgaupoint,
    2     .2113     7.2197   .49348E+02   .28596E+02  -.19539E+03    ygaupoint,sigmaxx,
    3     .7887     7.2424   .59292E+02   .10993E+03  -.45079E+03    sigmayy, sigmaxy]
    4     .7887     7.7970  -.19023E+03   .10993E+03  -.37031E+03
element no=,    2
    1     .7887     6.8281   .16513E+03  -.15092E+03   .18553E+02
    2     .2113     6.7992   .17244E+03  -.40439E+02  -.13318E+03
    3     .2113     6.2219   .26230E+02  -.40439E+02  -.22702E+02
    4     .7887     6.2508   .18919E+02  -.15092E+03   .12903E+03
element no=,    3
    1     .7887     5.8259  -.29548E+02  -.20516E+02  -.21806E+03
    2     .2113     5.7909  -.34875E+02  -.53446E+01  -.13102E+03
    3     .2113     5.1908   .54010E+02  -.53446E+01  -.11569E+03
    4     .7887     5.2424   .61877E+02  -.20516E+02  -.20229E+03
element no=,    4
    1     .7887     4.8175   .10311E+03  -.10606E+03   .11290E+02
    2     .2113     4.7598   .11109E+03  -.28420E+02  -.76191E+02
    3     .2113     4.1825   .31368E+02  -.28420E+02   .14534E+01
    4     .7887     4.2402   .23397E+02  -.10606E+03   .88935E+02
element no=,    5
    1     .7887     3.8175   .40009E+02  -.11320E+03  -.56658E+02
    2     .2113     3.7598   .32952E+02  -.30332E+02   .56270E+01
    3     .2113     3.1825   .10352E+03  -.30332E+02   .88496E+02
    4     .7887     3.2402   .11058E+03  -.11320E+03   .26212E+02
element no=,    6
    1     .7887     2.8092   .40688E+02  -.40859E+01   .20529E+03
    2     .2113     2.7576   .47958E+02  -.11261E+01   .12374E+03
    3     .2113     2.1741  -.36531E+02  -.11261E+01   .12682E+03
    4     .7887     2.2091  -.41454E+02  -.40859E+01   .20828E+03
element no=,    7
    1     .7887     1.7781   .38092E+02  -.16406E+03  -.10478E+03
    2     .2113     1.7492   .31153E+02  -.43960E+02   .27998E+02
    3     .2113     1.1719   .16993E+03  -.43960E+02   .14810E+03
    4     .7887     1.2008   .17687E+03  -.16406E+03   .15325E+02
element no=,    8
    1     .7887      .7803   .35125E+02   .11931E+03   .44359E+03
    2     .2113      .7576   .44553E+02   .32929E+02   .20789E+03
    3     .2113      .2030  -.19202E+03   .32929E+02   .12243E+03
    4     .7887      .2091  -.19454E+03   .11931E+03   .36061E+03
```

D Y N A M I C   S T O R A G E   A L L O C A T I O N   I N F O R M A T I O N

ARRAY NO.	ARRAY	ADDRESS	DIM1	DIM2	DIM3	PREC.
1	id	1	2	18	0	1
2	diag	37	23	0	0	1
3	alhs	61	206	0	0	1
4	brhs	267	23	0	0	1

```
ngaupoint        -number of gaupoint
xgaupoint        -x-coordinate of the gauss point
ygaupoint        -y-coordinate of the gauss point
sigmaxx          -the normal viscous stress sigmaxx at gauss point
sigmayy          -the normal viscous stress sigmayy at gauss point
sigmaxy          -the shear stress sigmaxy at gauss point
```